Ferhat ABBAS Sétif 1 University

Faculty of Sciences

Departement of Physics

A Thesis Submitted in fulfillment of the requirement for the Degree

of Doctorate

Presented by

Abdelouadoud GUERRA

Fabrication and characterization of chromium nitride (CrN) based micro-supercapacitors

---

Defended on 28 September 2022

Board of examiners:

Mebarek BOUKELKOUL	**MCA**	**Ferhat ABBAS Setif 1 University**	**Chairman**
Ammar MOSBAH	**MCA**	**Ferhat ABBAS Setif 1 University**	**Supervisor**
Abdelhafid MAHROUG	**MCA**	**Mohamed BOUDIAF 1 University-Msila**	**Examiner**
Mounir REFFAS	**MCA**	**Ferhat ABBAS Setif 1 University**	**Examiner**

Publication List

* Corresponding Author, + Equal contribution

- **Abdelouadoud Guerra***, Amine Achour, Sorin Vizireanu, Gheorghe Dinescu, Samira Messaci, Toufik Hadjersi,Rabah Boukherroub, Yannick coffinier, Jean Jacques Pireaux, ZnO/Carbon nanowalls shell/core nanostructures as electrodes for supercapacitors. Applied Surface Science, 2019, 481, 926-932.

- Emile Haye, Amine Achour, **Abdelouadoud Guerra**+, Fatsah Moulaï, Toufik Hadjersi, Rabah Boukherroub, Stephane Lucas, Achieving on chip micro-supercapacitors based on CrN deposited by bipolar magnetron sputtering at glancing angle. Electrochimica Acta, 2019. 324, 134890.

- **Abdelouadoud Guerra***, Emile Haye, Amine Achour, Mxime Harnois, Toufik Hadjersi, Jean-Francois Colomer, Jean-jacques Pireaux, Stephane Lucas, Rabah Boukherroub, High performance of 3D silicon nanowires array@ CrN for electrochemical capacitors. Nanotechnology, 2019, 31(3), 035407.

- Amine Achour., **Abdelouadoud Guerra**+, Fatsah Moulaï, Mohammad Islam, Toufik Hadjersi, Iftikhar Ahmad, Jean-Jaques Pireaux, MnOx thin film based electrodes: Role of surface point defects and structure towards extreme enhancement in specific capacitance. Materials Chemistry and Physics, 2019, 122487.

Abstract

The aim of this thesis work is the elaboration of micro-supercapacitor electrodes based on chromium nitride (CrN) deposited on a silicon current collector. Their electrochemical performance can be improved by increasing their specific surface area and/or porosity for better accessibility of the electrolyte to the active material to improve their charge storage.

The first part of the first chapter is devoted to the state of the art on supercapacitors and micro-supercapacitors as well as the different energy storage systems, various types and applications of supercapacitors and their storage mechanisms. In the second part, we describe the composition of a supercapacitor as well as materials and electrolytes used for the fabrication of supercapacitors.

The second chapter concerns the fabrication of electrodes based on a thin film of chromium nitride (CrN) deposited by bipolar magnetron sputtering at a glancing angle (PVD-GLAD). The use of this new technique allows controlling the morphology of the surface of the electrodes which directly affected their storage capacity. Subsequently, we will describe the fabrication of a micro-device with an inter-digital configuration based on chromium nitride with good electrochemical performances.

The third chapter is dedicated to the development of composite electrodes based on silicon nanowires (SiNWs) synthesized via a VLS mechanism and coated with a thin layer of highly pseudo-capacitive material of CrN. Post-coating SiNWs with CrN can offer benefits, such as enhanced faradaic capacitance and electrical conductivity of the composite made of the metal nitride and SiNWs. Furthermore, the double-layer capacitance of the SiNWs with a large specific surface area can be added to that of CrN.

The fourth chapter focuses on the development of composites electrodes made with carbon nanowalls (CNW) decorated with CrN. We will describe the benefits of using a template with a large specific surface area on the electrochemical performance of the composites electrodes. The large surface area of CNW and their good electrical conductivity allows improving not only the areal capacitance of CrN based electrodes but also its cycle life. Subsequently, we will describe the fabrication of a micro-device with a staked configuration based on CNW-CrN electrodes with robust electrochemical stability over 30000 cycles.

Abstract

Finally, the conclusion summarizes the obtained results during this thesis as well as the prospects envisaged.

Keywords: micro-supercapacitors, areal capacitance, carbon nanowalls, silicon nanowires, PVD, glancing Angle.

Résumé

L'objectif de cette thèse est l'élaboration des électrodes des micro-supercondensateurs (μSC) à base de nitrure de chrome déposé sur un substrat de silicium utilisé comme collecteur de courant. Leurs performances électrochimiques peuvent être améliorées en augmentant leurs surfaces spécifiques et/ou la porosité pour une meilleure accessibilité de l'électrolyte vers le matériau actif afin d'améliorer le stockage de charge des électrodes.

La première partie du premier chapitre est consacrée à l'état de l'art sur les supercondensateurs et micro-supercondensateurs ainsi qu'aux différents systèmes de stockage d'énergie, aux différents types et applications des supercondensateurs et de leurs mécanismes de stockage. Dans la deuxième partie, nous décrivons la composition d'un supercondensateur ainsi que les matériaux d'électrode et les électrolytes utilisés pour la fabrication des supercondensateurs.

Le deuxième chapitre concerne la fabrication des électrodes à base d'un film mince de nitrure de chrome (CrN) déposé par pulvérisation magnétron bipolaire sous incidence oblique. L'utilisation de cette nouvelle technique permet de contrôler la morphologie de la surface des électrodes qui affect direcetement leur capacité de stockage. Par la suite, nous décrirons la fabrication d'un micro-dispositif à configuration inter-digité à base de CrN avec de bonnes performances électrochimiques.

Le troisième chapitre est consacré au développement des électrodes composites à base de nanofils de silicium (NFSi) synthétisées via un mécanisme VLS et recouvertes d'une couche de CrN. Le revêtement des NFSi avec du CrN peut offrir des avantages, tels que la capacité faradique et la bonne conductivité électrique du composite de CrN et de NFSi. En outre, la capacité de double couche des NFSi avec une grande surface spécifique peut être ajoutée à celle du CrN.

Le quatrième chapitre se concentre sur le développement des électrodes composites de nanomur de carbone (NMC) décorées par des couches de CrN. Nous décrirons les avantages d'utilisation d'un template avec une grande surface spécifique sur les performances électrochimiques des électrodes composites. La grande surface spécifique de NMC et leur bonne conductivité électrique permettent d'améliorer non seulement la capacité surfacique des électrodes à base de CrN mais également leur durée de vie. Par la

suite, nous décrirons la fabrication d'un micro-dispositif avec une configuration empilé a base des électrodes CNW-CrN avec une excellente stabilité électrochimique aprés 30000 cycles.

Enfin, la conclusion résume les résultats obtenus au cours de cette thèse ainsi que les perspectives envisagées.

Mots clé : micro-supercondensateurs, silicium, capacité de stockage, nanomur de carbone, nanofils de silicium, PVD, incidence oblique.

ملخص

الهدف من هذه الأطروحة هو تطوير مكثفات عالية القدرة تتكون اساسا من رقائق السيليكون ونتريد الكروم حيث يمكن تحسين أداء هذه المكثفات عن طريق زيادة مساحة السطح / المسامية من أجل ضمان وصول أفضل للشحنات الكهربائية نحو المادة الفعالة لتخزين الشحنات الكهربائية داخل الأقطاب.

تم تخصيص الجزء الأول من الفصل الأول كمقدمة لأحدث التقنيات المتعلقة بالمكثفات العالية القدرة بالإضافة إلى أنظمة تخزين الطاقة المختلفة والأنواع ومجالات الاستعمال المختلفة للمكثفات عالية القدرة وآليات تخزينها. في الجزء الثاني، نصف تركيبة المكثفة المواد الاساسية المكونة للأقطاب الكهربائية ومختلف المحاليل الكهربائية المستخدمة.

يتعلق الفصل الثاني بتصنيع أقطاب كهربائية بطبقة رقيقة من نتريد الكروم باستخدام تقنية ثنائية القطب بزاوية متغيرة. حيث يسمح استخدام هذه التقنية الجديدة بالتحكم في شكل سطح الأقطاب الكهربائية والتي تؤثر بشكل مباشر على سعة تخزينها صغير. الاداء الجيد للأقطاب سمح لنا بعد ذلك بتصنيع جهاز دقيق يعتمد على نتريد الكروم مع أداء كهرو-كيميائي جيد.

الفصل الثالث مخصص لتطوير أقطاب كهربائية مركبة من أسلاك سيليكون نانومتريه مصنوعة باستعمال تقنية سائل/صلب ومغطاة بطبقة رقيقة من نتريد الكروم. استعمال نتريد الكروم كغطاء لأسلاك السيليكون يمنح الكثير من المزايا، مثل تعزيز سعة تخزين الطاقة وضمان توصيل الكهربائي عالي الجودة.
علاوة على ذلك، يمكن إضافة ميزة سعة الطبقة المزدوجة لأسلاك السيليكون ومساحة السطح الكبيرة إلى تلك الموجودة في نتريد الكروم.

يركز الفصل الرابع على تطوير أقطاب كهربائية مركبة من جدران الكربون نانومتريه مغطاة بطبقة رقيقة من نتريد الكروم. سنقدم خلال هذا المحور فوائد استخدام قطب كهربائي بمساحة كبيرة على أداء المكثفة المركبة حيث تسمح مساحة السطح الكبيرة لجدار الكربون النانومتري والتوصيل الكهربائي الجيد بتحسين ليس فقط السعة المساحية للأقطاب الكهربائية القائمة على نتريد الكروم ولكن أيضًا دورة حياتها.
بعد ذلك، سنصف كيفية تصنيع جهاز دقيق بتكوين ملتف من أقطاب الكربون النانو مترية ونتريد الكروم مع اداء كهروكيمياوي قوي وثابت على مدى ثلاثين ألف دورة.

أخيرًا، تلخص الخاتمة النتائج التي تم الحصول عليها خلال هذه الأطروحة بالإضافة إلى الآفاق المتوقعة.

الكلمات المفتاحية: المكثفات العالية القدرة، سعة التخزين، جدران الكربون النانومترية، أسلاك السيليكون النانومترية، الزاوية المتغيرة.

Acknowledgment

This thesis work has been prepared in Centre de Recherche en Technologie des Semiconducteurs pour Energétique -*CRTSE*- Algiers and Institut d'Electronique et de Microelectronique et de Nanotechnologie -*IEMN*- Lille through a collaboration between the University of Sétif -1- and the University of Lille.

I would like to express my deepest appreciation to my supervisor Dr.*Ammar Mosbah* for his guidance and modesty.

I would like to express my appreciation to Dr. *Toufik Hadjersi and* Dr. *Rabah Boukherroub* their help over the course of my Ph.D.

A very special thanks to the Examiners for agreeing to judge my thesis work.

My deepest appreciation for my uncle professor *Maamache Mustapha* for kind advice and great support and guidance. I am very grateful for his help and modesty.

I would like to also thank *Campus France* for funding and supporting this research work.

The best for last,

Thank God for the beautiful flower *Guerra Djouri Safaa* born on January 2, 2020.

A very special thank you to my wife *Imene* and my mother *Soraya* for their help and support.

Thank my father *Achour*, my brother *Houssem*.

Finally,

Condolence to my mother *Djabou Zoulikha* and my little flower *Guerra Assil Zahraa* Deceased during my last internship in Lille, 2019.

Lists of Figures

Lists of Figures

Lists of Figures

Lists of Tables

Table of Contents

Introduction

With the rapid increase demand in energy for electronic devices and the development of new hybrid electric vehicles, major research was carried out for the development of new stable and high power energy storage devices. Among these devices, rechargeable lithium (Li) batteries are considered as promising devices due to their high energy density. However, the moderate cycle of life and the lower power density of lithium batteries cannot provide a complete solution for energy storage systems. Besides, they are not suitable for industrial and military applications which required more energy resources with high energy and power density. In this context, the development of new storage systems, in particular supercapacitors (SCs), have attracted considerable attention due to their high power density, fast charge-discharge ability, long cycle life and environment-friendly merit compared to Li-ion batteries. SCs are widely employed in various systems, including hybrid electric vehicles, memory back-up and renewable energy devices. According to the known charge storage mechanism, supercapacitors can be classified into two categories: electrochemical double-layer capacitors (EDLCs) and pseudo-capacitors. The charge could be stored by EDLCs using charge accumulation of ions and electrons on the surface of the electrode without redox reactions. The pseudo-capacitors, however, rely on the fast and reversible faradaic reactions of pseudo-capacitive materials. Therefore, they are particularly suitable for applications that required power peaks in a short period.

The objective of this thesis work

With the continuous miniaturization of electronic devices (tablets, smartphones, etc...), the development of miniature power sources remains a great challenge. Micro-supercapacitors (*μSC*) meet these micro-electronics requirements in terms of power and long cycle life. However, the miniaturization of SC devices still a big challenge as the majority of electrode materials are not compatible with the micro-fabrication processes of power systems. That led to the research question: is it possible to develop a new high-performance *μSC*?

This thesis work is aimed at the development of high-performance on-chip μSC based on chromium nitride (CrN) active material that allows their integration into microelectronic devices. The major objectives of this thesis are as follows:

- To elaborate electrodes using low-cost active materials deposited on a silicon substrate.
- To evaluate the electrochemical performance of the as prepared-electrodes.
- To study the effects of the morphology and surface area on the electrochemical performance of electrodes.
- To fabricate on-chip micro-supercapacitors.
- To study the electrochemical performance of the fabricated devices.

This research work was funded by the Algerian-French cooperation program PHC Tassili.

Chapter 1. Literature Review

I. Introduction

Electrochemical capacitors (ECs), also called supercapacitors, have attracted considerable attention due to their high power density, fast charge-discharge ability, long cycle life and environment-friendly merit compared to Li-ion batteries [1-4]. Super-capacitors are widely employed in various systems, including hybrid electric vehicles, memory back-up and renewable energy devices [5, 6]. They have become an attractive power solution and may challenge batteries in the future as a general solution for power storage in many applications.

2. Historical background

The first capacitor, called the Leyden jar, which was invented by **Pieter van Musschenbroek** in 1746 at the University of Leyden in Holland. It was a glass jar wrapped inside and outside by a thin metal foil. The outer foil was connected to the ground, while a lead from inner foil was brought out through a plug at the mouth of the jar and connected to a source of electricity such as an electrostatic generator.

In 1879, the physicist Hermann Von Helmholtz proposed the first double-layer model which explains the principle of energy storage in the electrochemical double layer formed at the electrode/electrolyte interface. Energy is stored by distributing ions at the interface of each electrode, under the influence of electric potential.

The first patent was filed in 1957 by the American group GENERAL ELECTRIC [7] for a supercapacitor composed of aqueous electrolytes based on sulfuric acid and electrode made of porous carbon material. In 1969, a second patent from the American company SOHIO Corporation describes a new high-voltage device with an organic electrolyte. However, the first supercapacitor was commercialized in 1971 by the Japanese company NEC (NEC-TOKIN). Matsushita Electric Industrial Company, also, developed the "Gold Capacitor" series dedicated to memory backup in 1978.

Recently, supercapacitors are fabricated by many companies around the world (**Table 1)**. They are commercialized by several companies like Matsushita (Panasonic-AL135-137), Asahi Glass (AL130), NEC (AL138), Polystor, Econd, ESMA, ELIT, CAP-XX, SuperFard, EPCOS (Matsushita and Siemens), SAFT (AL 141, 142) and the world leaders in power supercapacitors are Maxwell and Batscap **[8].**

Table 1: Characteristics of various supercapacitors currently commercialized. [8]

Companies	**Voltage V**	**Capacity F**	**Specific Energy Wh.kg^{-1}**	**Maximum Power kW.kg^{-1}**	**Masse kg**
Batscap-France	2.7	2600	5.3	20	0.5
Maxwell-USA	2.7	3000	5.2	11.4	0.55
EPCOS Japon/ Germany	2.7	3400	4.3	6.7	0.6
NessCap-South Korea	2.7	5000	5.44	5.2	0.93
NipponChemi-Con-Japon	2.5	2400	4	3.8	0.52
LS-Cable South Korea	2.8	3000	5.2	10.4	0.63

1. Interest of supercapacitors

1.1. Different energy storage systems

Nowadays, energy storage systems can be classified into three categories: conventional capacitors, supercapacitors (SC) and batteries. They are characterized by the energy density corresponding to the number of charges stored per unit of surface or mass and the power density corresponding to the energy supplied per unit of time and per unit of surface or mass.

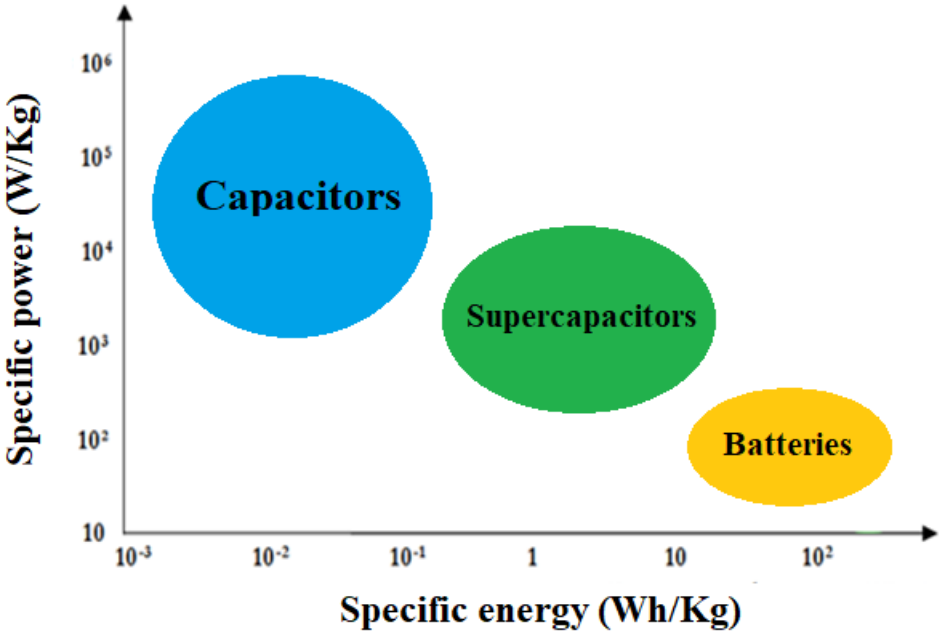

Figure 1: Ragone plot.

Figure 1 shows the Ragone plot (E vs P) of typical energy storage devices, it is clear that the batteries exhibit a high energy density (10-250 $Wh.kg^{-1}$) but a low power density (≤ 20 $W.kg^{-1}$), whereas conventional capacitors have a high power density (>> 50 $kW.kg^{-1}$) with low energy density (<0.1 $Wh.kg^{-1}$). SCs have high energy (1-10 $Wh.kg^{-1}$) than conventional capacitors. When compared to batteries, SCs have a longer cycle life (1,000,000 cycles) and can deliver much higher power (1-20 $kW.kg^{-1}$). They also show a lower series resistance with an energy efficiency of about 95% (less than 80% for batteries) (**Table 2**).

In a word, supercapacitors display a higher energy density than conventional capacitors and a higher power density than batteries and can fill the gap between batteries and conventional capacitors. Therefore, supercapacitors offer a promising approach to meet the power demands for applications that require a high energy density and a long cycle life.

Table 2: Comparison of characteristics of different energy storage systems [9, 10].

	Capacitors	Supercapacitors	Batteries
Charge time	10^{-6} – 10^{-3} s	1 – 30 s	1 – 5 h
Discharge time	10^{-6} – 10^{-3} s	1 – 30 s	0.3 – 3 h
Number of cycles	10^{10}	10^{6}	10^{3}
Specific Energy Wh.kg^{-1}	0,01 – 0,1	1 – 10	10 – 100
Specific Power W.kg^{-1}	$>10^{6}$	10^{4}	$<10^{3}$
Efficiency	≈ 100%	> 95%	70 – 85%

1.2. Recent applications of supercapacitors

Supercapacitor devices exhibit a high energy and power densities with excellent electrochemical stability. They can be used for various applications that require high powers. Their lifetime and almost low maintenance cost allow their integration in multiple areas such as energy recovery and storage. The main application of supercapacitors are shown in this section

- **Military**

Supercapacitors are used in radio transmitters, pulsed lasers, radar orientation systems for tracking ballistic missiles and satellites. They are tested on the ECCE bench (Essais des Composants de Chaine Electrique) [11]. The test bench is a hybrid electric vehicle series with 4 independent wheels with a main thermal engine (diesel in this case). The four electrical sources of ECCE are accumulators, an alternator, a supercapacitor and a fuel cell. The braking energy is recovered in a combination of accumulators with two supercapacitor modules [12].

- **Transport**

Currently, SCs are used in heavy hybrid vehicles. They are well suitable for public transport buses which can undergo several start/stop cycles; the energy recovered during the stop allows the vehicle to go to the next station. In the field of public transport, the French company PVI (Power Vehicle Innovation) developed the Watt system electric bus [13] (**Figure 2a**).

The integration of SC allows to producing an electric bus with the fastest recharge time in the world by the Chinese company Ningbo CSR New Energy Technology [14], Bluetram of the Bolloré Group [15], the Seoul Metro [16] and the Tramway with braking energy recovery from the TPG Group (Transports Publics Genevois) [17]. The use of SCs reduces significantly the energy consumption and pollution. Furthermore, several car companies integrate SC in their vehicles: BMW [18] (**Figure 2b**), Toyota [19], Volvo and Tesla [20].

Recently, a stationary system based on *SITRAS SES* SC was developed by Siemens and used to recover the braking energy of the tramway. The system now equips the metro systems of Madrid, Cologne and Dresden and saving up to 30% of energy and reducing the maximum power required by the network by 50% [21].

Supercapacitors can also be used in garbage trucks and delivery trucks, which can endure a thousand start/stop cycles per day.

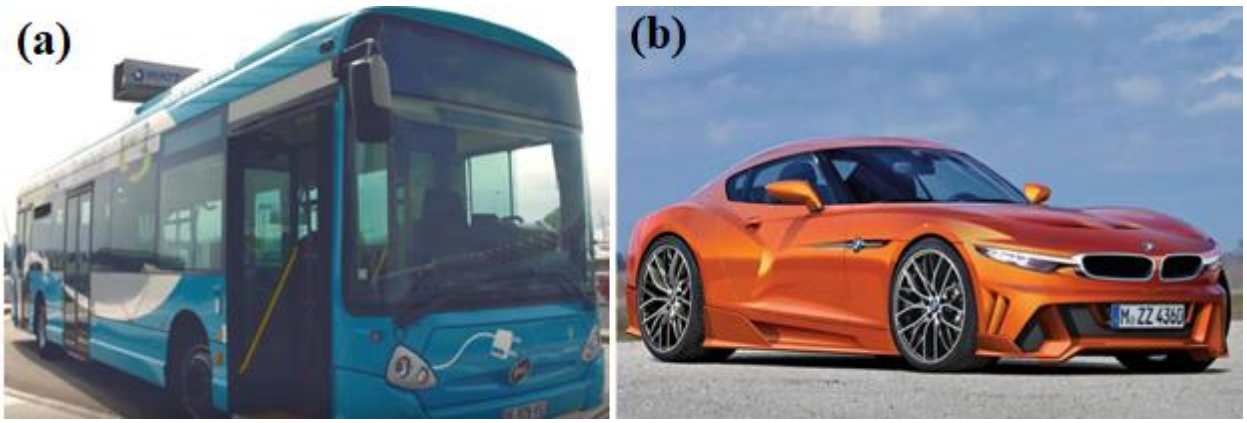

Figure 2: Application of supercapacitors in the transport sector. (a) Watt System supercapacitor bus from PVI [13]. (b) BMW hybrid sports car based on a supercapacitor developed by Toyota [18].

- **Industrial logistics area**

Supercapacitors are used in a wide range of commercial and industrial equipment. For example: in Japan, an airport crane with a supercapacitor system can recover kinetic energy when the carrier plate is lowered and to restore it during lifting. The use of supercapacitors has reduced its energy consumption by 40% (**Figure 3**).

Figure 3: Airport crane in Japan combining a diesel engine and supercapacitor modules. [22]

- **Public applications area**

Supercapacitors have been used as a power source for modern electronic equipment such as elevators [23], wind turbine blade orientation systems [24] and products powered by photovoltaic cells [25]. They are also used as an energy source for powering portable devices such as mobile phones [26-27], tools, toys, memory storage, etc… (**Figure 4**).

Figure 4: Common applications of supercapacitors: (a) Photovoltaic lamp [25]. (b) Wireless mouse with Genius DX-Eco supercapacitor [28].

2. Principle of supercapacitors

Conventional capacitors composed of two metal electrodes separated by an insulating dielectric material. When a voltage is applied between the two electrodes, opposite charges are accumulated on the surface of electrodes.

However, the charge is stored by redox reactions in batteries, which limits their cycle life due to the rapid degradation and modification of the chemical composition of the active materials during cycling.

Next to batteries, the charge storage mechanism of supercapacitors relies on the charge accumulation of ions and electrons on the surface of the electrode without redox reactions (**Figure 5**). In the discharged state, spontaneous charge accumulation occurs at the electrolyte-electrode interface (**Figure 5a**). When a potential difference is applied, charge separation takes place and the ionic species move towards the oppositely charged electrodes (**Figure 5b**).

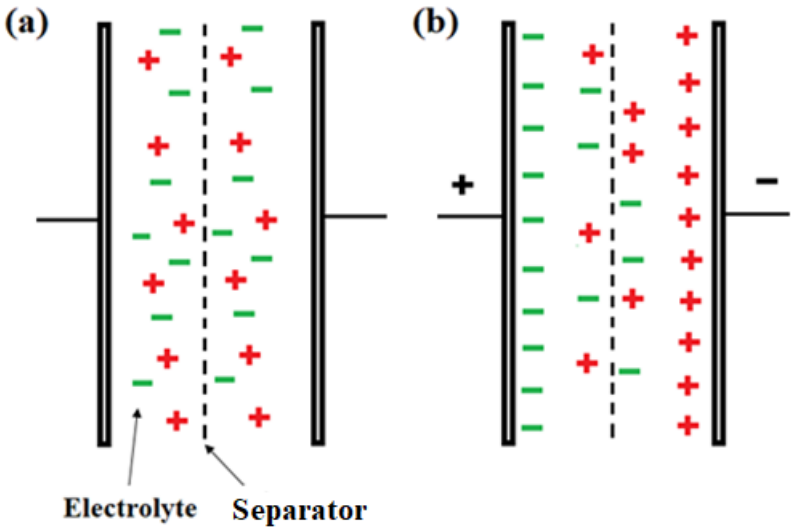

Figure 5: Schematic of a supercapacitor. (a) At the discharged state. (b) At the charged state.

In the case of conventional capacitors, the electrodes have a flat surface, whereas SCs have a much higher surface area. Thus, the capacitance calculated from equation (I-1) increases significantly over that of the conventional capacitors. The double-layer capacitance of supercapacitors can be calculated by [29]:

$$C = \frac{\varepsilon_r \varepsilon_0 A}{d}$$ **Equation I-1**

C : The specific capacitance

ε_0 : The vacuum permittivity

ε_r : The relative permittivity of the dielectric

A : The specific surface area of the electrode

d : The double-layer thickness

3. Types of supercapacitors

According to the storage mechanisms, supercapacitors can be classified into three main classes: electrochemical double-layer capacitors, pseudo-capacitors and hybrid supercapacitors [30-31] characterized by the pure electrostatic charge accumulation, the reversible faradaic redox process and a combination of the two, respectively (**Figure 6**).

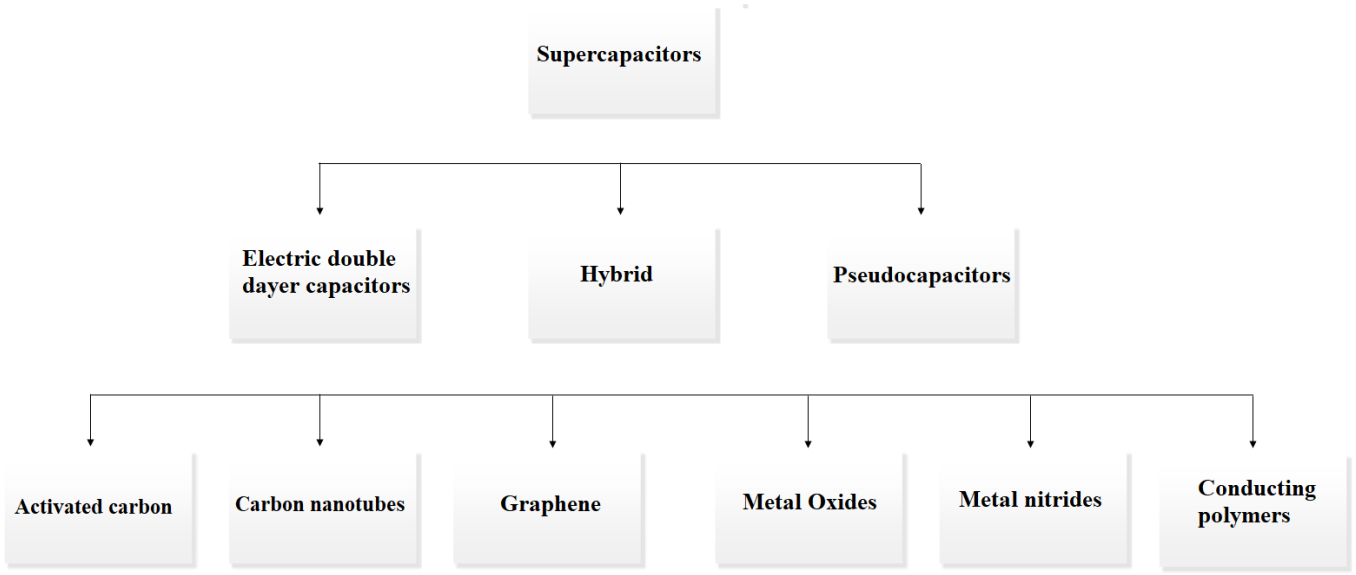

Figure 6: Classification of different supercapacitors.

3.1. Electrochemical double-layer capacitors EDLC

The charge can be stored by EDLCs (mainly restricted to carbon-based materials) using the charge accumulation of ions and electrons at the electrode/electrolyte interface without redox reactions. Opposite charges accumulate at the interface because of the applied potential.

Recently, different kinds of carbon-based materials such as activated carbons (ACs), carbon nanotubes and graphene are widely used as EDLC electrodes because of their higher surface area, low cost and high conductivity. Besides, the control of the specific surface area and the pore size adapted to the electrolyte is crucial to ensure a good electrochemical performances of the supercapacitors.

3.2. Pseudo-capacitors

The pseudo-capacitors, however, rely on faster and reversible faradaic reactions of pseudo-capacitive materials [30], which are mainly transition metal oxides such as VO_2 [32, 33], RuO_2 [34], MnO_2 [35-40], or conductive polymers [41-45]. Pseudo-capacitors exhibit a much higher specific capacity than EDLCs [46-47]. However, they suffer from moderate cyclic stability compared to carbon-based materials, because of the redox reactions between the electrolyte and electro active species occur on the surface of the electrodes. Their specific capacitance depends on the amount of charge transferred to the active material and the applied voltage.

$$C = \frac{dQ}{dU}$$ **Equation I-2**

C : Specific capacitance (F)

Q : Electrical charge (C)

U : Voltage (V)

3.3. Hybrid supercapacitors

Hybrid supercapacitors are classified into two main categories: asymmetric hybrids SC and composite hybrids SC. Asymmetric hybrids consist of an EDLC electrode and a pseudo capacitor electrode. They have better cycling stability than pseudo capacitors and can achieve higher energy and power densities than EDLCs.

The energy process of composite hybrid SCs is a combination of EDLC and the pseudo-capacitance with several combinations such as carbon and metal oxides [48-51] or conductive polymers [52-53] or Lithium [54] with improved electrochemical performances than those of symmetrical supercapacitors [48]. Nevertheless, their stability is limited compared to EDLCs.

4. Electrochemical double layer

The concept of the electrochemical double layer was developed in the 20th century based on the fundamental work of Helmholtz (1879) [55]. Helmholtz has discovered the phenomenon and describe it by a model assimilated to a planar capacitor where all the charges are adsorbed on the surface of the electrode. Gouy (1910) [56] and Chapman (1913) [57] modified the Helmholtz model by taking into

account the mobility of ions in the electrolyte solutions. Next, Stern (1924) [58] combined the Helmholtz and the Gouy-Chapman models. Their models are explained below.

4.1. Helmholtz double layer

The first model created by Helmholtz in 1879 [55] considered the concept of charge separation at the interface between a solid electronic conductor and a liquid ionic conductor. The thickness of the double layer (d) corresponds to the distance between the axis of the plane and the active material (**Figure 7**). The model is similair to that of two conventional capacitors. Nevertheless, the Helmholtz double-layer does not explain all the features, since it hypothesizes rigid layers of opposite charges.

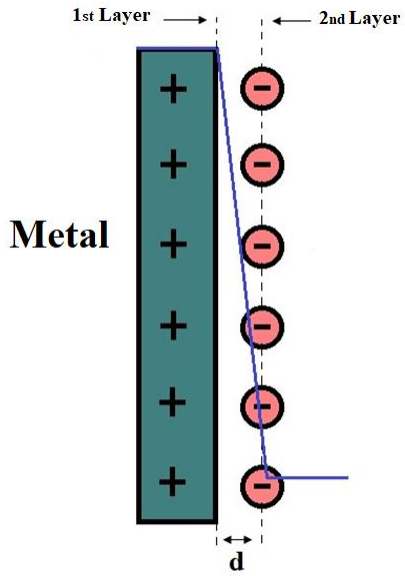

Figure 7: Helmholtz electrochemical double layer.

4.2. Gouy-Chapman double layer

Gouy (1910) [56] and Chapman (1913) [57] have proposed a model taking into account the mobility of ions in electrolytic solutions. The second layer is replaced by a diffused layer i.e. counter ions are not rigidly held but tend to diffuse into the liquid phase. The ions are also considered as point charges distributed near the surface of the electrode according to a statistical Boltzmann distribution (**Figure 8**).

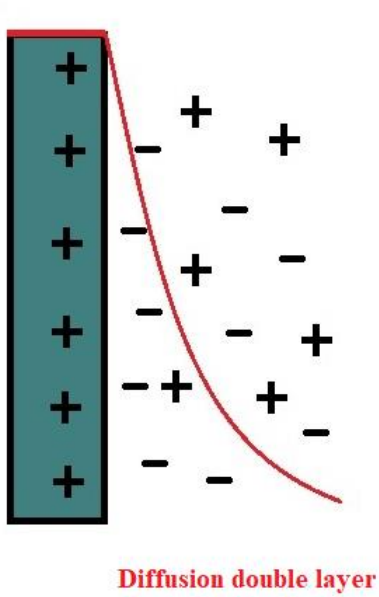

Figure 8: Gouy-Chapman double layer.

4.3. Stern double layer

In 1924, Stern [58] combined the two previous theories and divide the double electrochemical layer into two distinct layers, a compact layer called the Helmholtz layer with ions adsorbed at some distance (**d**) away from the surface of the electrode and a diffuse layer such as defined by Gouy and Chapman theory (**figure 9**).

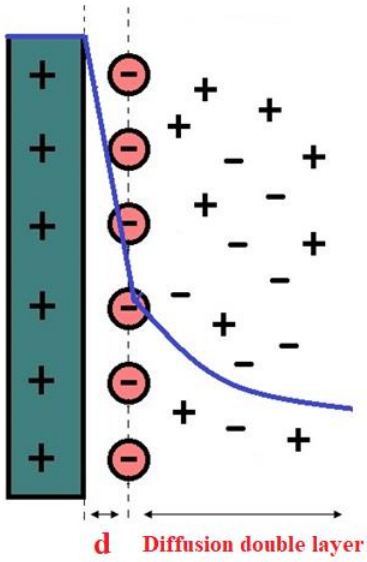

Figure 9: Stern double layer.

The total capacitance C_d of the electrochemical double layer can be computed as a Helmholtz layer capacitance C_H and a diffuse layer capacitance C_{diff} connected in series (**Equation I-3**). It also depends on the ionic concentration of the solution and the potential of the electrode. In the case of concentered

electrolytes (> 1 M), the Gouy-Chapman diffuse layer is compressed and the double-layer capacitance will be assimilated as Helmholtz capacitance.

$$\frac{1}{C_{dl}} = \frac{1}{C_H} + \frac{1}{C_{diff}}$$ **Equation I-3**

C_{dl} : Double layer capacitance

C_H : Helmholtz capacitance

C_{diff} : Gouy-Chapman capacitance

5. The characteristic parameters of supercapacitors

In general, the electrochemical performance of SCs can be evaluated by certain essential parameters. Capacitance (C), voltage (Um), energy density (Em) and power density (Pm) are used to evaluate the electrochemical performance of supercapacitors. Also, SCs can be assessed by their cycling stability.

5.1. Capacitance (C)

SCs can be considered as two capacitors connected in series. If the capacitance of the two electrodes is expressed as C_1 and C_2, the total capacitance is described according to the equation (**Equation I-4**):

$$\frac{1}{C_T} = \frac{1}{C_1} + \frac{1}{C_2}$$ **Equation I-4**

C_T **:** The total capacitance (F)

$C_1 C_2$: Capacitance of each electrode.

In the case of symmetric supercapacitor $C_1 = C_2$, the total capacitance (C_T) is half the capacitance of the electrodes. Besides, for an asymmetric supercapacitor, C_T is mainly dominated by the electrode with lower capacitance [30].

To further evaluate the performances of the electrode, specific capacitance is often used. It can be expressed in specific mass capacitance (C_S) or volume capacitance (C_V). Generally, Cs is normalized by mass loading ($F.g^{-1}$) according to the equation:

$$C_S = \frac{C}{m}$$ **Equation I-5**

C_S **:** Specific capacitance ($F.g^{-1}$)

C : Electrode capacitance (F)

m : The mass loading of active material (g)

If C_S is calculated for a device (a two-electrode system), the mass loading (**m** must be normalized by the total mass of the device, including the electrodes, the electrolyte and the separator. [59-60].

5.2. Power density

Power density (Pm) is an important parameter widely used to calculate the amount of energy supplied per unit of mass. It can be calculated using the equation:

$$P_m = \frac{U^2}{4 \times ESR \times m}$$ **Equation I-6**

U : The voltage of the device (V)

ESR : The equivalent series resistance (Ω)

m : The total mass of the device (kg)

To have a good power density (P_{max}), a supercapacitor should have a large maximum operating voltage and a lower ESR.

ESR is a key factor for determining the power density. It corresponds to the total of several contributions [59-60]: the internal resistance of the electrodes which results from the conductivity of the active material; the contact resistance between the active material and the current collector; the ionic resistance of the electrolyte due to the transport of ions to the pores and the resistance of ions transport through the separator.

5.3. Energy density

The energy density (Em) is an important parameter used to calculate stored charge per unit of mass. It can be calculated according to the equation:

$$E_m = \frac{C \times U^2}{2 \times m \times 3600}$$ **Equation I-7**

U : The voltage of the device (V)

C : Specific capacitance (F)

m : The mass loading of active material (g)

To have good energy density (Emax), it is necessary to have a large maximum operating voltage and a high capacitance value.

5.4. Cycling stability

The cycling stability is an important parameter that depends on many factors such as the active material, the electrolyte and the operating voltage. For example, electrochemical double-layer supercapacitors based on carbon electrodes generally exhibit high cycling stability [61]. When faradaic reactions are introduced, cycling stability is generally reduced due to the reversibility of interactions between ions and electrode materials [62].

6. Improvement and development of supercapacitors

Over the years, the development of high-performance and low cost supercapacitors devices have attracted considerable attention, so optimizing their performance allows improving their electrochemical performances. The basic principles to obtain a competitive supercapacitors are: high ionic conductivity of electrolyte and high conductivity of electrode materials associated with large surface area.

6.1. Electrode materials

Including current collectors and active material. Electrodes should be stable in the electrolyte and have a low internal resistance. Since the capacitance is proportional to the surface area, electrode materials with the highest specific surface area are used to ensure a good electrochemical performances of the supercapacitors.

6.2. Electrolytes

The choice of electrolytes is very important, they should have good ionic conductivity, low viscosity and a large operating electrochemical window. Therefore, they should provide high conductivity and high

electrochemical stability to ensure that the device can operated at the maximum voltages. Besides, the electrochemical window has a major influence on the power and energy densities (proportional to its square **Equation I-6, I-7**). Thus, using electrolyte with a large electrochemical stability window allows increasing the energy and power densities.

6.3. Resistance

Corresponding to the resistance of active material; the contact resistance between active material/collector, the resistance of the electrolyte and the resistance ions transport through the separator. The use of electrolyte with high conductivity as well as highly conductive active materials can significantly decrease the resistance cell and therefore increasing its power density.

6.4. Capacitance

Proportional to the specific surface area (**Equation I-1**). The use of electrodes with large specific surface area allows enhancing their specific capacitance and therefore increasing their energy density (**Equation I-7**).

7. Supercapacitors compositions

7.1. Electrodes

As mentioned above, a supercapacitor consists of two electrodes impregnated with electrolyte and separated by a porous membrane (**Figure 5**). The electrodes consist of active material deposited on the current collector. The electrodes are considered as the key factor which defines the storage mechanism of the based device. It should have a large specific surface area, good contact between active material/current collector and good electrical conductivity.

7.2. Active materials

In this part, we will present the different active materials (carbon, transition metal oxides and nitrides etc…) mainly used for the design of supercapacitors.

Carbonaceous materials

Carbon-based materials are widely used in electrochemical double-layer capacitors due to their low costs, large specific surface area and electrochemical/thermal stability. Also, activated carbon (AC) is the most

widely used electrode material for supercapacitors due to its large specific surface area (1000-2500 $m^2.g^{-1}$) [63], good conductivity and its relatively low cost [64]. In addition, different kinds of carbon materials with a large specific surface are widely used for supercapacitors application such as: carbon nano-onions (Carbon onions) [65-68], graphene [69-72], carbon walls (Carbon Nanowall, CNW) [34] [73, 74], Activated Carbon (AC) [75-78], carbon nanotube (Carbon NanoTube, CNT) [79-81]. The structure of these types of carbon is illustrated in **Figure 10**.

- *Carbon nanowalls*

Also named vertically oriented graphene sheets (**Figure 10a**) produced by expanding the radio frequency (RF) plasma beam [34]. The large specific surface area of (100-1500 $m^2.g^{-1}$) associated with excellent electrical conductivity makes carbon nanowall attractive for electrochemical energy storage applications [34].

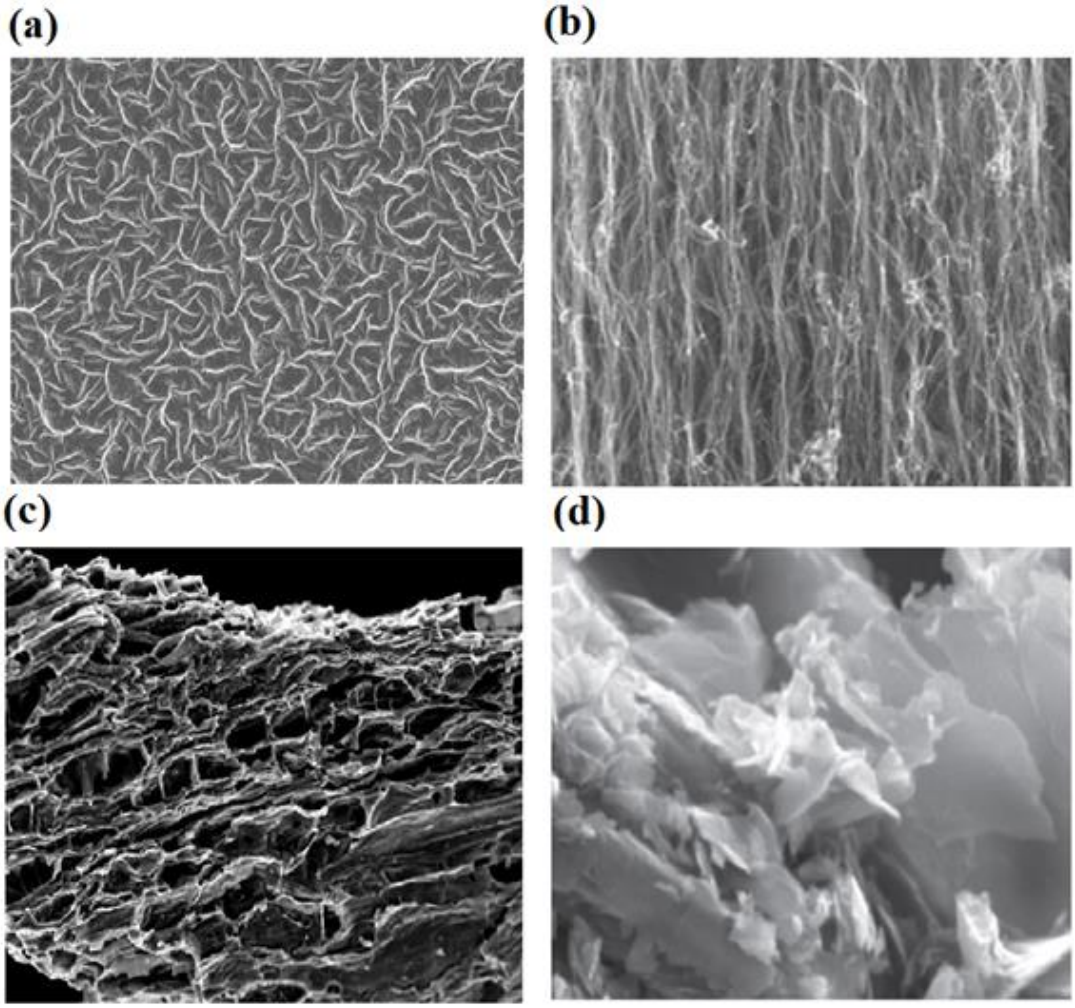

Figure 10: SEM images of (a) Carbon walls (CNW). (b) Carbon nanotube (CNT) [83]. (c) Activated carbon (AC) [82] and (d) Graphene [86].

- *Graphene*

As a new class of two-dimensional carbon nanostructure, graphene has attracted major interest in recent years because of its large specific surface (630 $m^2.g^{-1}$) [85], excellent electrical conductivity and chemical stability. Graphene sheets could be synthesized by mechanical cleavage of graphite and chemical exfoliation of graphite [85]. The high specific capacitance of 349 $F.g^{-1}$ was obtained for graphene electrodes in an aqueous electrolyte (**Figure 10d**) [87].

- *Activated carbon (AC)*

Activated carbon is the most widely used material for commercial supercapacitors because of its high surface area (3000 $m^2.g^{-1}$), good electrical properties and low cost. AC is derived from various carbon-rich precursors such as (charcoal, coconut, etc…) by physical or chemical activation in an inert atmosphere. The physical activation process requires high-temperature thermal treatment (700 - 1200 ° C) in the presence of an oxidizing gas (CO_2, air), whereas, the chemical activation is carried out at lower temperatures (400 - 700 ° C) with an activating agent such as (KOH, NaOH ...). Depending on the activation method, AC can reach a high specific capacitance of 100 - 300 $F.g^{-1}$ in an aqueous electrolyte [85] [88].

- *Carbon nanotubes*

The most promising materials used for electrochemical double-layer capacitors due to their excellent chemical stability, low resistivity (lower than that of activated carbon) and large specific surface area. There are two main types of carbon nanotubes: single-walled carbon nanotubes (SWCNT) consist of a single graphite sheet wrapped into a cylindrical tube and multi-walled carbon nanotubes (MWCNT) **Figure 11**). CNT is produced by laser ablation of carbon or chemical vapor deposition [84].

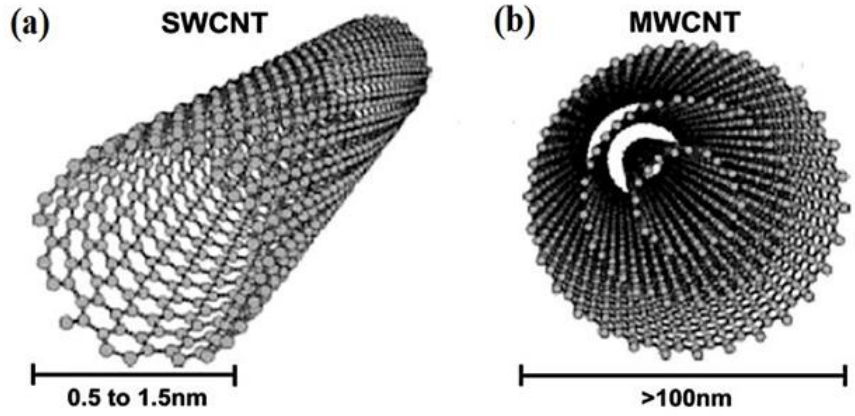

Figure 11: Schematic of carbon nanotubes. (a) Single-walled carbon nanotube (SWCNT). (b) Multi-walled carbon nanotube (MWCNT). [84]

a) Transition metal oxides

Transition metal oxides such as nickel oxide (NiO) [97], ruthenium dioxide (RuO_2) [34], vanadium oxide (VO_2) [32, 33], manganese oxide (MnO_2) [35-40] and iridium oxide (IrO_2) are considered as promising materials for supercapacitors because of their high conductivity and their higher specific capacitance than that of EDLCs. They can be produced by different methods such as electro-deposition [89-91], sol-gel [92] and chemical process [93]. Hydrous ruthenium dioxide ($hRuO_2$) currently show the highest reported specific capacitance [34].

- *Ruthenium oxide (RuO_2)*

RuO_2 has been widely studied as an electrode material because of its large specific surface area and high conductivity. Its energy storage mechanism relies on a pseudo-capacitive process with rapid electron transfer associated with the electro-adsorption of protons on its surface according to equation [8]:

$$RuO_2 + x\ H^+ + x\ e^- \leftrightarrow RuO_2\text{-}x\ (OH)\ x \qquad \text{with} \quad 0 \leq x \leq 2$$

The high specific capacitance of 768 $F.g^{-1}$ has been reported in an acidic aqueous electrolyte [94]. Hydrous ruthenium dioxide ($hRuO_2$) currently shows the highest reported specific capacitance [34]. However, its cost and its toxicity limit its wide commercial application.

- *Manganese oxide*

Less expensive metal oxide such as manganese oxide (MnO_2) has been considered as promising pseudo-capacitive material because of its low cost, abundance and nontoxicity.

The storage mechanism of MnO_2 is relying on the adsorption of cations of the electrolyte C^+ (Li^+, Na^+, K^+) on the electrode surface according to the redox reaction:

$$MnO_2 + C^+ + e^- \leftrightarrow MnOOC$$

Also, MnO_2 exists in a wide range of polymorphs such as α, β, γ, λ, and δ. It is found that specific capacitance measured for the MnO_2 strongly depended on its crystallographic structure with values in descending order: α-MnO_2 > δ-MnO_2 > β-MnO_2 [40].

- *Nickel oxide*

One of the most promising pseudo-capacitive materials; its low cost and high conductivity favor its wide application as electrode material for pseudo-capacitor. NiO can be produced by various methods such as thermal treatment of Ni $(OH)_2$ [95] and sol-gel [96]. Also, a high specific capacitance of 309 $F.g^{-1}$ has been reported in an aqueous electrolyte [97].

- *Binary metal oxides*

Recently, bimetallic oxides such as $NiCo_2O_4$ [98], $NiFe_2O_4$ [99] and $MnFe_2O_4$ [100] have attracted major interest. They offer an electrical conductivity and electrochemical activity higher than single metal oxide. For example, a high specific capacitance of 1450 $F.g^{-1}$ has been reported for $NiCo_2O_4$ electrodes in aqueous electrolytes [98] which is higher than that reported for NiO electrodes [97].

b) Transition metal nitrides

Recently, transition metal nitrides such as vanadium nitride [101,102], chromium nitride [103,104] and ruthenium nitride [105] are considered as potential electrode materials for pseudo-capacitors due to their excellent electrical conductivity, electrochemical stability and low toxicity.

- *Vanadium nitride (VN)*

Vanadium nitride has been identified as one of the most promising transition metal compounds for use in electrochemical capacitors with a specific capacitance as high as 1340 $F.g^{-1}$ [106]. This impressive capacitance was attributed to a combination of both double-layer type capacitance and pseudo-capacitance occurring at this nitride surface. However, VN suffer from poor cycling stability, which hinders its industrial application. In general, this poor cycling life is attributed to the dissolution of vanadium oxide layers which is responsible for the pseudo-capacitive behavior [101, 102, 106].

- *Chromium nitride (CrN)*

Chromium nitride has been developed as an alternative active material for supercapacitors application. Das et al. [107] were the first to study the electrochemical performance of CrN nanoparticles via nitriding of Cr_2O_3 and a high specific capacitance of 75 F.g-1 was obtained. Wei et al. [103] have reported the synthesis of CrN by DC magnetron sputtering with an areal capacitance of 12.8 $mF.cm^{-2}$ in aqueous acid

electrolyte along with excellent cycling stability after 20,000 cycles. The high performance of CrN was attributed to the high conductivity and chemical stability of CrN.

c) Conducting polymers

Other promising pseudo-capacitive materiasl commonly used in supercapacitors because of their high conductivity and low resistance series compared to carbon-based materials. The most commonly studied polymers are poly (pyrrole), poly (aniline) and poly (3-methyl thiophene).

Conducting polymers store charge by a redox reaction given by equations (**I-8**) and (**I-9**):

$$\textbf{Uncharged polymer} + \textbf{ne}^- + \textbf{nC}^+ \leftrightarrow \textbf{polymer n}^-, \textbf{nC}^+ \qquad \textbf{(I-8)}$$

$$\textbf{Uncharged polymer} + \textbf{nA}^- \leftrightarrow \textbf{polymer n}^+, \textbf{nA}^+, \textbf{ne}^- \qquad \textbf{(I-9)}$$

High capacity of 400 $F.g^{-1}$ is reported by Sharma et al. using polypyrrole films as the electrode [109]. Furthermore, Ghennatian et al. have prepared polyaniline nanofibers with a high specific capacity of 480 Fg^{-1} [110]. Besides, Poly (3, 4-ethylene dioxythiophene) synthesized by the electrochemical method shows a specific capacity of 130 Fg^{-1} [111].

d) Transition metal sulfides

In recent years, metal sulfides such as molybdenum disulfides [112], cobalt sulfide [113] and copper sulfide [114] have attracted particular interest in the manufacture of supercapacitors. Their superior physical and chemical properties (excellent electrical conductivity and mechanical and thermal stability) make them potential candidates for energy storage applications.

- *Molybdenum disulfide (MoS_2)*

MoS_2 has several advantages such as the high specific surface area, good electrical conductivity and sheet-like morphology. Various types of MoS_2 nanomaterials have been manufactured, such as MoS_2 nano-spheres [116] and MoS_2 nano-sheets [117] [118]. High specific capacitance of 330 Fg^{-1} has been reported for MoS_2 deposited on a glassy carbon substrate [119].

- *Cobalt sulfide (CoS)*

It has been considered as a potential candidate electrode material due to its high electrochemical activity and low cost. Yang et al. have synthesized hollow hexagonal nanosheets of CoS with good specific capacity of the order of 138 $F.g^{-1}$ [120]. A higher capacity of 475 $F.g^{-1}$ has been reported for CoSx synthesized by chemical precipitation [121].

- *Copper sulfide (CuS)*

Copper sulfide is an advantageous pseudo-capacitive material widely used as a supercapacitor electrode because of its excellent conductivity, low toxicity and abundance in nature. It can be produced using different physical and chemical synthesis methods. High capacities of 470 Fg^{-1} and 761 Fg^{-1} have been reported for Cu_2S films with different morphologies prepared by adsorption and successive ion layer reaction in an aqueous solution (SILAR) [122].

e) Silicon nanostructures

The mostly used micro-supercapacitors reported in the literature are generally based on carbon and metal oxides active materials. However, their integration in micro-electronics remains the main obstacle. On the other hand, silicon-based supercapacitors can be easily integrated since their fabrication technology is compatible with that of microelectronics. Also, silicon is the most widely used material in microelectronics technology due to its abundance on earth, high stability, low cost and toxicity. Thus it represents an attractive material for the fabrication of micro-supercapacitors.

The morphology of the surface of the electrodes has great importance since it determines the number of ions to be adsorbed. The surface of the silicon can be nanostructured in various forms such as porous silicon, silicon nanowires and nano-trees with high surface area allow increasing their specific capacitance.

- *Porous silicon*

Porous silicon (PSi) exhibits a relatively high surface area of about 600 $m^2.cm^{-2}$ [123], thus it represents an attractive material for the fabrication of SCs. It can be produced by chemical or electrochemical etching of p/n crystalline silicon. Electrochemical etching is the most commonly used method due to its reproducibility. The etching solution is a mixture of hydrofluoric acid (HF), ethanol and water. The

properties of porous silicon (porosity, depth and pore shape, etc.) can be controlled by the concentration of the etching solution, the density of the anodizing current and the etching time.

In 1999, Rowlands et al. [123] have reported the development of porous silicon by electrochemical anodization of a p-type crystalline silicon substrate in an etching solution of hydrofluoric acid (15%) for 10 min exhibiting an areal capacity of 130 µF .cm^{-2} in an organic electrolyte (NEt_4BF_4 / PC).

- *Silicon nanowires*

Very recently, silicon nanowires (SiNWs) have been proposed as electrode materials for micro-supercapacitors [124-126], due to their interesting capacitive characteristics where the capacitance of the electrode can be enhanced by increasing the specific surface area. They can be produced using chemical etching of crystalline silicon [127] or by chemical vapor deposition (CVD), in the presence of a gold catalyst [124-126]. Thissandier et al. [124] have reported the development of SiNWs by chemical vapor deposition (CVD). The optimization of the doping levels and their morphology allowed SiNWs to reach a high areal capacitance of 440 µF.cm^{-2} in an organic electrolyte (NEt_4BF_4 / PC). Besides, Berton et al. [126] have reported the use of ionic liquid electrolyte (EMI-TFSI) with a high operating voltage window of 4 V along with good specific power of 472 µW.cm^{-2}.

- *Silicon nanowires coated with active material*

SiNWs suffer from the rapid oxidation of the silicon surface in aqueous electrolytes and dissolution in mild saline solutions. Thus, their electrochemical stability and the capacitive performance of SiNWs can be enhanced by modifying their surfaces with highly conductive active material such as manganese oxide MnO_2 [93], carbon [127] and silicon carbide SiC [129].

Table 3 summarizes the performance of silicon nanowires based electrodes.

Table 3: Electrochemical performance of SiNWs based electrodes.

Electrode materials	Electrolyte	Areal capacitance $mF.cm^{-2}$	Number of cycles	References
MnO_2@SiNWs	$LiClO_4$-PMPyrrBTA	13.38	5000	[93]
SiC@SiNWs	KCl	1.7	1000	[130]
C@SiNWs	Na_2SO_4	25,64	25 000	[127]

f) Nanocomposites

The composite electrodes Fare made of a carbon-based material (graphene, CNTs, CNW ...) coated with highly pseudo-capacitance material of metal oxides or metal nitrides. They exhibit a large specific surface area, which increases the contact surface between the pseudo-capacitive material and the electrolyte. For example, a composite electrode made of MnO_2 / reduced graphene oxide (rGO) can achieve a high specific capacitance of 255 $F.g^{-1}$ [131]. Besides, Dinh et al. have reported the fabrication of composites electrodes based on hydrous ruthenium oxide (hRuO) coated carbon nanowalls (CNW) with an excellent areal capacitance of 1097 $mF.cm^{-2}$ [34]. In addition, Liu et al. have reported the synthesis of the graphene / poly-pyrrole composite exhibiting a high capacity of 420 $F.g^{-1}$ in an acid electrolyte [132]. Qin et al. have reported the electrochemical performance of activated carbon modified with poly-aniline (PANI). The PANI-Carbon composite electrode shows a specific capacity of 587 $F.g^{-1}$ [133]. Zhang et al. have reported the growth of vanadium nitride (VN) on a carbon nanotube fiber (CNT) which gave a very high specific capacity of 715 $mF.cm^{-2}$ [134].

7.3. Electrolytes

Besides electrodes, the electrolytes are the most influential component of the performance of supercapacitors (energy, power, stability…). They can be classified into three categories: aqueous, organic and ionic liquids electrolytes. However, the choice of electrolyte is important, it should be inert, uninflammable, have a large electrochemical window, low viscosity and high ionic conductivity.

According to the equations (**I-5**, **I-6**), the power and energy densities are proportional to the square of the voltage U which is limited by the electrochemical stability window. The larger electrochemical window implies a maximum voltage and therefore a better power and energy densities.

The ionic conductivity of the electrolyte plays an important role, a high ionic conductivity limits the internal resistance of the device and therefore enhances its power densities (the resistance is inversely proportional to the power density **equation I-5**).

The low viscosity allows good diffusion of the ions to the active material and reduces the resistance of the supercapacitors.

In general, there are three types of electrolytes used for supercapacitors: aqueous electrolytes, organic electrolytes and ionic liquids. Aqueous electrolytes have a high ionic conductivity but their electrochemical window is limited. However, organic and ionic liquid electrolytes allow larger potential window but their ionic conductivity remains much lower compared to the aqueous electrolyte. **Table 4** summarizes the characteristic of the various electrolytes.

Table 4: comparison of the properties of aqueous, organic and ionic liquid electrolytes [8].

Electrolytes	Stability window V	Viscosity mPa.s	Ionic conductivity $mS.cm^{-1}$
Aqueous	< 1.2	1	> 400
Organic	2 - 3	0.3 - 2.6	50
Ionic liquid	3 - 6	50 - 400	< 15

7.3.1. Aqueous electrolytes

The aqueous electrolytes contain acid (H_2SO_4, H_3PO_4 etc...), basic (KOH, NaOH etc…) and neutral salt (KCl, Na_2SO_4 etc…). According to **Table 3**, these electrolytes exhibit a high ionic conductivity> 0.4 $S.cm^{-1}$ (up to 0.8 $S.cm^{-1}$ for sulfuric acid at 25 ° C) [30]. Their advantages are low cost and low toxicity. However, the electrochemical window of aqueous electrolytes is impeded by the limited cell voltage (around 1V), which is linked to the decomposition of water at 1.23 V. Besides, the freezing/boiling point of water limits their working temperature.

7.3.2. Organic electrolytes

Organic electrolytes are the mixture of a conductive salt (usually ammonium or phosphonium) dissolved in an organic solvent such as propylene carbonate ($C_4H_6O_3$) or acetonitrile (CH_3CN). Tetraethylammonium tetrafluoroborate (Et_4NBF_4) is the most used salt. Their main advantage is the large electrochemical window (2-3 V) which allows storing a large amount of energy. However, supercapacitors with organic electrolytes generally have a higher cost, low specific capacitance and lower ionic conductivity (0.05 $S.cm^{-1}$) as well as their high flammability and toxicity compared to aqueous electrolytes.

7.3.3. Ionic liquids

Ionic liquids (IL) can offer a great advantage for supercapacitors due to their large windows of electrochemical stability (3-6 V), high thermal and chemical stability. They are composed of ions (anions and cations) with a melting temperature below 100 °C.

Several combinations (anions/cations) are possible to produce ionic liquids. The cations mostly used are: centered at a nitrogen atom (imidazolium, pyrrolidinium and ammonium), on a phosphorus atom (phosphonium) or a sulfur atom (sulfonium). The most used anions are chloride (Cl), bromide (Br), tetrafluoroborate (BF_4), hexafluorophosphate (PF_6) and bis (trifluoromethylsulfonyl) imide [$TFSI^-$].

Their main advantage is the larger electrochemical window (can reach 6V and limited by the instability of the electrolyte, reduction of the cation and the oxidation of the anion). The larger potential window assures a high energy density. However, ionic liquids are more viscous and less ionic conductors than organic or aqueous electrolytes. Their ionic conductivity is less than 0.015 $S.cm^{-1}$. However, the properties

of ionic liquids can be enhanced by dilution of the ionic salts in an organic solvent to combine their properties (electrochemical stability of ionic liquids and low viscosity of the solvent). In this case, the electrochemical window is limited by the solvent used.

7.4. Separator

The separator is a porous membrane placed between the two electrodes of the supercapacitor. It must be electrically insulating to prevent the short-circuiting, highly porous to ensure the ionic conductivity, chemically and electro-chemically stable. The choice of separator depends on the type of electrolyte and electrode used. In the case of organic electrolytes, cellulose and polymer membrane (polyethylene PE, polypropylene PP) are commonly used. Glass fibers can be used in the case of aqueous electrolytes [30].

I. Micro-supercapacitors

The rapid development of microelectronic devices has spurred research on new energy storage micro-devices. Generally, micro-batteries are widely used to ensure sufficient energy density. However, their short cycle life and low power density limit their wide application in microelectronics where high power densities are required. Thanks to their long cycle life (> 100,000 cycles) and their higher power density, micro-supercapacitors with two configurations commonly used to integrate a micro-device: the stacked configuration and the inter-digital configuration (Figure 10) [135] should overcome these limitations.

1. The stacked configuration

The stacked configuration consists of two films of electrodes (active material deposited on a current collector) stacked and separated by a solid electrolyte, the solid electrolyte also plays the role of separator (**Figure 12a**). The maximum voltage of the device is identical to that of the single electrode. It is also possible to design an asymmetric devices with supercapacitors electrode and battery electrode. The main advantages of the stacked configuration are: reliable process, high productivity and low costs.

2. The inter-digital configuration

The inter-digital configuration consists of the integration of the two electrodes on a planar surface (generally a silicon substrate) in the form of inter-digital combs (**Figure 12b**). The two inter-digited electrodes are isolated by physical separation to prevent any contact which would cause short circuits. This configuration, therefore, does not require a separator. Their performance depends on the materials used (active material, electrolyte, etc.) and the geometry of the micro-device. The electrodes (of length L)

are separated by an isolated space (of width l). However, a large space between the inter-digital electrodes implies a higher resistance. Consequently, maximizing the ratio (L / l) will reduce significantly the resistance and therefore enhancing the power density [136].

Each configuration has advantages and inconvenients, the stacked configuration often suffers from short circuits and the dislocation of the electrodes. However, inter-digital configuration on a flat substrate can solve these problems [135]. On the other hand, the inter-digital configuration can reduce the energy density due to the thin thickness of the electrodes.

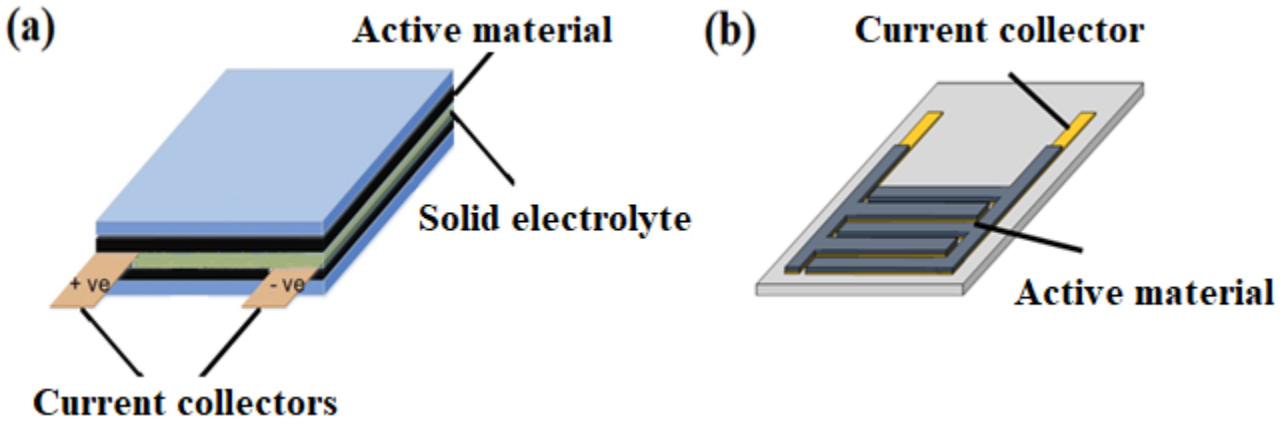

Figure 12: Schematic of micro-supercapacitors configurations. (a) Stacked configuration and (b) inter-digital configuration.

3. Performances of micro-supercapacitors

The performances of supercapacitors are generally reported using gravimetric values. The specific capacitance (Fg^{-1}), the specific power ($W.kg^{-1}$), the specific energy ($Wh.kg^{-1}$) and cycling stability are the main parameters for the evaluation of supercapacitors. In the case of micro-supercapacitors, the material quantity available is very low, and therefore, the mass of the electrode is negligible compared to the total weight of the micro-device. Consequently, capacitance, power and energy densities are expressed per unit of surface area ($F.cm^{-2}$, $W.cm^{-2}$ and $Wh.cm^{-2}$).

The active material of the electrode, the electrolyte and the configuration of the device are the main key factor to improve the electrochemical performance of micro-supercapacitors. Next, the electrolyte is an important factor to determine the maximum voltage window of the micro-device which is limited by the degradation of the electrolyte. Hydrogels (gel of an aqueous ionic solution) and ionogels (gel containing an ionic liquid) are the most used electrolytes [8].

The configuration of micro-devices, in particular the inter-digital configuration, can also improve their performance. For stacked microdevices, the main parameter is the thickness of the electrode layer: increasing the thickness of the electrode increases the storage capacity. For the inter-fingered micro-devices: increasing the number of inter-digital electrodes and reducing the space between them improves their performance.

4. Micro-supercapacitors electrodes materials

4.1. Transition metal nitrides-based micro-supercapacitors

Transition metal nitrides are promising pseudo-capacitive materials with good electrochemical characteristics such as a high specific capacity and excellent electrical conductivity, which makes them potential candidates as micro-supercapacitors (*µSC*) electrodes.

Robert et al. [137] have reported the fabrication of an inter-digital *µSC* based on vanadium nitride (VN) using an ICP (Inductive Coupled Plasma) etching method. The fabricated device shows a good areal capacitance of 40 $mF.cm^{-2}$.

Wei et al. [103] have fabricated *µSC* based on thin layers of chromium nitride (CrN) by DC sputtering. The areal capacitance of the micro-device was as high as 6.5 $mF.cm^{-2}$ at a current density of 1 $mA.cm^{-2}$. Furthermore, thin porous layers of CrN have been synthesized by Wei et al. [138] using chemical etching of CrCuN. Its integration in symmetrical micro-supercapacitors allows obtaining a capacity of 10.9 $mF.cm^{-2}$ for 2 $mA.cm^{-2}$.

Table 5 summarizes the capacity values of metal nitride-based *µSC* reported in the literature.

Table 5: Performance of transition metal nitride-based micro-supercapacitors.

Active material	Electrolyte	Areal capacitance ($mF.cm^{-2}$)	References
VN	KOH	40	[137]
CrN	H_2SO_4	6.5	[103]
Porous CrN	H_2SO_4	10.9	[138]

4.2. Carbon-based micro-supercapacitors

Due to their large specific surface, carbon-based materials are widely used to manufacture of double-layer micro-supercapacitors (*μSC*) (**Table 4**). Pech et al. have reported the manufacture of inter-digital micro-device based on activated carbon in an ethylene glycol solvent and an organic binder of polytetrafluoroethylene (PTFE) [139]. The fabricated device exhibits a large voltage window of 2.5 V and a maximum specific capacity of 2.1 $mF.cm^{-2}$. A micro-device based on carbon nano-onions has been fabricated exhibit a specific capacity of 0.9 $mF.cm^{-2}$ at a high scanning speed of 100 $V.s^{-1}$[140]. Furthermore, inter-digital *μSC* based on carbide-derived carbon films (CDC) has been manufactured by Huang et al. [141]. These micro-devices achieved good electrochemical performance with an areal capacitance of 1.5 $mF.cm^{-2}$. Gao et al. have reported the synthesis of a reduced graphene-based *μSC* exhibits a specific capacitance of 0.51 $mF.cm^{-2}$ [142]. Besides, inter-digital micro- *μSC* based on graphene oxide composite (rGO) and carbon nanotubes (CNT) electrodes have been reported by Beidaghi and Wan et al. [143].

Table 6: Performance of carbon-based micro-supercapacitors.

Active material	Electrolyte	Areal capacitance ($mF.cm^{-2}$)	References
Activated carbon AC	1M Et_4NBF_4/PC	2.1	[139]
Carbon onions	1M Et_4NBF_4/PC	0.9	[140]
carbide-derived carbon	1M Et_4NBF_4/PC	1.5	[141]
Reduced Graphene Oxide	Hydrated GO	0.51	[142]
Reduced Graphene Oxide – Carbon nanotube	3M KCl	6.1	[143]

Summary

This chapter highlights the major interest of supercapacitors (*SC*) and micro-supercapacitors (*μSC*), the theory of double-layer models, the electrode, electrolyte, active materials and recent applications of *SC* in many fields such as logistics, military and microelectronics. The electrodes of *SC* are mainly based on carbon or transition metal-based compounds. However, the main challenge is their integration into microelectronic circuits. Thus, the development of high-performance electrodes based on transition metal nitrides such as chromium nitride (CrN) deposited on silicon current collectors should facilitate their integration into micro-electronics circuits.

The *μSC* based electrodes also should be stable in the electrolyte and have a large developed surface area. Besides, the use of new strategy combining physical vapor deposition (PVD) with glancing angle (GLAD) is envisaged in order to fabricate a porous CrN thin films with high surface area/porosity allows improving its electrochemical storage. Another strategy using a high conductive nanostructures consisting of silicon nanowires (SiNWs) and carbon nanowalls (CNW) with high surface area for the growth of CrN thin film will be investigated.

References

[1] X. Xiao, B. Han, G. Chen, L. Wang, Y. Wang, Preparation and electrochemical performances of carbon sphere@ ZnO core-shell nanocomposites for supercapacitor applications, Scientific Reports, 7 (2017) 40167.

[2] Y. Zhang, H. Li, L. Pan, T. Lu, Z. Sun, Capacitive behavior of graphene–ZnO composite film for supercapacitors. Journal of Electroanalytical Chemistry. 634(1) (2009) 68-71.

[3] L. Fang, B. Zhang, W. Li, J. Zhang, K. Huang, Zhang, Q. Fabrication of highly dispersed ZnO nanoparticles embedded in graphene nanosheets for high performance supercapacitors. Electrochimica Acta, 148 (2014) 164-169.

[4] P. Simon, Y. Gogotsi, Materials for electrochemical capacitors. Nature Materials, 7(11) (2008) 845-854.

[5] G. R. Li, Z. L. Wang, F. L. Zheng, Y. N. Ou, Y. X. Tong, ZnO@ MoO_3 core/shell nanocables: facile electrochemical synthesis and enhanced supercapacitor performances. Journal of Materials Chemistry, 21(12) (2011) 4217-4221.

[6] P. M. Kulal, D. P. Dubal, C. D. Lokhande, V. J. Fulari, Chemical synthesis of Fe_2O_3 thin films for supercapacitor application. Journal of Alloys and Compounds, 509(5) (2011) 2567-2571.

[7] H. Becker, Low voltage electrolytic capacitor. US2800616 1957.

[8] F.Thissandier, thèse de doctorat, Elaboration de micro-supercondensateurs à base d'électrodes en silicium nanostructuré: des nanomatériaux aux dispositifs université de GRENOBLE (2013).

[9] H. Gualous, R. Gallay, A. Berthon, Utilisation des supercondensateurs pour le stockage de l'energie embarquee: applications transport. Revue de l'Electricité et de l'Electronique. (8) (2004) 83-90.

[10] M.H. Kacem, T. Souhir, N. Rfik, Utilisation des supercondensateurs et des batteries pour le stockage de l'énergie embarquée pour véhicule électrique. International Conference on Green Energy and Environmental Engineering (2014).

[11]https://www.defense.gouv.fr/dga/actualite-dga/2010/dix-huit-tonnes-ont-roule-a-la-pile-a-combustible.

[12] J. Come, thèse de doctorat «Caractérisation électrochimique de matériaux à insertion de Li pour supercondensateurs hybrides à haute densité d'énergie » Institut Carnot CIRIMAT Université Toulouse III – Paul Sabatier (2012).

[13] http://www.supercondensateur.com/watt-system-bus-a-supercondensateur.

[14] http://www.supercondensateur.com/bus-electrique-10-secondes-charge-supercondensateur.

[15] http://www.supercondensateur.com/bluetram-tramway-a-supercondensateur-made-in-france.

[16] http://www.supercondensateur.com/metro-seoul-economie-energie-supercondensateurs.

[17]http://www.supercondensateur.com/tramway-supercondensateur-avec-recuperation-energie-du-freinage.

[18]http://www.supercondensateur.com/bmw-voiture-sport-hybride-supercondensateur-avec-toyota.

[19] http://www.supercondensateur.com/toyota-yaris-hybrid-r-supercondensateur-400-chevaux.

[20] http://www.supercondensateur.com/volvo-batterie-structurelle-supercondensateur-voiture.

[21]http://www.batterypoweronline.com/images/PDFs_articles_whitepaper_appros/Maxwell%20Techno logies.pdf

[22] J. R. Miller, P. Simon, Electrochemical capacitors for energy management. Science Magazine, 321(5889) (2008) 651-652.

[23] P. Barrade, A. Rufer, Supercapacitors as energy buffers: a solution for elevators and for electric busses supply. In Power Conversion Conference.PCC-Osaka 2002. (3) (2002) 1160-1165.

[24] C. Abbey, G. Joos, Supercapacitor energy storage for wind energy applications. IEEE Transactions on Industry Applications, 43(3) (2007) 769-776.

[25] http://www.lampadaire-photovoltaique.com/

[26] J. Monteiro, N. Garrido, R. Fonseca, Efficient supercapacitor energy usage in mobile phones. In Consumer Electronics-Berlin (ICCE-Berlin EEE International Conference on Consumer Electronics-Berlin (ICCE-Berlin) (2011) (318-321).

[27] L. Palma, P. Enjeti, J. W. Howze, An approach to improve battery run-time in mobile applications with supercapacitors IEEE 34th Annual Conference on Power Electronics Specialist, (2), (2003), (918-923).

[28]www.supercondensateur.com/souris-sans-fil-supercondensateur-recharge-instantanee-genius-dx-eco

[29] P. Simon, Y. Gogotsi, Materials for electrochemical capacitors. In Nanoscience and Technology: A Collection of Reviews from Nature Journals, (2010), (320-329).

[30] C. Zhong, Y. Deng, W. Hu, J. Qiao, L. Zhang, J. Zhang, A review of electrolyte materials and compositions for electrochemical supercapacitors. Chemical Society Reviews, 44(21) (2015) 7484-7539.

[31] Y. Wang, Y. Song, Y. Xia, Electrochemical capacitors: mechanism, materials, systems, characterization and applications. Chemical Society Reviews, 45(21) (2016) 5925-5950.

[32] X. Xiao, S. Li, H. Wei, D. Sun, Y. Wu, G. Jin, F. Wang, Y.Zou, Synthesis and characterization of VO_2 (B)/graphene nanocomposite for supercapacitors. Journal of Materials Science: Materials in Electronics 26(6) (2015) 4226-4233.

[33] X. Xia, D. Chao, C. F. Ng, J. Lin, Z. Fan, H. Zhang, Z.X. Shen, H. J. Fan, VO_2 nanoflake arrays for supercapacitor and Li-ion battery electrodes: performance enhancement by hydrogen molybdenum bronze as an efficient shell material. Materials Horizons, 2(2) (2015) 237-244.

[34] T. M. Dinh, A. Achour, S.Vizireanu, G. Dinescu, L. Nistor, K. Armstrong, D. Guay, D. Pech, Hydrous RuO_2/carbon nanowalls hierarchical structures for all-solid-state ultrahigh-energy-density micro-supercapacitors, Nano Energy, 10 (2014) 288-294.

[35] S. Hassan, M. Suzuki, A.A. El-Moneim. Capacitive behavior of manganese dioxide/stainless steel electrodes at different deposition currents.American Journal of Materials Science, 2(2) (2012) 11-14.

[36] J. Yan, E. Khoo, A. Sumboja, P. S. Lee, Facile coating of manganese oxide on tin oxide nanowires with high-performance capacitive behavior. ACS Nano, 4(7) (2010) 4247-4255.

[37] S. Chou, F. Cheng, J. Chen, Electrodeposition synthesis and electrochemical properties of nanostructured γ-MnO_2 films. Journal of Power Sources, 162(1) (2006) 727-734.

[38] M.S. Wu, Z.S. Guo, J.J. Jow, Highly regulated electrodeposition of needle-like manganese oxide nanofibers on carbon fiber fabric for electrochemical capacitors.Journal of Physical Chemistry C 114(49) (2010) 21861-21867.

[39] G.A. Ali, M.M. Yusoff, Y.H. Ng, H.N. Lim, K. F. Chong, Potentiostatic and galvanostatic electrodeposition of manganese oxide for supercapacitor application: A comparison study. Current Applied Physics, 15(10) (2015) 1143-1147.

[40] S. Hassan, M. Suzuki, S. Mori, A.A. El-Moneim. MnO_2/carbon nanowalls composite electrode for supercapacitor application. Journal of Power Sources, 249 (2014) 21-27.

[41] G. A. Snook, P. Kao, A. S. Best, Conducting-polymer-based supercapacitor devices and electrodes. Journal of Power Sources, 196(1) (2011) 1-12.

[42] E. Frackowiak, V. Khomenko, K. Jurewicz, K. Lota, F. Béguin, Supercapacitors based on conducting polymers/nanotubes composites. Journal of Power Sources, 153(2) (2006) 413-418.

[43] S. Ghosh, O. Inganäs, Conducting polymer hydrogels as 3D electrodes: applications for supercapacitors. Advanced Materials, 11(14) (1999) 1214-1218.

[44] J. Zhang, X. S. Zhao, Conducting polymers directly coated on reduced graphene oxide sheets as high-performance supercapacitor electrodes. The Journal of Physical Chemistry C, 116(9) (2012) 5420-5426.

[45] K. S. Ryu, K. M. Kim, N. G. Park, Y. J. Park, S. H. Chang, Symmetric redox supercapacitor with conducting polyaniline electrodes. Journal of Power Sources, 103(2) (2002) 305-309.

[46] J. Yan, E. Khoo, A.Sumboja, P. S. Lee, Facile coating of manganese oxide on tin oxide nanowires with high-performance capacitive behavior. ACS Nano 4(7) (2010) 4247-4255.

[47] B. Pant, M. Park, P.G. Ouellet, J. Park, Y.S. Kuk, E.J. Lee, S.j. Park. Carbon Nanofibers Wrapped with Zinc Oxide Nano-flakes as Promising Electrode Material for Supercapacitors. Journal of Colloid and Interface Science 522 (2018) 40-47.

[48] R. R. Salunkhe, J. Tang, Y. Kamachi, T. Nakato, J. H. Kim, Y. Yamauchi, Asymmetric supercapacitors using 3D nanoporous carbon and cobalt oxide electrodes synthesized from a single metal–organic framework. ACS Nano, 9(6) (2015) 6288-6296.

[49] G. Sun, X. Zhang, R. Lin, J. Yang, H. Zhang, P. Chen, Hybrid fibers made of molybdenum disulfide, reduced graphene oxide, and multi-walled carbon nanotubes for solid-state, flexible, asymmetric supercapacitors. Angewandte Chemie International Edition, 54(15) (2015) 4651-4656.

[50] D. W. Wang, F. Li, , H. M. Cheng, Hierarchical porous nickel oxide and carbon as electrode materials for asymmetric supercapacitor. Journal of Power Sources, 185(2) (2008) 1563-1568.

[51] V. Khomenko, E. Raymundo-Pinero, F. Béguin, Optimisation of an asymmetric manganese oxide/activated carbon capacitor working at 2 V in aqueous medium. Journal of Power Sources, 153(1) (2006) 183-190.

[52] A. Laforgue, P. Simon, J. F. Fauvarque, M. Mastragostino, F. Soavi, J. F. Sarrau, S. Saguatti, Activated carbon/conducting polymer hybrid supercapacitors. Journal of the Electrochemical Society, 150(5) (2003) 645-651.

[53] D. Villers, D. Jobin, C. Soucy, D. Cossement, R. Chahine, L. Breau, D. Bélanger, The influence of the range of electroactivity and capacitance of conducting polymers on the performance of carbon conducting polymer hybrid supercapacitor.Journal of the Electrochemical Society, 150(6) (2003) 747-752.

[54] K. Naoi, S. Ishimoto, Y. Isobe, S. Aoyagi, High-rate nano-crystalline Li4Ti5O12 attached on carbon nano-fibers for hybrid supercapacitors.Journal of Power Sources, 195(18) (2010) 6250-6254.

[55] H. V. Helmholtz, Studien über electrische Grenzschichten. Annalen der Physik, 243(7) (1879) 337-382.

[56] M. Gouy, Sur la constitution de la charge électrique à la surface d'un électrolyte. Journal of Physics and Theoretical Application. 9(1) (1910) 457-468.

[57] D. L. Chapman, Contribution to the theory of electrocapillarity. The London, Edinburgh, and Dublin philosophical magazine and journal of science, 25(148) (1913) 475-481.

[58] O. Stern, Zur theorie der elektrolytischen doppelschicht. Zeitschrift für Elektrochemie und Angewandte Physikalische Chemie, 30(21) (1924) 508-516.

[59] H. Chen, T. N. Cong, W. Yang, C. Tan, Y. Li, Y. Ding, Progress in electrical energy storage system: A critical review. Progress in Natural Science, 19(3) (2009) 291-312.

[60] Y. Shao, M. F. El-Kady, J. Sun, Y. Li, Q. Zhang, M. Zhu, R. B. Kaner, Design and mechanisms of asymmetric supercapacitors. Chemical Reviews, 118(18) (2018) 9233-9280.

[61] R. R. Devarapalli, S. Szunerits, Y. Coffinier, M. V. Shelke, R. Boukherroub, Glucose-derived porous carbon-coated silicon nanowires as efficient electrodes for aqueous micro-supercapacitors. ACS Applied Materials & Interfaces, 8(7) (2016) 4298-4302.

[62] V. Augustyn, P. Simon, B. Dunn, Pseudo capacitive oxide materials for high-rate electrochemical energy storage.Energy & Environmental Science, 7(5) (2014) 1597-1614.

[63] E. Frackowiak, Q. Abbas, F. Béguin, Carbon/carbon supercapacitors. Journal of Energy Chemistry, 22(2) (2013) 226-240.

[64] A. González, E. Goikolea, J. A. Barrena, R. Mysyk, Review on supercapacitors: technologies and materials, Renewable and Sustainable Energy Reviews, 58 (2016) 1189-1206.

[65] D. Pech, M. Brunet, H. Durou, P. Huang, V. Mochalin, Y. Gogotsi, P. Simon, Ultrahigh-power micrometere-sized supercapacitors based on onion-like carbon, Nature Nanotechnology, 5(9) (2010) 651.

[66] J. K. McDonough, A. I. Frolov, V. Presser, J. Niu, C. H. Miller, T. Ubieto, Y. Gogotsi, Influence of the structure of carbon onions on their electrochemical performance in supercapacitor electrodes. Carbon, 50(9) (2012) 3298-3309.

[67] Y. Gao, Y. S. Zhou, M. Qian, X. N. He, J. Redepenning, P. Goodman, Y. F. Lu, Chemical activation of carbon nano-onions for high-rate supercapacitor electrodes, Carbon, 51(2013) 52-58.

[68] E. G. Bushueva, P. S. Galkin, A. V. Okotrub, L. G. Bulusheva, N. N. Gavrilov, V. L. Kuznetsov, S. I. Moiseekov , Double layer supercapacitor properties of onion like carbon materials. Physica Status Solidi (b), 245(10) (2008) 2296-2299.

[69] J. J. Yoo, K. Balakrishnan, J. Huang, V. Meunier, B. G. Sumpter, A. Srivastava, P. M. Ajayan, Ultrathin planar graphene supercapacitors, Nano Letters, 11(4) (2011), 1423-1427.

[70] Y. Zhu, S. Murali, M. D. Stoller, K. J. Ganesh, W. Cai, P. J. Ferreira, D. Su, Carbon-based supercapacitors produced by activation of graphene, Science, 332(6037) (2011), 1537-1541.

[71] C. Liu, Z. Yu, D. Neff, A. Zhamu, B. Z. Jang, Graphene-based supercapacitor with an ultrahigh energy density.Nano Letters, 10(12) (2010) 4863-4868.

[72] Y. Wang, Z. Shi, Y. Huang, Y. Ma, C. Wang, M. Chen, Y. Chen, Supercapacitor devices based on graphene materials, The Journal of Physical Chemistry C, 113(30) (2009) 13103-13107.

[73] S. Hassan, M. Suzuki, S. Mori, A. A. El-Moneim, MnO2/carbon nanowalls composite electrode for supercapacitor application, Journal of Power Sources, 249 (2014) 21-27.

[74] H. F. Yen, Y. Y. Horng, M. S. Hu, W. H. Yang, J. R. Wen, A. Ganguly, L. C. Chen, Vertically aligned epitaxial graphene nanowalls with dominated nitrogen doping for superior supercapacitors Carbon, 82 (2015), 124-134.

[75] T. Brousse, P. L. Taberna, O. Crosnier, R. Dugas, P. Guillemet, Y. Scudeller, P. Simon, Long-term cycling behavior of asymmetric activated carbon/MnO_2 aqueous electrochemical supercapacitor. Journal of Power Sources, 173(1) (2007) 633-641.

[76] J. Gamby, P. L. Taberna, P. Simon, J. F. Fauvarque, M. Chesneau, Studies and characterisations of various activated carbons used for carbon/carbon supercapacitors, Journal of Power Sources, 101(1) (2001) 109-116.

[77] J. Gamby, P. L. Taberna, P. Simon, J. F. Fauvarque, M. Chesneau, Studies and characterisations of various activated carbons used for carbon/carbon supercapacitors, Journal of power sources, 101(1) (2001) 109-116.

[78] P. Liu, M. Verbrugge, S. Soukiazian, Influence of temperature and electrolyte on the performance of activated-carbon supercapacitors, Journal of Power Sources, 156(2) (2006) 712-718.

[79] D. Yu, L. Dai, Self-assembled graphene/carbon nanotube hybrid films for supercapacitors, The Journal of Physical Chemistry Letters, 1(2) (2009) 467-470.

[80] C. Masarapu, H. F. Zeng, K. H. Hung, B. Wei, Effect of temperature on the capacitance of carbon nanotube supercapacitors, ACS Nano, 3(8) (2009) 2199-2206.

[81] K. H. An, W. S. Kim, Y. S. Park, Y. C. Choi, S. M. Lee, , D. C. Chung, Y. H. Lee, Supercapacitors using single-walled carbon nanotube electrodes. Advanced Materials, 13(7) (2001) 497-500.

[82] Y. Omidi-Khaniabadi, A. Jafari, H. Nourmoradi, F. Taheri, S. Saeedi, Adsorption of 4-chlorophenol from aqueous solution using activated carbon synthesized from aloe vera green wastes, Journal of Advances in Environmental Health Research, 3(2) (2015) 120-129.

[83] Y. van de Burgt, Laser-assisted growth of carbon nanotubes, A review.Journal of Laser Applications, 26(3) (2014) 032001.

[84] B. Ribeiro, E. C. Botelho, M. L. Costa, C. F. Bandeira, Carbon nanotube buckypaper reinforced polymer composites, A review. Polímeros, 27(3) (2017) 247-255.

[85] Z. S. Iro, C. Subramani, S. S. Dash, A brief review on electrode materials for supercapacitor, International Journal of Electrochemical. Science 11(12) (2016) 10628-10643.

[86] A. Shalaby, D. Nihtianova, P. Markov, A. D. Staneva, R. S. Iordanova, Y. B. Dimitriev, Structural analysis of reduced graphene oxide by transmission electron microscopy, Bulgarian Chemical Communications, 47(1) (2015) 291-295.

[87] J. Yan, J. Liu, Z. Fan, T. Wei, L. Zhang, High-performance supercapacitor electrodes based on highly corrugated graphene sheets, Carbon, 50(6) (2012) 2179-2188.

[88] G. ALCICEK, thèse de doctorat, Contribution à l'étude du vieillissement et à l'intégration des supercondensateurs dans une chaîne de propulsion électrique (CPE) haute tension pour des applications véhicule électrique. Université de technologie Belfort-Montbéliard (2014).

[89] S. Chou, F. Cheng, J.Chen, Electrodeposition synthesis and electrochemical properties of nanostructured γ-MnO2 films, Journal of Power Sources, 162(1) (2006) 727-734.

[90] S. T. Navale, V. V. Mali, S. A. Pawar, R. S. Mane, M. Naushad, F. J. Stadler, V. B. Patil, Electrochemical supercapacitor development based on electrodeposited nickel oxide film. RSC Advances, 5(64) (2015) 51961-51965.

[91] S. G. Kandalkar, H. M. Lee, H. Chae, C. K. Kim, Structural, morphological, and electrical characteristics of the electrodeposited cobalt oxide electrode for supercapacitor applications, Materials Research Bulletin, 46(1) (2011) 48-51.

[92] C. C. Wang, C. C. Hu, Electrochemical and Textural Characteristics of (Ru Sn) Ox· n H 2 O for Supercapacitors Effects of Composition and Annealing, Journal of the Electrochemical Society, 152(2) (2005) 370-376.

[93] D. P. Dubal, D. Aradilla, G. Bidan, P. Gentile, T. J. Schubert, J. Wimberg, P. Gomez-Romero, 3D hierarchical assembly of ultrathin MnO 2 nanoflakes on silicon nanowires for high performance micro-supercapacitors in Li-doped ionic liquid, Scientific Reports, 5 (2015) 9771.

[94] J. P. Zheng, P. J. Cygan, T. R. Jow, Hydrous ruthenium oxide as an electrode material for electrochemical capacitors, Journal of the Electrochemical Society, 142(8) (1995) 2699-2703.

[95] V. Srinivasan, J. W. Weidner, An electrochemical route for making porous nickel oxide electrochemical capacitors, Journal of the Electrochemical Society, 144(8) (1997) 210-213.

[96] K. C. Liu, M. A. Anderson, Porous nickel oxide/nickel films for electrochemical capacitors, Journal of the Electrochemical Society, 143(1) (1996) 124-130.

[97] X. H. Xia, J. P. Tu, X. L. Wang, C. D. Gu, X. B. ZhaoHierarchically porous NiO film grown by chemical bath deposition via a colloidal crystal template as an electrochemical pseudocapacitor material Journal of Materials Chemistry, 21(3) (2011) 671-679.

[98] C. Yuan, J. Li, L. Hou, X. Zhang, L. Shen, X. W. Lou, Ultrathin mesoporous NiCo2O4 nanosheets supported on Ni foam as advanced electrodes for supercapacitors, Advanced Functional Materials, 22(21) (2012) 4592-4597.

[99] V. Venkatachalam, R. Jayavel, Novel synthesis of Ni-ferrite (NiFe2O4) electrode material for supercapacitor applications, In AIP Conference Proceedings 1665(1) (2015) 140016.

[100] S. L. Kuo, J. F. Lee, N. L. Wu, Study on pseudocapacitance mechanism of aqueous $MnFe_2O_4$ supercapacitor, Journal of the Electrochemical Society, 154(1) (2007) 34-38.

[101] D. Choi, G. E. Blomgren, P. N. Kumta, Fast and reversible surface redox reaction in nanocrystalline vanadium nitride supercapacitors. Advanced Materials, 18(9) (2006) 1178-1182.

[102] X. Lu, M. Yu, T. Zhai, G. Wang, S. Xie, T. Liu, Y. Li, High energy density asymmetric quasi-solid-state supercapacitor based on porous vanadium nitride nanowire anode. Nano Letters, 13(6) (2013) 2628-2633.

[103] B. Wei, H. Liang, D. Zhang, Z. Wu, Z. Qi, Z. Wang, CrN thin films prepared by reactive DC magnetron sputtering for symmetric supercapacitors. Journal of Materials Chemistry A, 5(6) (2017), 2844-2851.

[104] M. Arif, A. Sanger, A. Singh, Sputter deposited chromium nitride thin electrodes for supercapacitor applications. Materials Letters, 220 (2018), 213-217.

[105] S. Bouhtiyya, R. L. Porto, B. Laïk, P. Boulet, F. Capon, J. P. Pereira-Ramos, J. F. Pierson, Application of sputtered ruthenium nitride thin films as electrode material for energy-storage devices. Scripta Materialia, 68(9) (2013) 659-662.

[106] D. Choi, P. N. Kumta, Chemically synthesized nanostructured VN for pseudocapacitor application. Electrochemical and Solid-State Letters, 8(8) (2005) 418-422.

[107] B. Das, M. Behm, G. Lindbergh, M. V. Reddy, B. V. R. Chowdari, High performance metal nitrides, MN (M= Cr, Co) nanoparticles for non-aqueous hybrid supercapacitors. Advanced Powder Technology, 26(3) (2015) 783-788.

[108] C. M. Ghimbeu, E. Raymundo-Piñero, P. Fioux, F. Béguin, C. Vix-Guterl, Vanadium nitride/carbon nanotube nanocomposites as electrodes for supercapacitors. Journal of Materials Chemistry, 21(35) (2011) 13268-13275.

[109] R. K. Sharma, A. C. Rastogi, S. B. Desu, Pulse polymerized polypyrrole electrodes for high energy density electrochemical supercapacitor. Electrochemistry Communications, 10(2) (2008) 268-272.

[110] H. R. Ghenaatian, M. F. Mousavi, S. H. Kazemi, M. Shamsipur, Electrochemical investigations of self-doped polyaniline nanofibers as a new electroactive material for high performance redox supercapacitor. Synthetic Metals, 159(17-18) (2009) 1717-1722.

[111] K. Liu, Z. Hu, R. Xue, J. Zhang, J. Zhu, Electropolymerization of high stable poly (3, 4-ethylenedioxythiophene) in ionic liquids and its potential applications in electrochemical capacitor. Journal of Power Sources, 179(2) (2008) 858-862.

[112] M. Acerce, D. Voiry, M. Chhowalla, Metallic 1T phase MoS2 nanosheets as supercapacitor electrode materials. Nature Nanotechnology, 10(4) (2015) 313.

[113] Z. Yang, C. Y. Chen, H. T. Chang, Supercapacitors incorporating hollow cobalt sulfide hexagonal nanosheets. Journal of Power Sources, 196(18) (2011) 7874-7877.

[114] J. Zhang, H. Feng, J. Yang, Q. Qin, H. Fan, C. Wei, W. Zheng, Solvothermal synthesis of three-dimensional hierarchical CuS microspheres from a Cu-based ionic liquid precursor for high-performance asymmetric supercapacitors. ACS Applied Materials & Interfaces, 7(39) (2015) 21735-21744.

[115] M. A. Bissett, I. A. Kinloch, R. A. Dryfe, Characterization of MoS_2–graphene composites for high-performance coin cell supercapacitors. ACS Applied Materials & Interfaces, 7(31) (2015) 17388-17398.

[116] X. Zhou, B. Xu, Z. Lin, D. Shu, L. Ma, Hydrothermal synthesis of flower-like MoS_2 nanospheres for electrochemical supercapacitors. Journal of Nanoscience and Nanotechnology, 14(9) (2014) 7250-7254.

[117] J. Zhu, W. Sun, D. Yang, Y. Zhang, H. H. Hoon, H. Zhang, Q. Yan, Multifunctional Architectures Constructing of PANI Nanoneedle Arrays on MoS_2 Thin Nanosheets for High-Energy Supercapacitors. Small, 11(33) (2015) 4123-4129.

[118] A. Hamdi, L. Boussekey, P. Roussel, A. Addad, H. Ezzaouia, R. Boukherroub, Y. Coffinier, Hydrothermal preparation of MoS_2/TiO_2/Si nanowires composite with enhanced photocatalytic performance under visible light. Materials & Design, 109 (2016) 634-643.

[119] B. D. Falola, T. Wiltowski, I. I. Suni, Electrodeposition of MoS2 for charge storage in electrochemical supercapacitors. Journal of the Electrochemical Society, 163(9) (2016) 568-574.

[120] Z. Yang, C. Y. Chen, H. T. Chang, Supercapacitors incorporating hollow cobalt sulfide hexagonal nanosheets. Journal of Power Sources, 196(18) (2011) 7874-7877.

[121] F. Tao, Y. Q. Zhao, G. Q. Zhang, H. L. Li, Electrochemical characterization on cobalt sulfide for electrochemical supercapacitors. Electrochemistry Communications, 9(6) (2007) 1282-1287.

[122] R. N. Bulakhe, S. Sahoo, T. T. Nguyen, C. D. Lokhande, C. Roh, Y. R. Lee, J. J. Shim, Chemical synthesis of 3D copper sulfide with different morphologies for high performance supercapacitors application. RSC Advances, 6(18) (2016) 14844-14851.

[123] S. E. Rowlands, R. J. Latham, W. S. Schlindwein, Supercapacitor devices using porous silicon electrodes. Ionics, 5(1-2) (1999) 144-149.

[124] F. Thissandier, P. Gentile, N. Pauc, T. Brousse, G. Bidan, S. Sadki, Tuning silicon nanowires doping level and morphology for highly efficient micro-supercapacitors.Nano Energy, 5 (2014) 20-27.

[125] F. Thissandier, N. Pauc, T. Brousse, P. Gentile, S. Sadki, Micro-ultracapacitors with highly doped silicon nanowires electrodes. Nanoscale Research Letters, 8(1) (2013) 38.

[126] N. Berton, M. Brachet, F. Thissandier, J. Le Bideau, P. Gentile, G. Bidan, S. Sadki, Wide-voltage-window silicon nanowire electrodes for micro-supercapacitors via electrochemical surface oxidation in ionic liquid electrolyte. Electrochemistry Communications, 41 (2014) 31-34.

[127] R. R. Devarapalli, S. Szunerits, Y. Coffinier, M. V. Shelke, R. Boukherroub, Glucose-derived porous carbon-coated silicon nanowires as efficient electrodes for aqueous micro-supercapacitors. ACS Applied Materials Interfaces, 8(7) (2016) 4298-4302.

[128] S. Chatterjee, R. Carter, L. Oakes, W. R. Erwin, R. Bardhan, C. L. Pint, Electrochemical and corrosion stability of nanostructured silicon by graphene coatings: toward high power porous silicon supercapacitors. The Journal of Physical Chemistry C, 118(20) (2014) 10893-10902.

[129] F. Gao, G. Lewes-Malandrakis, M. T. Wolfer, W. Müller-Sebert, P. Gentile, D. Aradilla, , C. E. Nebel, Diamond-coated silicon wires for supercapacitor applications in ionic liquids. Diamond and Related Materials, 51 (2015), 1-6.

[130] J. P. Alper, M. Vincent, C. Carraro, R. Maboudian, Silicon carbide coated silicon nanowires as robust electrode material for aqueous micro-supercapacitor. Applied Physics Letters, 100(16) (2012) 163901.

[131] Q. Zhang, X. Wu, Q. Zhang, F. Yang, H. Dong, J. Sui, L. Dong, One-step hydrothermal synthesis of MnO2/graphene composite for electrochemical energy storage.Journal of Electroanalytical Chemistry 837 (2019) 108-115.

[132] Y. Liu, Y. Zhang, G. Ma, Z. Wang, K. Liu, H. Liu, Ethylene glycol reduced graphene oxide/polypyrrole composite for supercapacitor. Electrochimica Acta, 88 (2013) 519-525.

[133] W. Qin, J. L. Li, G. Fei, W. S. Li, K. Z. Wu, X. D. Wang, Activated carbon coated with polyaniline as an electrode material in supercapacitors. New Carbon Materials, 23(3) (2008), 275-280.

[134] Q. Zhang, X. Wang, Z. Pan, J. Sun, J. Zhao, J. Zhang, Z. Zhang, Wrapping aligned carbon nanotube composite sheets around vanadium nitride nanowire arrays for asymmetric coaxial fiber-shaped supercapacitors with ultrahigh energy density. Nano Letters, 17(4) (2017) 2719-2726.

[135] J. Wang, F. Li, F. Zhu, O. G. Schmidt, Recent Progress in Microsupercapacitor Design, Integration, and Functionalization.Small Methods, 3(8) (2018) 1800367.

[136] N. Liu, Y. Gao, Recent Progress in Micro-Supercapacitors with In-Plane Interdigital Electrode Architecture.Small, 13(45) (2017) 1701989.

[137] K. Robert, C. Douard, A. Demortière, F. Blanchard, P. Roussel, T. Brousse, C. Lethien, On Chip Interdigitated Micro-Supercapacitors Based on Sputtered Bifunctional Vanadium Nitride Thin Films with Finely Tuned Inter-and Intracolumnar Porosities. Advanced Materials Technologies, 3(7) (2018) 1800036.

[138] B. Wei, G. Mei, H. Liang, Z. Qi, D. Zhang, H. Shen, Z. Wang, Porous CrN thin films by selectively etching CrCuN for symmetric supercapacitors. Journal of Power Sources, 385 (2018) 39-44.

[139] D. Pech, M. Brunet, P. L. Taberna, P. Simon, N. Fabre, F. Mesnilgrente, H. Durou, Elaboration of a microstructured inkjet-printed carbon electrochemical capacitor.Journal of Power Sources, 195(4) (2010) 1266-1269.

[140] D. Pech, M. Brunet, H. Durou, P. Huang, V. Mochalin, Y. Gogotsi, P. Simon, Ultrahigh-power micrometre-sized supercapacitors based on onion-like carbon. Nature Nanotechnology, 5(9) (2010), 651.

[141] P. Huang, M. Heon, D. Pech, M. Brunet, P. L. Taberna, Y. Gogotsi, P. Simon, Micro-supercapacitors from carbide derived carbon (CDC) films on silicon chips. Journal of Power Sources, 225 (2013) 240-244.

[142] W. Gao, N. Singh, L. Song, Z. Liu, A. L. M. Reddy, L. Ci, P. M. Ajayan, Direct laser writing of micro-supercapacitors on hydrated graphite oxide films. Nature Nanotechnology, 6(8) (2011) 496.

[143] M. Beidaghi, C. Wang, Micro-supercapacitors based on interdigital electrodes of reduced graphene oxide and carbon nanotube composites with ultrahigh power handling performance. Advanced Functional Materials, 22(21) (2012) 4501-4510.

[144] M. Arulepp, L. Permann, J. Leis, A. Perkson, K. Rumma, A. Jänes, E. Lust, Influence of the solvent properties on the characteristics of a double layer capacitor. Journal of Power Sources, 133(2) (2004) 320-328.

Chapter 2. Achieving on Chip Micro-Supercapacitors Based on CrN Deposited by Bipolar Magnetron Sputtering at Glancing Angle

1. Introduction

Physical vapor deposition (PVD) techniques are widely used for material synthesis, in the form of films, for different applications including semiconductor technology, medical devices, smart coatings, or cutting tools [1–4]. Recently, there has been an impressive research effort toward the fabrication of electrodes deposited by PVD for energy storage devices such as Li-ions/micro-batteries [5,6] or electrochemical capacitors (ECs)/micro-supercapacitors (μSCs) [7–9]. In particular, in the case of ECs electrodes, the PVD techniques offer alternative solution to most of the problems faced during the processing of powder into packed films [6,8,9]. These problems consist of bad adhesion to the current collector, loss of accessible volume to the electrolyte and incompatibility with standard micro-fabrication protocols. Indeed, PVD can produce films with good adhesion, controlled thickness, composition and morphology [1–4,6,9]. Thus, using PVD to fabricate electrodes for ECs, and especially for micro-supercapacitors, would be an interesting alternative solution to most of the problems encountered during the processing of powder into packed films.

Metal oxides including RuO_2 [10], MnO_2 [11] and transition metal nitrides such as TiN [12,13], VN [14], TiVN [15]**,** RuN[16] and CrN [17,18], have been deposited by PVD methods for use as electrodes in ECs. Besides, the deposition parameters were also adjusted, to increase the porosity of the films, and thus, enhance their specific capacitance. For instance, nitrogen flux has been controlled in the case of TiN electrodes [12], while the pressure and deposition temperature have been adjusted in the case of VN [19] and CrN [17] electrodes to produce porous films with enhanced electrochemical energy storage. In this work, we used bipolar magnetron sputtering at a glancing angle (GLAD) as a new strategy, in the field of ECs, to improve the apparent porosity of CrN films. The GLAD strategy simply entails substrate tilting to the target during film deposition. The GLAD method allows modifying the morphology of the deposited coating, from dense to porous, and the formation of inclined columns. Such features have found applications in optical devices (polarized light emitters), sensors devices (humidity sensors) or energy devices (solar energy conversion) [20–22]. Herein, four different tilt angles of 0, 45, 60 and 75° were explored. The areal capacitance value of the resulting CrN electrodes can reach capacitance values as high as 35.4 $mF.cm^{-2}$ at a current density of 1.2 $mA.cm^{-2}$, with a stable cycle life exceeding 10,000 cycles.

Moreover, the apparent porosity of the CrN electrode can be controlled by tailoring the deposition angle inside the chamber during film growth, which affects both the areal capacitance and power density of the electrodes. In contrast to the method used in Ref [18] involving selective etching of Cu from CrCuN film to obtain porous CrN films, our method is simple and consists of a single-step process. Besides, it is scalable and can be easily generalized for other types of materials deposited by PVD techniques to obtain high porous electrodes for energy storage applications.

1. Chromium nitride (CrN) as an active material for SC applications

Transition metal-based materials (TMs) have been explored as promising electrode materials for supercapacitors application due to their unique properties such as high capacity, excellent conductivity and low cost [10-18]. Among those TMs, chromium nitride (CrN) has been explored as a potential candidate for many industrial applications due to its chemical stability and excellent electrical conductivity [17, 18]. However, only a few reports are available on the use of CrN as supercapacitor electrode materials. Das et al. [32] were the first to develop the synthesis of CrN nanoparticles by nitriding Cr_2O_3 at a relatively low temperature. The specific capacitance of the CrN based electrode was as high as 75 F g^{-1} at a current density of 30 mA.g^{-1}. Very recently, Wei et al. have reported the fabrication of a symmetrical SC (CrN / CrN) using reactive magnetron sputtering method with high energy density (of 8.2 mWh.cm^{-3}, a high power density of 0.7 W.cm^{-3} along with excellent electrochemical stability over 20000 cycles [17]. Arif et al. have reported the synthesis of a thin-film CrN electrode with a high specific capacitance of 41.6 Fg^{-1} at a scan rate of 5 mV.s^{-1} and good cyclic stability over 2000 cycles [44].

Most recently, Qi et al. [45] reported the synthesis of nanostructured porous CrN thin layers by combining magnetron sputtering and glancing angle deposition (GLAD). The thin-film electrode exhibited a high specific capacity of 17.7 mF.cm^{-2} at a current density of 1.0 mA.cm^{-2}. A symmetric supercapacitor using the CrN electrode was proposed to achieve maximum energy and power densities of 7.4mWh cm^{-3} and 18.2W cm^{-3}, respectively with good stability (retention of 92.2% capacity after 20,000 cycles). The recent studies reported show the advantage of using CrN as an active material for the fabrication of high performance supercapacitors.

2. Experimental methods

2.1. Synthesis of CrN films

The CrN thin films have been synthesized by combining magnetron sputtering and glancing angle deposition (GLAD) in a 1m³ semi-industrial hexagonal chamber from D&M Vacuumsystemen (**Figure 13a**) [2]. Two planar chromium targets (7.5 × 35 cm, 99.99% purity, from Neyco) have been sputtered in an argon and nitrogen gas mixture, respectively 150 and 120 sccm, with gas injected at the surface of the target. The pressure was set at 5 mTorr (0.66 Pa) and continuously adjusted with a throttle valve. The targets are sputtered in bipolar mode, using a Magpuls QP-1000/20 10 kW pulse unit, at a mean current of 2 A, a duty cycle of 50% and a frequency of 2500 Hz (**Figure 13b**).

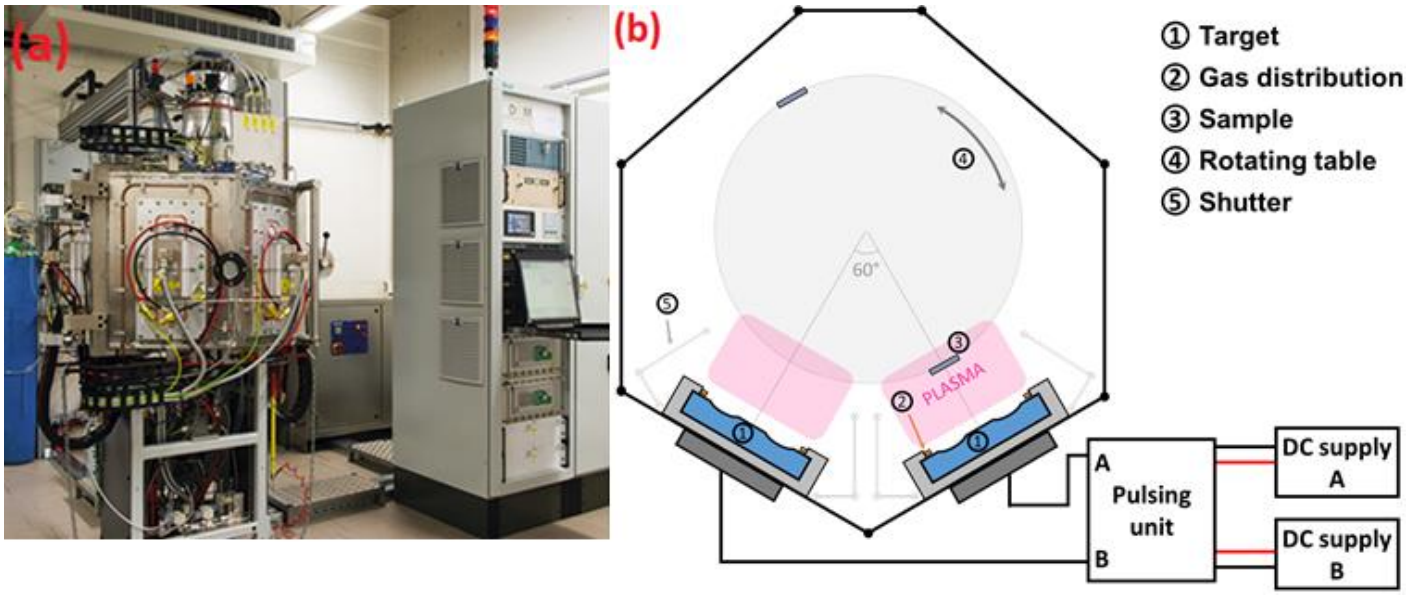

Figure 13: (a) Laboratoire d'Analyse par Reaction Nucléaire (LARN) sputtering machine. (b) Schematic of the Sputtering method.

The operating cycle (ratio between T_{ON} and $T_{ON} + T_{OFF}$), as well as the frequency, are adjustable. In our case, the T_{ON} and T_{OFF} were fixed at 100µs (**Figure 14a**). Silicon substrates were static and mounted in front of one cathode, with tilted substrate holder at 0, 45, 60 and 75°. When the sample holder is tilted, the deposition flow is no longer orthogonal to the substrate but forms an angle α with it leading to the formation of columns with inclination β (**Figure 14b**).

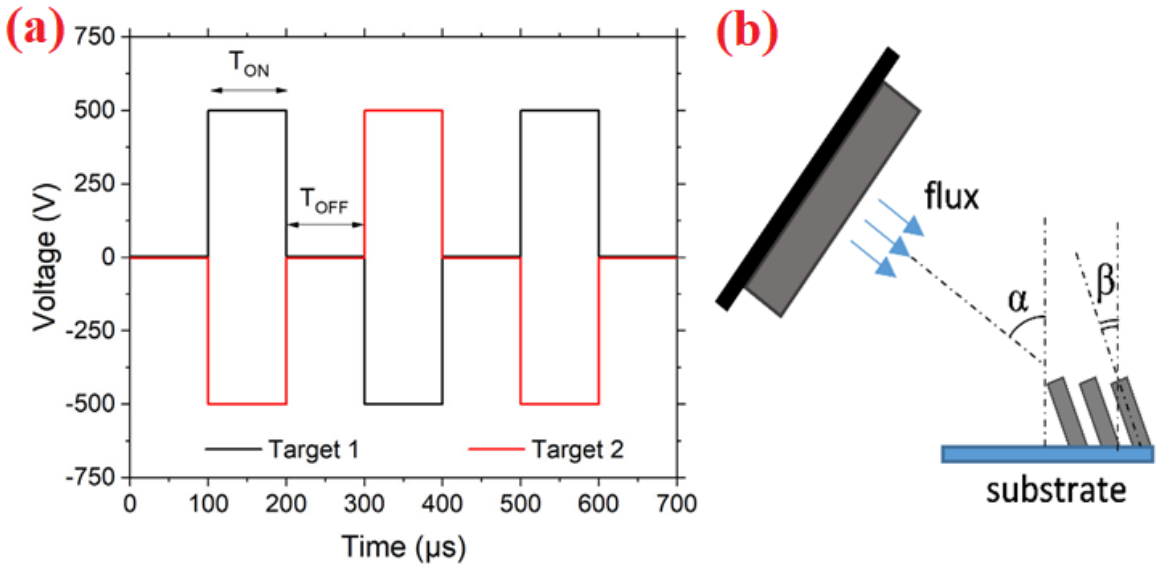

Figure 14: (a) Evolution of the voltage during a bipolar discharge. (b) Schematic of the GLAD deposition.

Before the deposition of CrN film, an interface layer of Ti and Au with a thickness of 80 nm is deposited. The Ti/Au layers were chosen as substrates for CrN deposition because the device is made of gold as the current collector deposited on a Ti buffer layer (as explained in **Figure 20**). The role of the Ti buffer is the improvement of the gold adhesion on silicon. Therefore, to make an honest comparison between CrN films tested in the three-electrode configurations and the CrN deposited on the device (made of gold current collector), we have chosen Ti/Si as a buffer in the case of CrN film to exclude any effect of the substrate concerning the resistivity and CV shapes.

1.2. Electrochemical measurements

Electrochemical studies of the CrN electrodes were carried out using a potentiostat/galvanostat Metrohm-Autolab PGSTAT128N at room temperature in a typical three-electrode electrochemical cell. The cell is composed of two parts assembled face to face. The lower part has a copper current collector and the upper part is made of Teflon and filled with the electrolyte. It also has a hole at the bottom to enable the contact between the electrode and the electrolyte. The CrN sample was used as a working electrode, Ag/AgCl as a reference electrode and Pt foil as a counter electrode. In this cell, only the side coated with CrN was in contact with the electrolyte (S = 0.5 cm^2). The other side of the samples was contacted with the copper current collector by using a silver paste to ensure good electrical contact. The electrodes were characterized by cyclic voltammetry (CV) and Galvanostatic Charge-Discharge (GCD) in H_2SO_4 (0.5 M)

aqueous solution. The charge transfer and ion diffusion properties study of the CrN thin-film electrodes were conducted by electrochemical impedance spectroscopy (EIS) measurements. The EIS measurements were carried out in the frequency range of 100 kHz–10 mHz by plotting spectra using 10 points per frequency decade at open circuit potential (OCP) in 0.5 M H_2SO_4 electrolyte at room temperature. The capacitance calculation details according to Reference [21-22] are given in **Annex**.

In the present work, only areal and volumetric capacitance of the CrN deposits and the corresponding micro-devices are provided. It should be noted that the mass of the device has no meaning because the most important is the area that is occupied by the device and not its mass [8].

3. Results and discussion

3.1. Evaluation of CrN electrodes deposited at different angles

3.1.1. Structural and surface characterization

Figure 15 shows the cross-section and top-view SEM images of the CrN films deposited at different glancing incidence. All the samples exhibit a dense columnar structure, a typical morphology obtained under similar conditions [2,23], with small cubic crystallites growing normal to the surface. The tilting of the sample (**Figure 14b**) leads to a (i) change of the morphology, (ii) a decrease of the thickness, from 1870 nm at 0° down to 1210 nm at 75° of incidence, and (iii) a global increase of the tilting angle of the columns β. The increase of β is observed up to α = 60°, while the columns are slightly less tilted than for α = 60°. This evolution has already been reported by Besnard et al. [20], where the saturation of the tilting angle occurs. It is worth to mention that in our case, the nanostructures are deposited on silicon substrates, which means that material quantity available is very low, and therefore, in contrast to powder, the Brunauer-Emmett-Teller (BET) analysis is not possible. The only possible way to estimate the surface area is from SEM images.

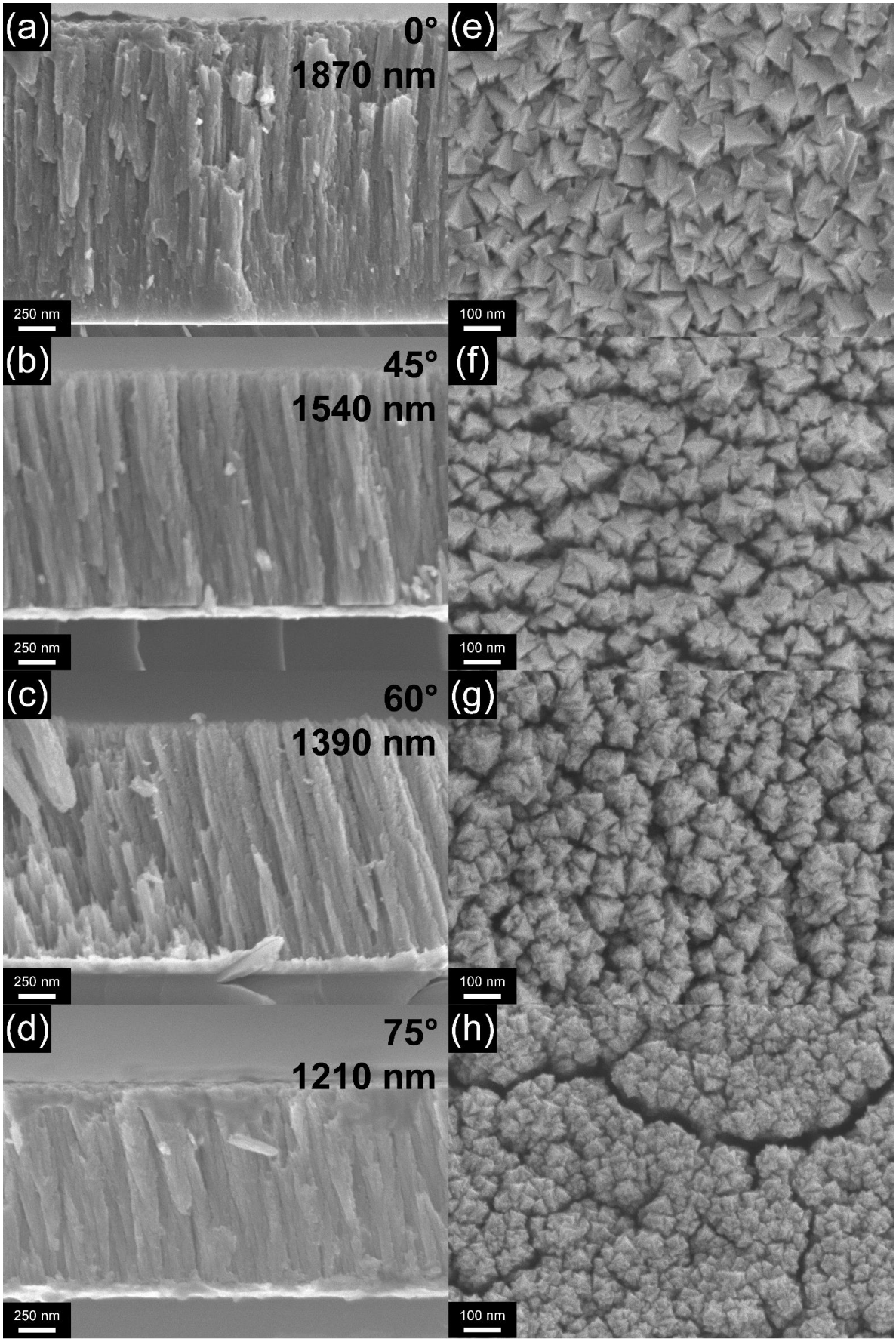

Figure 15: Top view SEM images of CrN films : (a) CrN0° (b) CrN45°, (c) CrN60° and (d) CrN75°.Cross-section SEM images of CrN films: (e) CrN0° (f) CrN45°, (g) CrN60° and (h) CrN75 °.

Overall, the increase of tilt angle results in a more porous structure: at 0°, the structure is denser, without voids between columns (**Figure 15a & e**), and cubic crystallites of ≈100 nm are observed on the top surface. Both CrN45° and CrN60° exhibit similar morphology, but a different tilting angle (respectively 10.8 ± 0.8° and 16.4 ± 0.7°), with smaller cubic crystallites, about 50-100 nm (**Figure 15f & g**), and more open voids between the top of the columns. The increase of the incidence up to 75° does not significantly affect the shape of the columns. However, it drastically reduces the crystallites size (<50 nm) which merges to close open porosity as can be observed on the top surface from Figure 1h. The same evolution has recently been reported for TiN thin films [21]. It results in lower mobility of adatoms and lower crystallite size, in addition to the creation of voids between columns [26,27]. It is worth mentioning that the difference of grain size, as well as the separation of columns by voids and defects in each case, can deeply influence both the electrical and electrochemical performance (inter-columnar porosity) behavior of CrN electrodes deposited at different tilt angles. Finally, the voids between columns, estimated from SEM observations, are less than 20 nm, suggesting the presence of a mesoporous network in CrN45° and CrN60° samples. Due to the low amount of active material and to the limited surface of thin-film samples, it was not possible to further estimate the pores size distribution by gas adsorption techniques.

3.1.2. Physico-chemical characterization

The cubic structure is also confirmed by GA-XRD measurements (**Figure 16a**), with diffraction peaks at 37.5°, 43.6°, 63.4° and 76.0° attributed to (111), (200), (220) and (311) planes, respectively. All the diffraction peaks have a significant increase of the full width at half maximum (FWHM) as the deposition angle increases. The FWHM of (111) diffraction peak has been used to estimate the grain size using the Scherrer formula; the grain size decreases from 18 to 9 nm as the deposition angle increases from 0 to 75°, in good agreement with the SEM observation. Due to the tilted columnar morphology and the use of GA-XRD, the intensity ratio strongly depends on the measurement method and the sample position during the measurement. Thus, the comparison of intensity is convenient. However, a shift of the diffraction peaks is observed as the deposition angle increases. This effect is attributed to the increase of the oxygen content at high angles, due to the lower deposition rate. The presence of oxygen in metal nitride thin film is frequently reported [28,29], and its content decreases as the deposition rate increases.

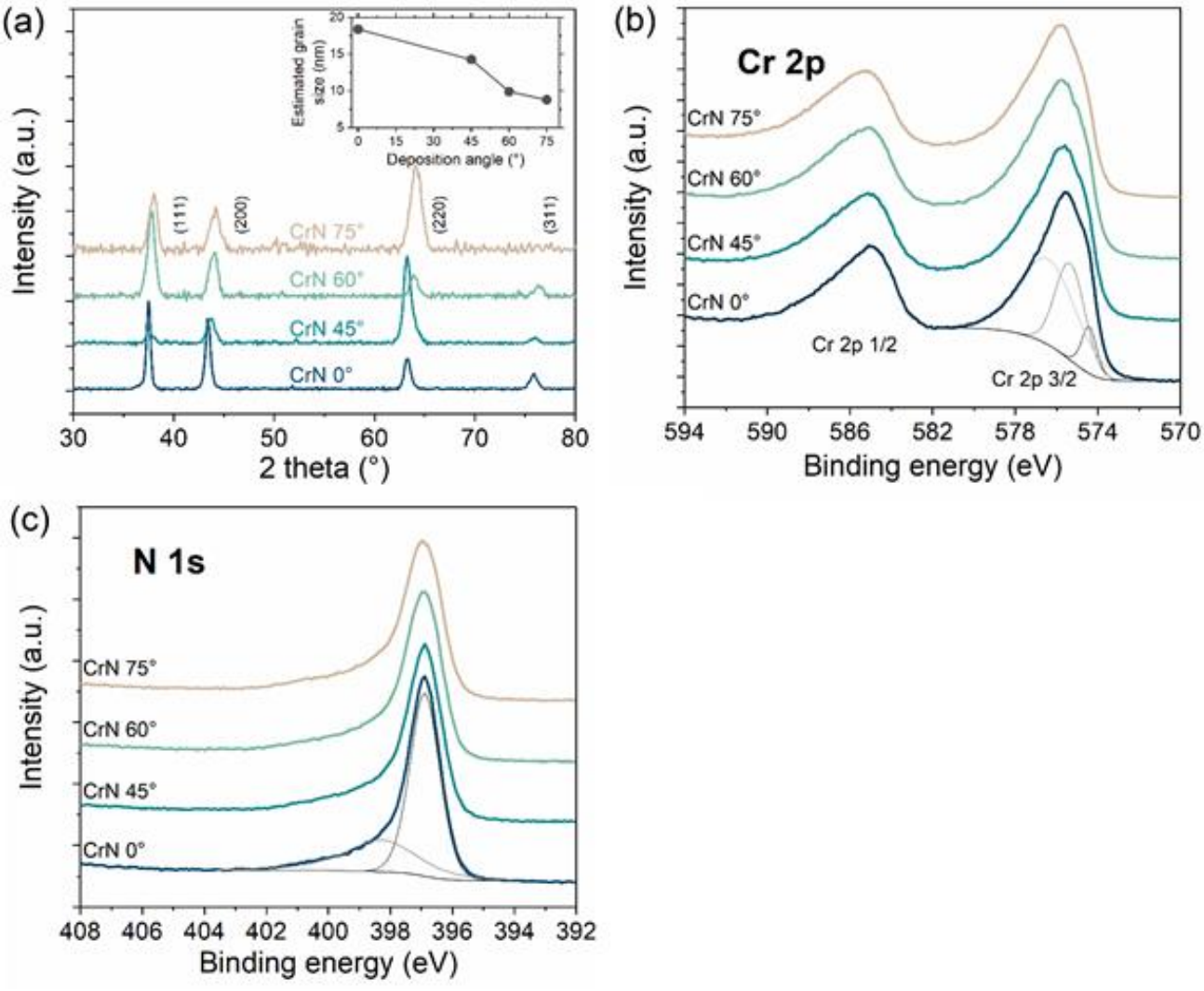

Figure 16: (a) XRD patterns, and XPS high-resolution spectra of (b) N 1s and (c) Cr 2p of CrN films.

The surface chemistry of the chromium nitride thin films has been investigated by XPS measurements, on Cr 2p and N 1s core-level spectra (**Figures 16b and c**). No significant differences between samples are evidenced, which is expected since neither the working pressure nor the gas flux has been modified. The survey spectra (not shown here) reveal the presence of oxygen, with higher content as the tilting angle increases. Cr $2p_{3/2}$ is fitted with three contributions, centered at 574.6, 575.5 and 576.6 eV that can be assigned to CrN, Cr(O, N) and Cr_2O_3, respectively [30]. Such surface oxidation is expected, as no sample etching is done before the analysis. Nitride formation is attested by the N 1s core-level spectra (**Figure 16c**) with a major contribution at 396.9 eV in addition to oxynitride formation as depicted from the contribution at 398.3 eV [30,31]. Since the specific capacitance of electrochemical capacitors is influenced by both the surface chemistry and the surface area of the active materials, one should consider

that, in the case of our CrN electrodes, any difference of the electrochemical behavior will be only attributed to the effect of surface area and structure, because the surface chemistry of all the CrN electrodes deposited at different tilt angles is almost the same.

3.1.3. Electrochemical characterization

The charge transfer and ion diffusion properties of the CrN thin-film electrodes were investigated by electrochemical impedance spectroscopy (EIS) measurements. **Figure 17** shows the typical Nyquist and bode plots of CrN thin-film electrodes (CrN0°, CrN45°, CrN60° and CrN75°) recorded in 0.5 M H_2SO_4 aqueous solution at open circuit potential (OCP).

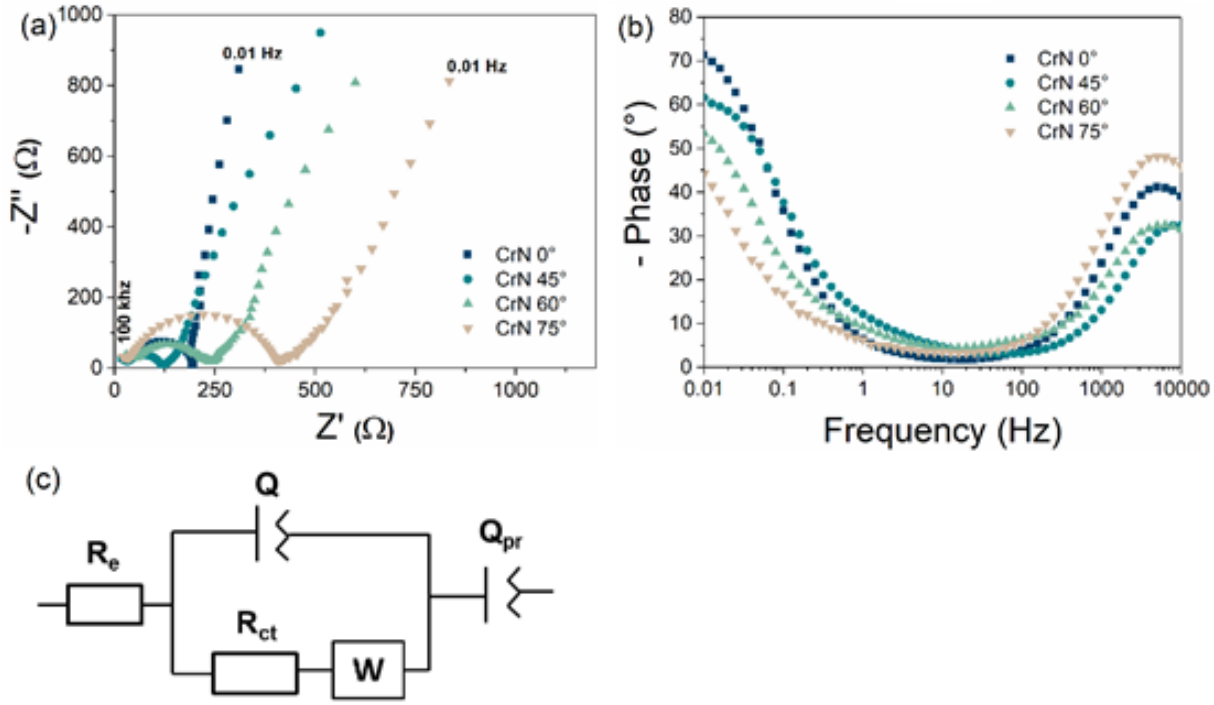

Figure 17: Analysis of EIS plots of the CrN film electrodes (CrN0°, CrN45°, CrN60° and CrN75°): (a) Nyquist plots, (b) Bode plots recorded in 0.5 M H_2SO_4 at OCP, and (c) the related equivalent circuit.

Three domains can be identified for the EIS spectra as depicted in **Figure 17**; at high frequencies region, a semicircle is observed which can be attributed to the surface properties and charge transfer resistance of the material; the domain at mid frequencies region corresponds to a straight line (except for CrN0°) with a slope < 45° followed by a straight line at higher phase angle. These features indicate a non-perfect capacitive-like behavior. The slope of the straight line making an angle lower than 45° in the mid-

frequency region is due to the diffusion effect of ions at the electrode-electrolyte interface and reflects the diffusive behavior, including proton diffusion in the electrolyte trapped in the porosity of the CrN film. These slopes are followed by a straight line with a slope > 45° indicating the capacitive behavior of the CrN films. These results are in accordance with the literature on the electrochemical behavior of CrN in the acidic electrolyte [17,32,33]. The intercept of the beginning of the semicircle with Z' axis is very close for all the samples and it is related to the resistance of the 0.5M H_2SO_4 electrolyte (Re). Wider arcs or semi-circles mean greater resistance to charge transfer and a steeper slope means a lower ion diffusion rate [34]. In the low-frequency region, a vertical plot is observed, suggesting a capacitive behavior of the CrN electrodes. The phase angles determined in the Bode plot (**Figure 17b**) at low frequencies are >45° for all electrodes, which is lower than the expected value for an ideal capacitor (90°). The Randles equivalent circuit of CrN electrodes in **Figure 17c** presents three series networks, one of them related to the electrolyte, the second to the film area, and the third to the pores. The electrolyte resistance is represented by resistor $\mathbf{R_e}$, the area occupied by CrN film is represented by a parallel **R//Q** network that refers to the associated interfacial process ($\mathbf{R_{ct}}$, $\mathbf{C_{dl}}$ **and W**), standing for the charge transfer resistance, double layer capacitance and diffusion effect, respectively, in series with a $\mathbf{Q_{pr}}$ corresponding to the pseudocapacitance of CrN electrodes. The Nyquist plot was fitted using the Randles equivalent circuit and its parameter values were summarized in **table 1**. The resistance of the electrolyte R_e was varied from 28 to 17 **Ω** which due to the difference in contact of the backside of the electrodes. The charge transfer resistance (R_{ct}) value determined for CrN45° electrode was 120 **Ω**, lower than that for CrN0°, CrN60° and CrN75° electrodes with values of 204, 237, and 409 **Ω**, respectively. The results indicate that the CrN45° electrode is electrochemically more active than the other samples deposited at different grazing angles. This implies that the deposition angle has a drastic influence on the electrochemical behavior of the CrN films. This can be explained by the morphology and the apparent porosity of the sample. The relative low charge transfer resistance ($\mathbf{R_{ct}}$) values are helpful to provide good electrochemical performance [35].

Table 6: EIS equivalent circuit fitting parameter values of the CrN electrodes.

	R_e (Ω)	Q (F)	R_{ct} (Ω)	W ($S.sec^{0.5}$)	B ($sec^{0.5}$)	Q_{pr} ($S.sec^{0.n}$)	n
0°	17.24	6.27E-8	204.5	0.003578	4.768E9	5.024E-6	0.8532
45°	18.06	0.007685	120.5	0.001956	2.353E5	5.113E-6	0.7833
60°	28.65	5.802E-4	237.57	0.005861	3.133E8	3.444E-5	0.5864
75°	19.8	6.28E-7	409.49	0.004907	2.378E9	9.583E-7	0.9443

Figure 18a shows cycling voltammograms (CV) of the CrN (0-75°) electrodes at a scan rate of 10 $mV.s^{-1}$. The CVs of CrN45° and CrN60° are bit distorted even at a low scan rate, which could indicate that the CrN deposit is resistive. In the case of CrN0° and CrN75°, the CVs do not show any capacitive behavior even at a low scan rate of 5 $mV.s^{-1}$ (not shown here), and the current is very weak, thus indicating a poor double-layer capacitance. This can be assigned to the dense structure of the CrN0° and CrN75° electrodes as observed by SEM and in agreement with EIS analyses. The effect of surface chemistry can be ruled out as already discussed in the XPS section. The CVs at different scan rates (10-100 $mV.s^{-1}$) of the CrN films, deposited at tilt angles of 45° and 60°, are presented in **Figures 18b and 18c**, respectively. At a low scan rate, both CVs exhibit small distortion, indicative of the resistivity nature of the deposit (more portably due to the increased oxygen amount in the films). However, at higher scan rates, the CrN45° and CrN60° electrodes display poor capacitance retention, which may be due to the porosity of the electrodes.

Galvanostatic charge-discharge curves at a current density of 0.4 $mA.cm^{-2}$ are depicted in **Figure 18d**. It can be seen that the CrN45° and CrN60° electrodes display an IR drop of 0.088 V and 0.192 V respectively, suggesting a superior electrical conductivity of CrN45°, as well as more accessible porosity

by the electrolyte. This is consistent with the CV and EIS results. Indeed, at the same scan rate, the CVs of the CrN60° electrode are more distorted than those of the CrN45° electrode.

The areal capacitance values were calculated from the charge-discharge curves at a current density of 0.4 $mA.cm^{-2}$. The values are 70.0 and 54.2 $mF.cm^{-2}$ for CrN45° and CrN60° electrodes, respectively. Such a difference cannot be due to the smaller thickness of CrN60° compared to CrN45°. Indeed, when the capacitance is normalized to the thickness, the volumetric capacitance of CrN 45° and CrN60° become 454.5 and 389.9 $F.cm^{-3}$, respectively.

Figures 18e and f depicts the variation of the areal capacitance versus scan rate and current density, respectively. It can be seen that the capacitance decreases with increasing the scan rate and current density, suggesting that parts of the surface are inaccessible at high scan rates and/or at fast charging-discharging rates. The difference of areal capacitance between the two electrodes can be attributed to the small differences in their thicknesses.

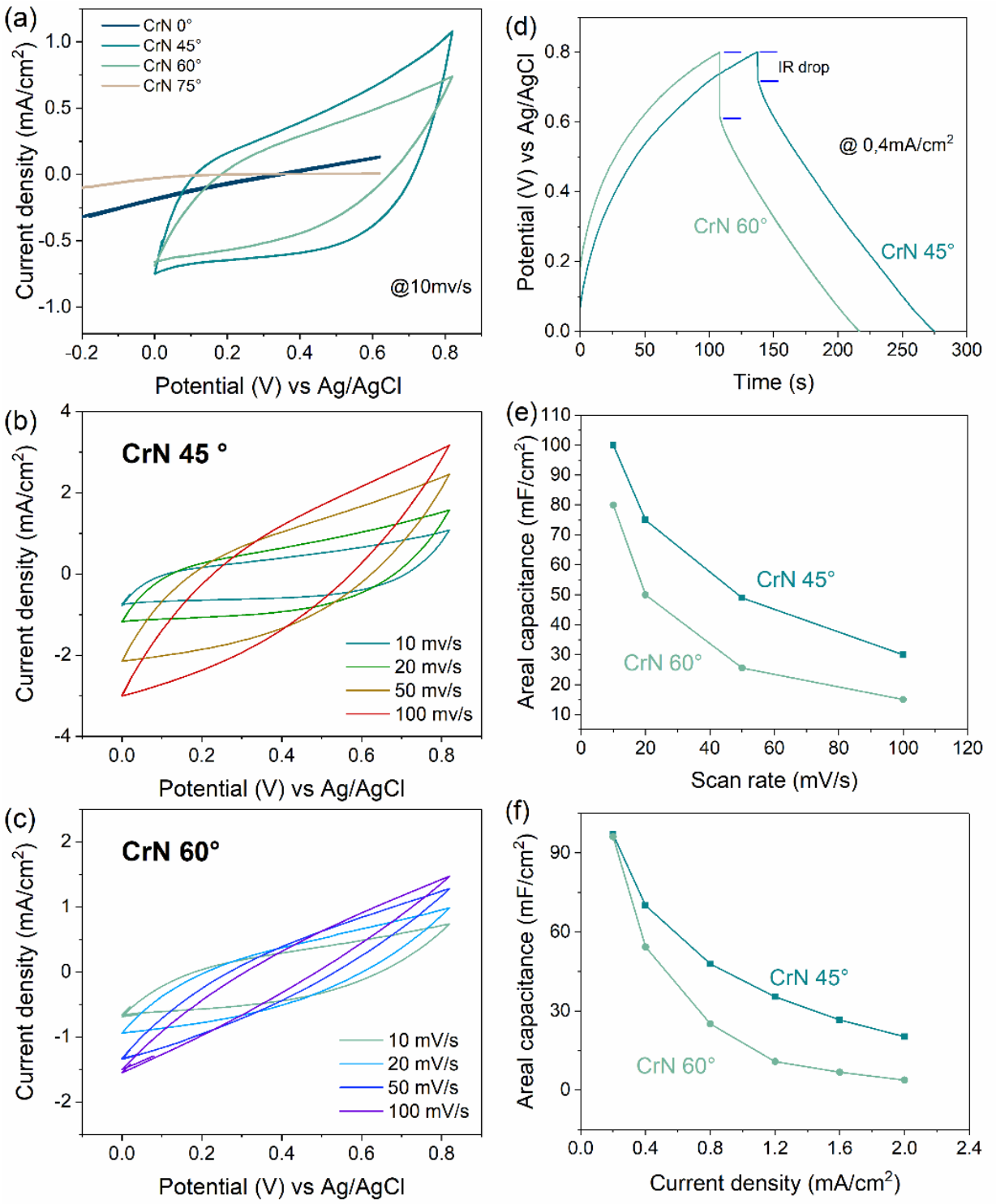

Figure 18: (a) Comparison of cyclic voltammograms of CrN electrodes in 0.5M H_2SO_4 at a scan rate of 10 mV.s $^{-1}$, (b) cyclic voltammograms of CrN45° at different scan rates and (c) cyclic voltammograms of CrN60° at different scan rates, (d) comparison of GCD curves at 0.4 mA cm^{-2} for CrN45° and CrN60° electrodes, (e) areal capacitance of CrN45° and CrN60° films versus scan rate, (f) areal capacitance of CrN45° and CrN60° films versus current density.

The capacity loss after 10,000 consecutive cycles at a scan rate of 100 $mV.s^{-1}$ is only 5.5%, as shown in Figure 7, indicative of a fair long-term electrochemical stability [6-8], which is even higher than those of transition metal nitride materials [36]. Such good electrochemical stability enables one to envision the use of CrN electrodes in micro-supercapacitors [8]. The sudden drop in capacitance at the ~5000 cycle could be due to day/night room temperature change.

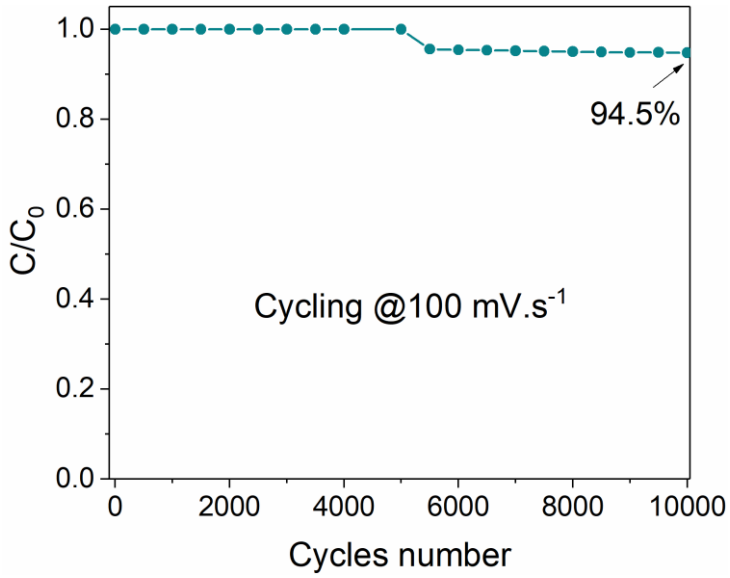

Figure 19: Cycling stability test of CrN45° film in 0.5M H_2SO_4 at a scan rate of 100 $mV.s^{-1}$.

From a practical point of view, the areal capacitance of 35.4 $mF.cm^{-2}$ at a current density of 1.2 $mA.cm^{-2}$ for the CrN45° electrode compares to 31.0 $mF\,cm^{-2}$ at 1.0 $mA.cm^{-2}$ for the porous CrN electrodes recently reported in [18] and 2.5 fold higher than the best CrN electrode deposited by sputtering (13 $mF.cm^{-2}$ at 1.0 $mA.cm^{-2}$) recently reported in [17]. When compared to other transition metal nitrides, the areal capacitance of our CrN electrodes is still much higher than for TiN electrodes (27 $mF.cm^{-2}$ at 1.0 $mA.cm^{-2}$) [37], HfN electrode (6 $mF{\cdot}cm^{-2}$ at 1.0 $mA{\cdot}cm^{-2}$) [38], or GaN membrane (21 $mF\ cm^{-2}$ at 0.1 $mA\ cm^{-2}$) [39] (**Table 7**).. Therefore, our CrN electrodes are competing quite well with the state of the art transition metal nitride thin film electrodes, not only in the term of cycling stability but also in the term of specific capacitance.

Table 7: Performances of CrN electrodes.

Electrodes	**Areal capacitance $mF.cm^{-2}$**	**Current density $mA.cm^{-2}$**	**references**
CrN-GLAD	35,4	1.2	This work
Porous CrN	31,0	1.0	[18]
CrN thin film	13	1.0	[17]
TiN	27	1.0	[36]
HfN	6	1.0	[37]
GaN	21	0.1	[38]

3.2. Integration of CrN thin film electrode in a planar symmetrical µSC

CrN 60° was chosen in this study to be integrated into the micro-device as shown in **Figure 20**. As the volumetric capacitance is close to each other for both orientations, we choose the more tilted sample, namely CrN 60°. Besides, due to the size of the device and to avoid deposition on the current collector side of the device, orientation of 60 ° was chosen as the safe angle to deposit the CrN on the device. Moreover, more than 95% of the 30 fabricated MSCs did not exhibit any short-circuit between the two electrodes, indicating the high reproducibility of the technological process. Furthermore, the electrodes are deposited without intentional heating of the silicon substrate. Therefore, our complete process is compatible with semiconductor technology.

Figure 20c illustrates the geometrical parameters of the unit cell. A 100 µm wide spacing was used to isolate the interdigitated electrodes (2 mm long/1.7 mm wide). The SEM cross-section of the CrN coated µSC is reported in **Figure 20d**, with a similar morphology with previous coatings.

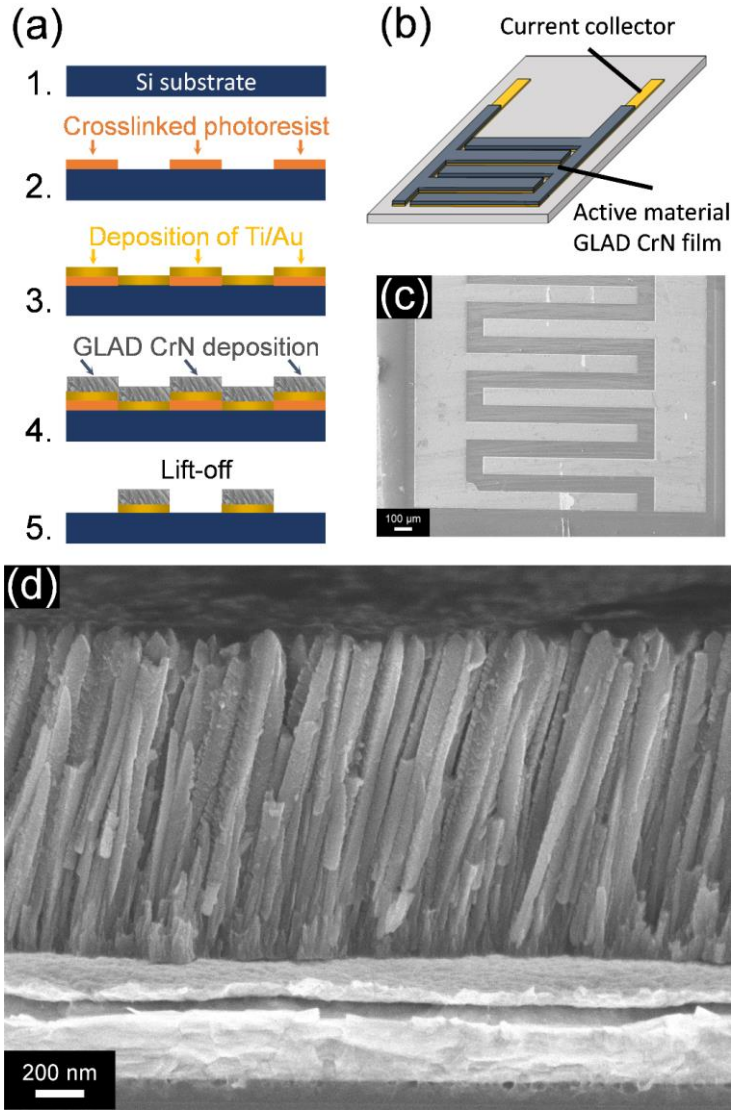

Figure 20: Micro-supercapacitor fabrication and design. (a) Schematic illustration of the fabrication process using the lift-off process of the active material (not to scale). Schematic (b) and optical image (c) of the micro-device. (d) Cross-section of the electrode observed with scanning electron microscopy.

3.2.1. Electrochemical properties of µSC

The CV plots of CrN based µSC were recorded at various scan rates from 0.01 to 10 $V.s^{-1}$ to test the rate capability of the µSC. Indeed, the integration of CrN on-chip µSCs allows decreasing the series resistance thus improving the power density of the microsystem [40].

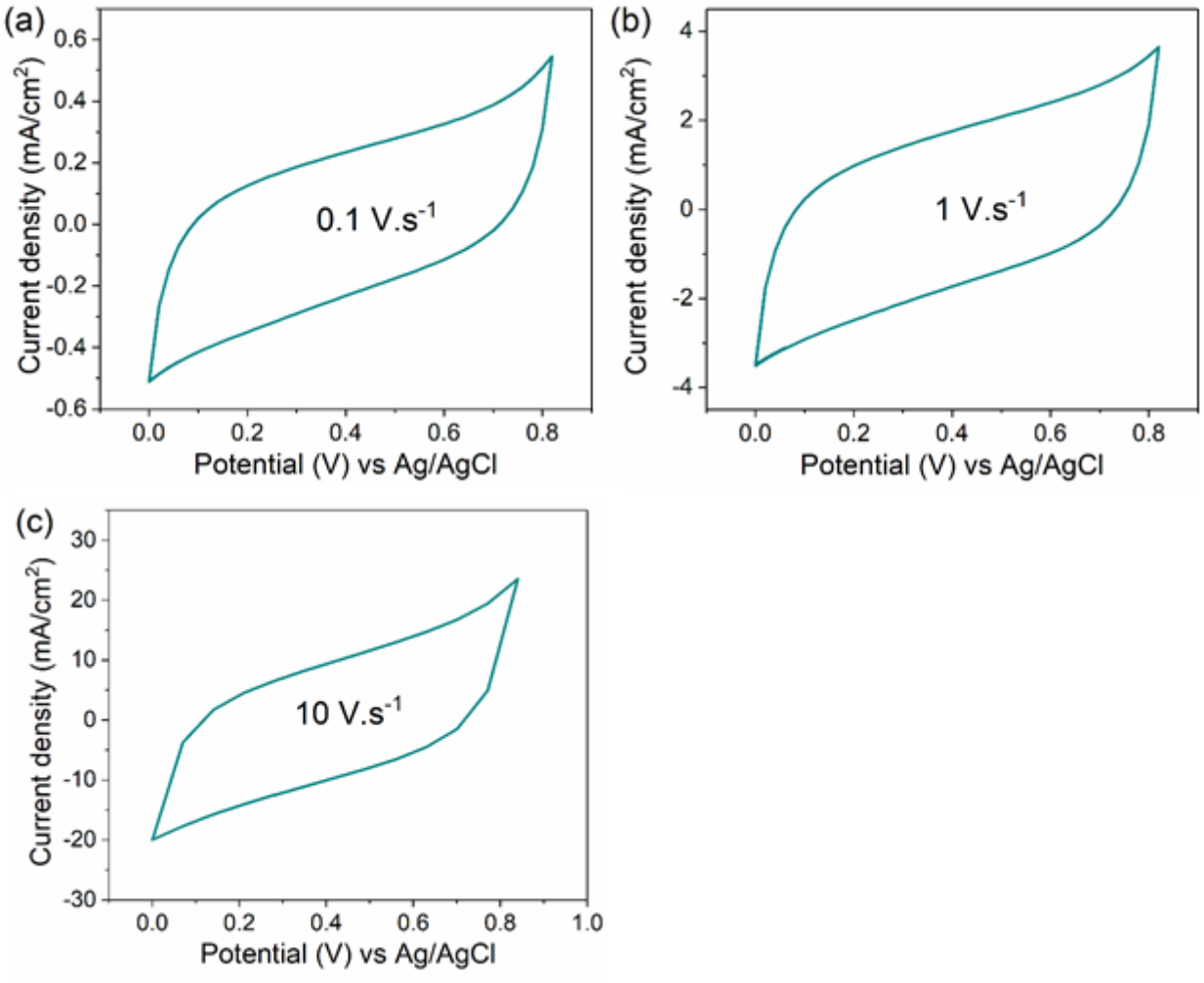

Figure 21: CVs obtained at scan rates of (a) 0.1, (b) 1 and (c) 10 $V.s^{-1}$ for CrN 60° based micro-supercapacitors device.

Electrochemical impedance spectroscopy was used to investigate the CrN micro-supercapacitor device. The shape of the Nyquist plots (**Figure 22**) confirms no short circuit between the electrodes, thus validating again the technological process. The electrolyte resistance between the two CrN electrodes is 13.0 Ω and the charge transfer resistance values (R_{ct}) determined for the symmetric micro-supercapacitors is 36.8 Ω.

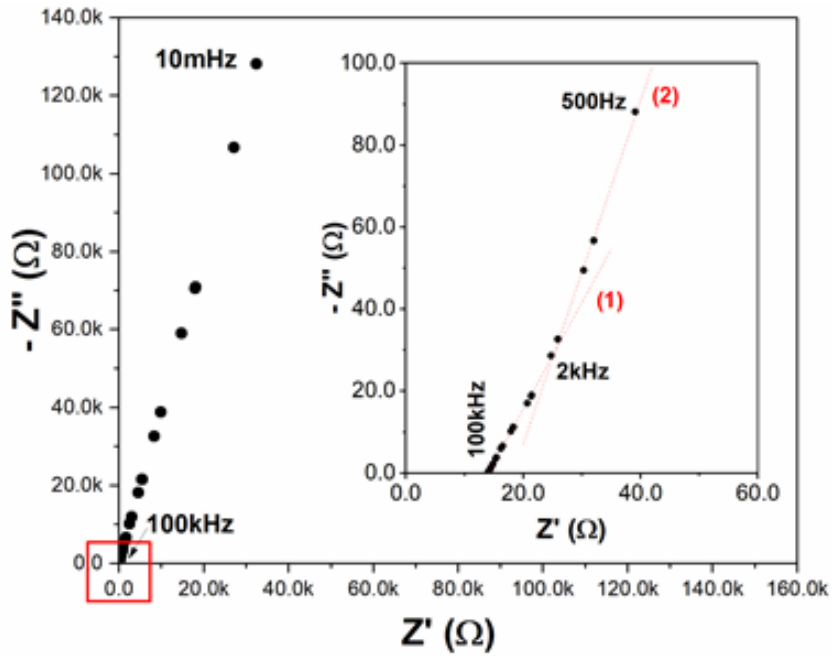

Figure 22: Nyquist plot of the CrN-based symmetric micro-supercapacitor (the inset shows the enlarged Nyquist plot at high-frequency region).

The galvanostatic charge-discharge curves at different current densities of the μSC in 0.5 M H_2SO_4 are displayed in **Figure 23a**. The areal capacitance measured at the lower current density (0.05 mA cm^{-2}) is 10.3 mF cm^{-2}. Since the surface area of a single electrode is less than 1/3 of the total surface of the micro-device, this capacitance value is in good agreement with the previous findings from the study of single electrodes. Indeed, a capacitance of 10.3 mF cm^{-2} for the μSC is 25% of that of the corresponding thin film (≈ 35.4 mF cm^{-2} per electrode), in agreement with surface ratio.

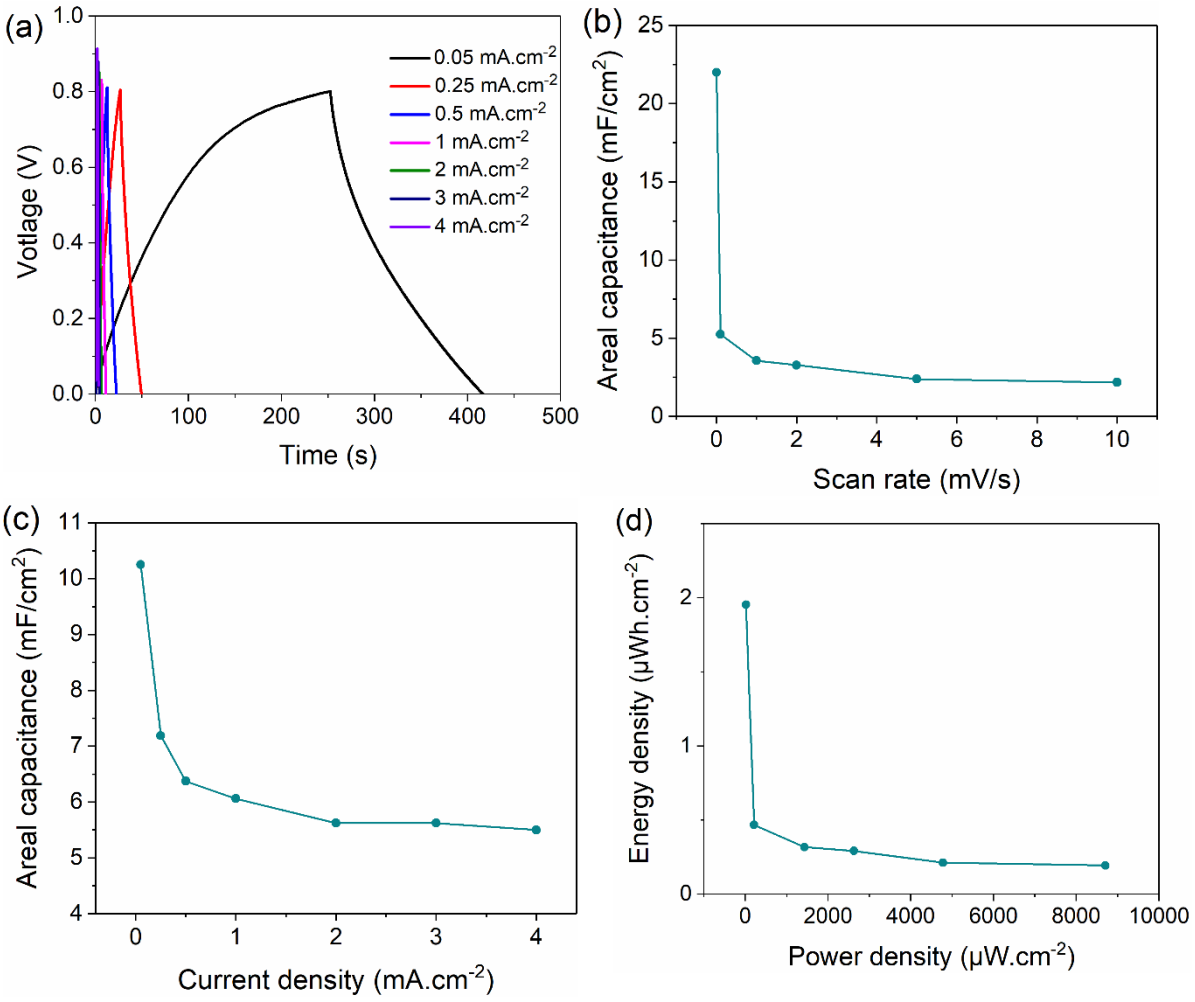

Figure 23: (a) GCD curves of CrN 60° based micro-supercapacitor at different current densities, (b) its areal capacitance versus scan rate and (c) its areal capacitance versus current density, (d) Ragone plot.

It can be seen that at a current density of 0.05 mA.cm^{-2}, the CrN60° based MSC displays an IR drop of 0.088 V versus 0.192 V for CrN60° thin film electrode (**Figure 18d**), indicating less resistance in series for the µSC. This is also the reason why the integrated CrN60° can be cycled at a higher scan rate compared to the same deposit tested in the three electrodes configuration. **Figure 23b and c** depicts the variation of the areal capacitance with scan rate and current density, respectively. The values of areal capacitances experience a drastic drop upon increasing the scan rate from 2 to 100 mV.s^{-1} (from 21.0 to 5.5 mF.cm^{-2}), whereas a relatively high capacitance level is retained over scan rates in the wide range of 0.1–10 V.s^{-1} (from 5.5 to 2.2 mF.cm^{-2}). The decrease in capacitance with a scan rate increase from 2 to 100 mV.s^{-1} occurs not only due to the limited ion diffusion in porous electrodes but also to the limitation from charge transfer rate for pseudo-capacitive electrodes. The same phenomenon happens for current densities in the range of 0.05-1 mA.cm^{-2} and 1- 4 mA.cm^{-2}. For the former current range, the areal

capacitance is stable around 6.0 and 5.5 mF. cm^{-2}, while it drops from 10.3 to 6.0 mF. cm^{-2} within the of 0.05- 1 $mA.cm^{-2}$ current range. Considering the thickness of the coating, the volumetric capacitance is stable around 40-45 F cm^{-3}.

The areal capacitance of the symmetric CrN/CrN based µSC is higher than the silicon chip CDC MSCs (1.5 $mF.cm^{-2}$ at 100 $mV.s^{-1}$) [41], and comparable to the PS–TiN in-chip device (5 $mF.cm^{-2}$) [36], photoresist derived carbon (3.2 mF cm^{-2} at 0.5 $mA.cm^{-2}$) [42], or asymmetric flexible MXene-reduced graphene oxide (2.4 mF cm^{-2} at 2 $mV.s^{-1}$) [43].

The maximum surface power density of the 1.3µm thick CrN60°/CrN60° symmetrical µSC was 8.7 $mW.cm^{-2}$ at an energy density of 0.2 $\mu Wh.cm^{-2}$ (**Figure 23d**). This energy can be increased up to 2 $\mu Wh.cm^{-2}$ while decreasing the power density to 20 $\mu W.cm^{-2}$. Although the energy density is impeded by the limited cell voltage (0.8 V) due to the use of the symmetrical device in the acidic electrolyte, the high values of power density depict the optimum geometry of our electrodes and micro-devices. The cycling stability test of the based µSC shows that 91.5% of initial capacitance was retained after 10000 cycles (**Figure 24**). This test reveals that the µSC CrN / CrN is stable, which ensures the long use of the µSC.

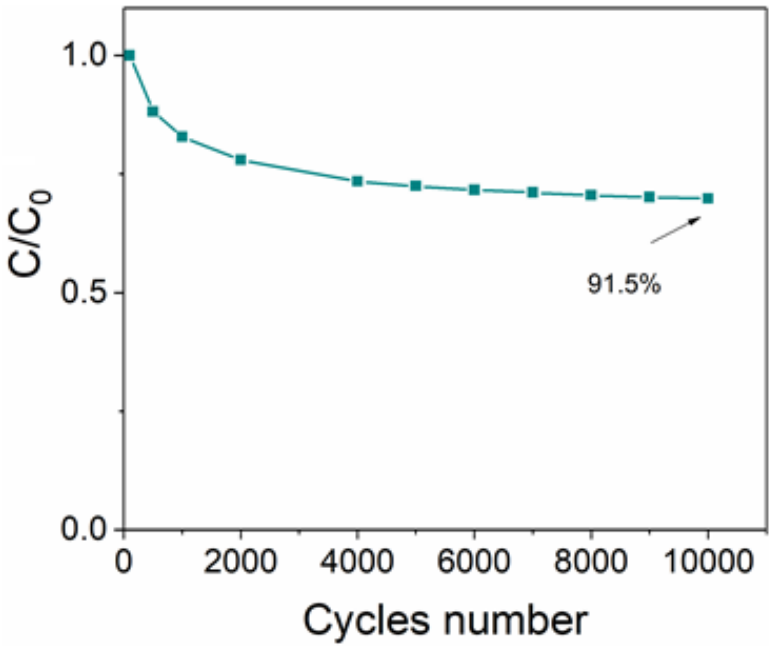

Figure 24: Cycling stability test of CrN based micro-supercapacitor at a scan rate of 1$V.s^{-1}$.

4. Conclusion

In this work, the GLAD deposition technique was used to deposit CrN films for use as electrodes for electrochemical capacitors. The films deposited at 0° and 75° are electrochemically inactive for charge storage, more probably due to inappropriate morphologies (too dense at 0° and unaccessible columns closed on the top at 75°), while films deposited at 45 and 60° exhibit a columnar morphology, with open voids that allow access for ion diffusion onto the electroactive interface, resulting in electrode with high specific capacitance (35.4 mF cm^{-2} at a current density of 1.2 $mA.cm^{-2}$) and long cycling life (94.5% of retention after 10.000 cycles). Besides, our symmetric on-chip micro-supercapacitor based on porous CrN60° demonstrate a maximum energy density of 2 $\mu Wh.cm^{-2}$ (15.3 $mWh.cm^{-3}$) at a power density of 20 $\mu W.cm^{-2}$ (0.15 $W.cm^{-3}$). Moreover, power densities can be increased up to 8.7 $mW.cm^{-2}$. Although preliminary, these first results open the way for the fabrication of on-chip CrN based micro-supercapacitors using GLAD deposition technique. Further work should aim at enlarging the cell voltage of the microdevice by coupling CrN as a positive electrode with another negative electrode such as vanadium nitride.

References

[1] K. Ait Aissa, A. Achour, J. Camus, L. Le Brizoual, P.-Y. Jouan, M.-A. Djouadi, Comparison of the structural properties and residual stress of AlN films deposited by dc magnetron sputtering and high power impulse magnetron sputtering at different working pressures, Thin Solid Films. 550 (2014) 264–267.

[2] E. Haye, J.L. Colaux, P. Moskovkin, J.-J. Pireaux, S. Lucas, Wide range investigation of duty cycle and frequency effects on bipolar magnetron sputtering of chromium nitride, Surf Coat. Technol. 350 (2018) 84–94.

[3] L. Bait, L. Azzouz, N. Madaoui, N. Saoula, Influence of substrate bias voltage on the properties of TiO 2 deposited by radio-frequency magnetron sputtering on 304L for biomaterials applications, Appl. Surf. Sci. 395 (2017) 72–77.

[4] Z. Ben Cheikh, F. El Kamel, O. Gallot-Lavallée, M.A. Soussou, S. Vizireanu, A. Achour, K. Khirouni, Hydrogen doped BaTiO 3 films as a solid-state electrolyte for micro-supercapacitor applications, J. Alloys Compd. 721 (2017) 276–284.

[5] J.F.M. Oudenhoven, Loïc. Baggetto, P.H.L. Notten, All-Solid-State Lithium-Ion Microbatteries: A Review of Various Three-Dimensional Concepts, Adv. Energy. Mater. 1 (2011) 10–33.

[6] J. Freixas, E. Eustache, P. Roussel, C. Brillard, D. Deresmes, N. Nuns, N. Rolland, T. Brousse, C. Lethien, Sputtered Titanium Nitride: A Bifunctional Material for Li-Ion Micro batteries, J. Electrochem. Soc. 162 (2015) A493–A500.

[7] P. Simon, Y. Gogotsi, Materials for electrochemical capacitors, Nature Mater. 7 (2008) 845–854.

[8] N.A. Kyeremateng, T. Brousse, D. Pech, Microsupercapacitors as miniaturized energy-storage components for on-chip electronics, Nature Nanotechnol. 12 (2017) 7–15.

[9] P. Huang, C. Lethien, S. Pinaud, K. Brousse, R. Laloo, V. Turq, M. Respaud, A. Demortière, B. Daffos, P.L. Taberna, B. Chaudret, Y. Gogotsi, P. Simon, On-chip and freestanding elastic carbon films for micro-supercapacitors, Science. 351 (2016) 691–695.

[10] M.-J. Lee, J.S. Kim, S.H. Choi, J.J. Lee, S.H. Kim, S.H. Jee, Y.S. Yoon, Characteristics of thin film supercapacitor with ruthenium oxide electrode and Ta_2O_{5+x} solid oxide thin film electrolyte, J Electroceram. 17 (2006) 639–643.

[11] A. Kumar, A. Sanger, A. Kumar, Y. Kumar, R. Chandra, Sputtered Synthesis of MnO_2 Nanorods as Binder Free Electrode for High Performance Symmetric Supercapacitors, Electrochim. Acta. 222 (2016) 1761–1769.

[12] A. Achour, R.L. Porto, M.-A. Soussou, M. Islam, M. Boujtita, K.A. Aissa, L. Le Brizoual, A. Djouadi, T. Brousse, Titanium nitride films for micro-supercapacitors: Effect of surface chemistry and film morphology on the capacitance, J. Power. Sources. 300 (2015) 525–532.

[13] A. Achour, M. Chaker, H. Achour, A. Arman, M. Islam, M. Mardani, M. Boujtita, L. Le Brizoual, M.A. Djouadi, T. Brousse, Role of nitrogen doping at the surface of titanium nitride thin films towards capacitive charge storage enhancement, Journal. Power. Sources. 359 (2017) 349–354.

[14] A. Achour, R. Lucio-Porto, S. Solaymani, M. Islam, I. Ahmad, T. Brousse, Reactive sputtering of vanadium nitride thin films as pseudo-capacitor electrodes for high areal capacitance and cyclic stability, J Mater Sci: Mater Electron. 29 (2018) 13125–13131.

[15] A. Achour, R. Lucio-Porto, M. Chaker, A. Arman, A. Ahmadpourian, M.A. Soussou, M. Boujtita, L. Le Brizoual, M.A. Djouadi, T. Brousse, Titanium vanadium nitride electrode for micro-supercapacitors, Electrochem. Comm. 77 (2017) 40–43.

[16] S. Bouhtiyya, R. Lucio Porto, B. Laïk, P. Boulet, F. Capon, J.P. Pereira-Ramos, T. Brousse, J.F. Pierson, Application of sputtered ruthenium nitride thin films as electrode material for energy-storage devices, Scripta Mater. 68 (2013) 659–662.

[17] B. Wei, H. Liang, D. Zhang, Z. Wu, Z. Qi, Z. Wang, CrN thin films prepared by reactive DC magnetron sputtering for symmetric supercapacitors, J. Mater. Chem. A. 5 (2017) 2844–2851.

[18] B. Wei, G. Mei, H. Liang, Z. Qi, D. Zhang, H. Shen, Z. Wang, Porous CrN thin films by selectively etching CrCuN for symmetric supercapacitors, J. Power Sources. 385 (2018) 39–44.

[19] K. Robert, C. Douard, A. Demortière, F. Blanchard, P. Roussel, T. Brousse, C. Lethien, On-Chip Interdigitated Micro-Supercapacitors Based on Sputtered Bifunctional Vanadium Nitride Thin Films with Finely Tuned Inter- and Intracolumnar Porosities, Adv. Mater. Tech. 3 (2018) 1800036.

[20] A. Besnard, N. Martin, C. Millot, J. Gavoille, R. Salut, Effect of sputtering pressure on some properties of chromium thin films obliquely deposited, IOP Conf. Ser.: Mater. Sci. Eng. 12 (2010) 012015.

[21] B. Bouaouina, C. Mastail, A. Besnard, R. Mareus, F. Nita, A. Michel, G. Abadias, Nanocolumnar TiN thin film growth by oblique angle sputter-deposition: Experiments vs. simulations, Materials & Design. 160 (2018) 338–349.

[22] X. Xu, M. Arab Pour Yazdi, J.-B. Sanchez, A. Billard, F. Berger, N. Martin, Exploiting the dodecane and ozone sensing capabilities of nanostructured tungsten oxide films, Sensors and Actuators B: Chemical. 266 (2018) 773–783.

[23] G. Greczynski, J. Jensen, J. Böhlmark, L. Hultman, Microstructure control of CrNx films during high power impulse magnetron sputtering, Surf. Coat. Technol. 205 (2010) 118–130.

[24] J. Dervaux, P.-A. Cormier, S. Konstantinidis, P. Moskovkin, S. Lucas, R. Snyders, Nanostructured Ti thin films by combining GLAD and magnetron sputtering: a joint experimental and modelling study, 22nd International Symposium on Plasma Chemistry. (2015) 4.

[25] J. Dervaux, P.-A. Cormier, S. Konstantinidis, R. Di Ciuccio, O. Coulembier, P. Dubois, R. Snyders, Deposition of porous titanium oxide thin films as anode material for dye sensitized solar cells, Vacuum. 114 (2015) 213–220.

[26] J. Lintymer, J. Gavoille, N. Martin, J. Takadoum, Glancing angle deposition to modify microstructure and properties of sputter deposited chromium thin films, Surf. Coat. Technol. 174–175 (2003) 316–323.

[27] A. Barranco, A. Borras, A.R. Gonzalez-Elipe, A. Palmero, Perspectives on oblique angle deposition of thin films: From fundamentals to devices, Prog. Mater. Sci. 76 (2016) 59–153.

[28] A. Trenczek-Zajac, M. Radecka, K. Zakrzewska, A. Brudnik, E. Kusior, S. Bourgeois, M.C.M. de Lucas, L. Imhoff, Structural and electrical properties of magnetron sputtered Ti(ON) thin films: The case of TiN doped in situ with oxygen, J. Power. Sources. 194 (2009) 93–103.

[29] N.K. Ponon, D.J.R. Appleby, E. Arac, P.J. King, S. Ganti, K.S.K. Kwa, A. O'Neill, Effect of deposition conditions and post deposition anneal on reactively sputtered titanium nitride thin films, Thin Solid Films. 578 (2015) 31–37.

[30] I. Milošev, H.-H. Strehblow, B. Navinšek, Comparison of TiN, ZrN and CrN hard nitride coatings: Electrochemical and thermal oxidation, Thin Sol. Films. 303 (1997) 246–254.

[31] H.C. Barshilia, N. Selvakumar, B. Deepthi, K.S. Rajam, A comparative study of reactive direct current magnetron sputtered CrAlN and CrN coatings, Surf. Coat. Technol. 201 (2006) 2193–2201.

[32] B. Das, M. Behm, G. Lindbergh, M.V. Reddy, B.V.R. Chowdari, High performance metal nitrides, MN (M=Cr, Co) nanoparticles for non-aqueous hybrid supercapacitors, Adv. Powder Technol. 26 (2015) 783–788.

[33] Y. Wu, F. Ran, Vanadium nitride quantum dot/nitrogen-doped microporous carbon nanofibers electrode for high-performance supercapacitors, J. Power. Sources. 344 (2017) 1–10.

[34] P.R. Jadhav, M.P. Suryawanshi, D.S. Dalavi, D.S. Patil, E.A. Jo, S.S. Kolekar, A.A. Wali, M.M. Karanjkar, J.-Hyeok. Kim, P.S. Patil, Design and electro-synthesis of 3-D nanofibers of MnO_2 thin films and their application in high performance supercapacitor, Electrochim. Acta. 176 (2015) 523–532.

[35] H. Shen, B. Wei, D. Zhang, Z. Qi, Z. Wang, Magnetron sputtered NbN thin film electrodes for supercapacitors, Mater. Lett. 229 (2018) 17–20.

[36] K. Grigoras, J. Keskinen, L. Grönberg, E. Yli-Rantala, S. Laakso, H. Välimäki, P. Kauranen, J. Ahopelto, M. Prunnila, Conformal titanium nitride in a porous silicon matrix: A nanomaterial for in-chip supercapacitors, Nano Energy. 26 (2016) 340–345.

[37] B. Wei, H. Liang, D. Zhang, Z. Qi, H. Shen, Z. Wang, Magnetron sputtered TiN thin films toward enhanced performance supercapacitor electrodes, Mater. Renewable Sustain Energy. 7 (2018).

[38] Z. Gao, Z. Wu, S. Zhao, T. Zhang, Q. Wang, Enhanced capacitive property of HfN film electrode by plasma etching for supercapacitors, Mater. Lett. 235 (2019) 148–152.

[39] L. Zhang, S. Wang, Y. Shao, Y. Wu, C. Sun, Q. Huo, B. Zhang, H. Hu, X. Hao, One-step fabrication of porous GaN crystal membrane and its application in energy storage, Sci. Rep. 7 (2017).

[40] D. Pech, M. Brunet, T.M. Dinh, K. Armstrong, J. Gaudet, D. Guay, Influence of the configuration in planar interdigitated electrochemical micro-capacitors, J. Power Sources. 230 (2013) 230–235.

[41] P. Huang, M. Heon, D. Pech, M. Brunet, P.-L. Taberna, Y. Gogotsi, S. Lofland, J.D. Hettinger, P. Simon, Micro-supercapacitors from carbide derived carbon (CDC) films on silicon chips, J. Power Sources. 225 (2013) 240–244.

[42] B. Hsia, M.S. Kim, M. Vincent, C. Carraro, R. Maboudian, Photoresist-derived porous carbon for on-chip micro-supercapacitors, Carbon. 57 (2013) 395–400.

[43] C. Couly, M. Alhabeb, K.L. Van Aken, N. Kurra, L. Gomes, A.M. Navarro-Suárez, B. Anasori, H.N. Alshareef, Y. Gogotsi, Asymmetric Flexible MXene-Reduced Graphene Oxide Micro-Supercapacitor, Adv. Elect. Mater. 4 (2018) 1700339.

[44] M. Arif, A.Sanger, A. Singh, Sputter deposited chromium nitride thin electrodes for supercapacitor applications. Mater. Lett, 220, (2018), 213-217.

[45] Z. Qi, B. Wei, J. Wang, Y. Yang, Z. Wang, Nanostructured porous CrN thin films by oblique angle magnetron sputtering for symmetric supercapacitors, Journal of Alloys and Compounds, 806 (2019) 953-959.

Chapter 3. High performance of 3D silicon nanowires array@CrN for electrochemical capacitors

1. Introduction

Electrochemical capacitors (ECs), have attracted increasing attention as a potential candidate for energy storage and conversion due to their high power density and long cycling life compared to batteries and electrolytic capacitors [1-4]. Supercapacitors can be classified into two categories: electrochemical double-layer supercapacitors (EDLCs) and pseudo-capacitors [5, 6]. The second category (pseudo-capacitors) which are widely common for transition metal oxides and polymers, offer high specific capacitance but dotted with moderate cyclic stability and low power density which can be limiting for some applications, where both high power density and long cycling life stability are needed [1].

Recently, silicon nanowires (SiNWs) have been investigated as electrodes in electrochemical capacitors with a special focus on their use as the future on-chip micro-supercapacitors [7-10]. However, the rapid oxidation of silicon surface and the degradation of SiNWs during electrochemical cycling in aqueous electrolytes is the main obstacle for their wide application in the field of ECs and micro-supercapacitors [11, 12]. Nonetheless, this limitation can be overcome by the growth of nanostructures onto the SiNWs surface to increase the specific capacitance without scarifying too much the power density and cycling stability of SiNWs. For example, Alper et al. [7] have fabricated silicon carbide/SiNWs composites with enhanced capacitive behavior and higher capacitance values. Furthermore, carbon/SiNWs have also been reported as composites for ECs with good capacitance and improved cycling life stability [11].

Transition metal nitrides (TMNs) including TiN [13-15], VN [16-18], Mo_2N [19] seem to be a suitable choice due to their high specific capacitance, excellent electrical conductivity and electrochemical stability. Among these TMNs, chromium nitride (CrN) [20, 21] has been recently studied as a promising electrode material for ECs, owing to its excellent conductivity and electrochemical stability [21]. Therefore, coupling the high conductivity of the CrN combined with the large surface area of SiNWs can improve the electrochemical performance and thereby produce enhanced capacitance.

In this chapter, we report the electrochemical investigation of silicon nanowires, coated with CrN layers as electrode materials for ECs. The CrN layers with different thicknesses were grown on SiNWs by magnetron sputtering using the one-step process. The areal capacitance of SiNWs@CrN was enhanced by 116 fold compared to that of pristine SiNWs in 0.5 M H_2SO_4 electrolyte, with excellent cycling stability

over 15000 cycles. These results demonstrate that coating SiNWs with TMNs such as CrN can push forward toward the use of SiNWs in micro-supercapacitors.

2. Silicon nanowires as supercapacitors electrode material

Over the past years, the development of high-performance µ-SC has attracted considerable attention. Most µ-SC have been developed with various carbon-based materials such as graphene or pseudo-capacitive materials such as MnO_2, NiO and RuO_2. However, their integration in microelectronic devices stills the main obstacle for its commercial application. In this context, SiNWs have been studied with the attempt to use it as electrode materials for SC application because of their high surface area and quasi-ideal double-layer capacitive behavior [7-12]. Besides, the low cost, abundance and the nontoxic nature of silicon make SiNWs potential candidates for supercapacitors application [1-10]. Moreover, only a few reports exist on the use of SiNWs as supercapacitor electrode material according to our knowledge. Recently, Thissandier group have reported a detailed study on SiNWs as µSC electrode material in organic, ionic or an ionic-organic mixture electrolytes to avoid corrosion of nanowires [8-10]. However, SiNWs-based µ-SCs exhibit a moderate specific capacitance (in the range of 10 to 440 $\mu F.cm^{-2}$) [10]. This capacity value is not adequate for powering micro-electronic devices.

Most recently, a new strategy based on the post-coating of SiNWs with thin films of highly capacitive and pseudo-capacitive materials allows improving the electrochemical performances of the wires SiNWs [1, 7, 11, 12]. Ortaboy et al. have reported the fabrication of carbonized porous silicon nanowires modified with layers of manganese oxide (MnOx) (**Figure 25**) [1]. The prepared electrode exhibits a high specific capacitance of 635 $F.g^{-1}$, a high power density of 25 kW kg^{-1}, a high energy density of 261 Wh kg^{-1} and good cyclic stability after 10,000 cycles.

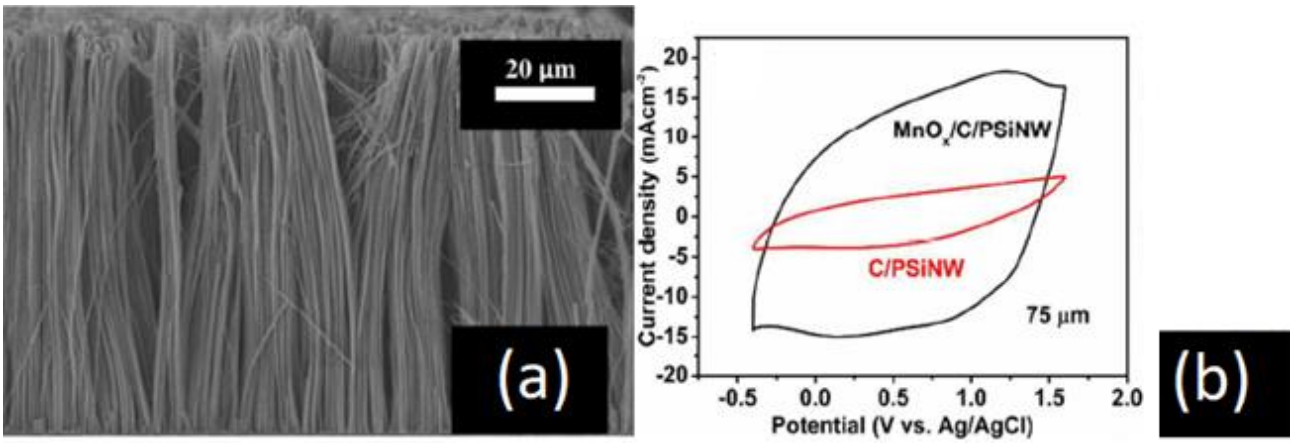

Figure 25: (a) SEM image and (b) CVs at various scan rates of carbonized silicon nanowires modified by MnOx [1].

Devarapalli et al. have reported the coating of vertically aligned SiNWs with carbon layers via a simple hydrothermal process using glucose as the carbon precursor (**Figure 26**). The measured capacity is 25.64 mF.cm^{-2} with good stability up to 25 000 cycles [11].

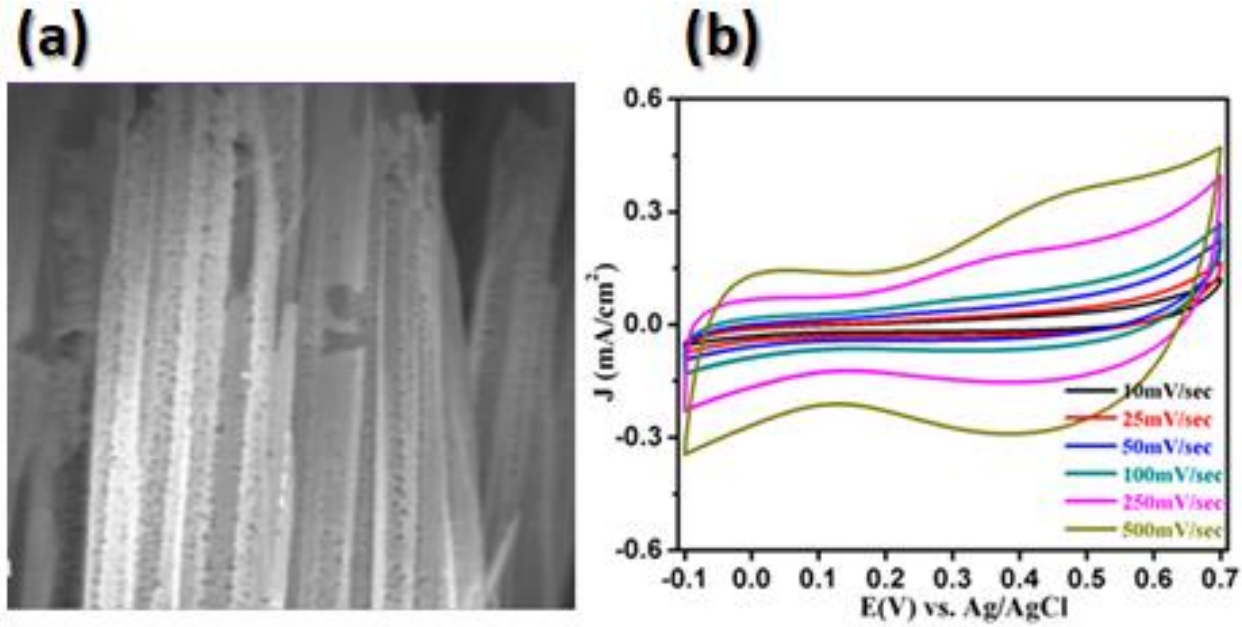

Figure 26: (a) SEM image and (b) CVs at various scan rates of carbon-coated silicon nanowires [11].

Alper et al. have reported the fabrication of silicon nanowires modified with silicon carbide (SiC) layers exhibiting a high areal capacitance of 1.7 mF.cm^{-2} [7] (**Figure 27**).

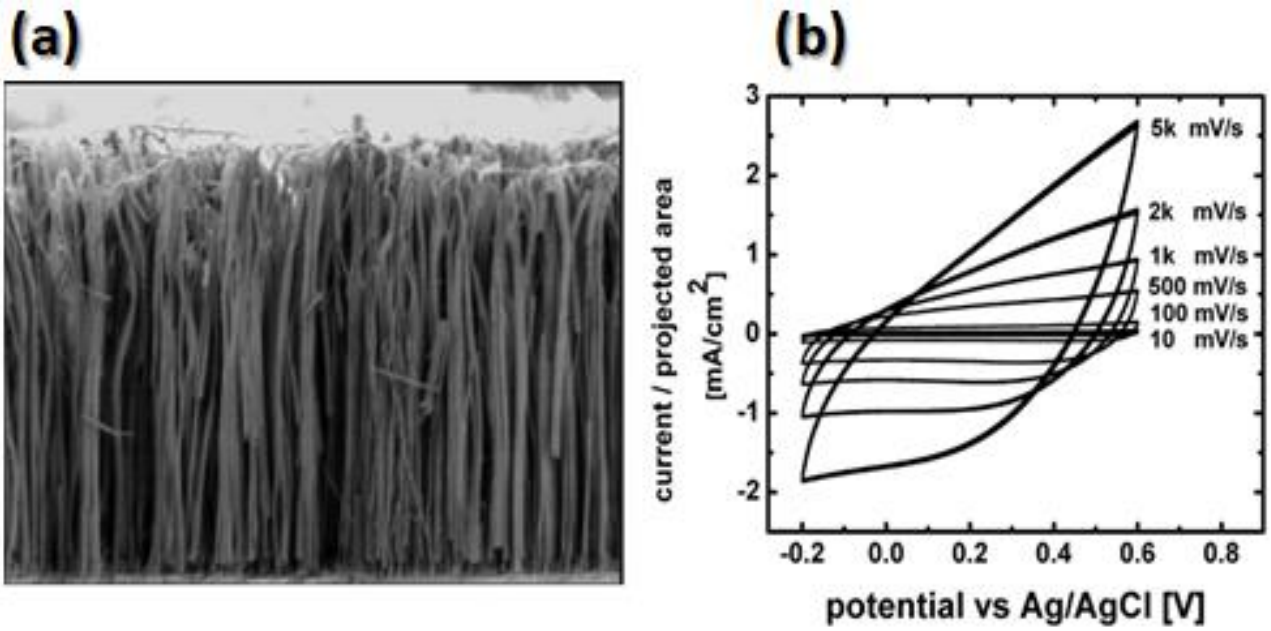

Figure 27: (a) SEM image and (b) CVs at various scan rates of SiC-coated silicon nanowires [7].

Most recently, silicon nanowires synthesized by chemical vapor deposition (CVD) via the VLS mechanism modified by MnO_2 (**Figure 28**) have been reported exhibit good areal capacitance of 13.38 $mF.cm^{-2}$ [12].

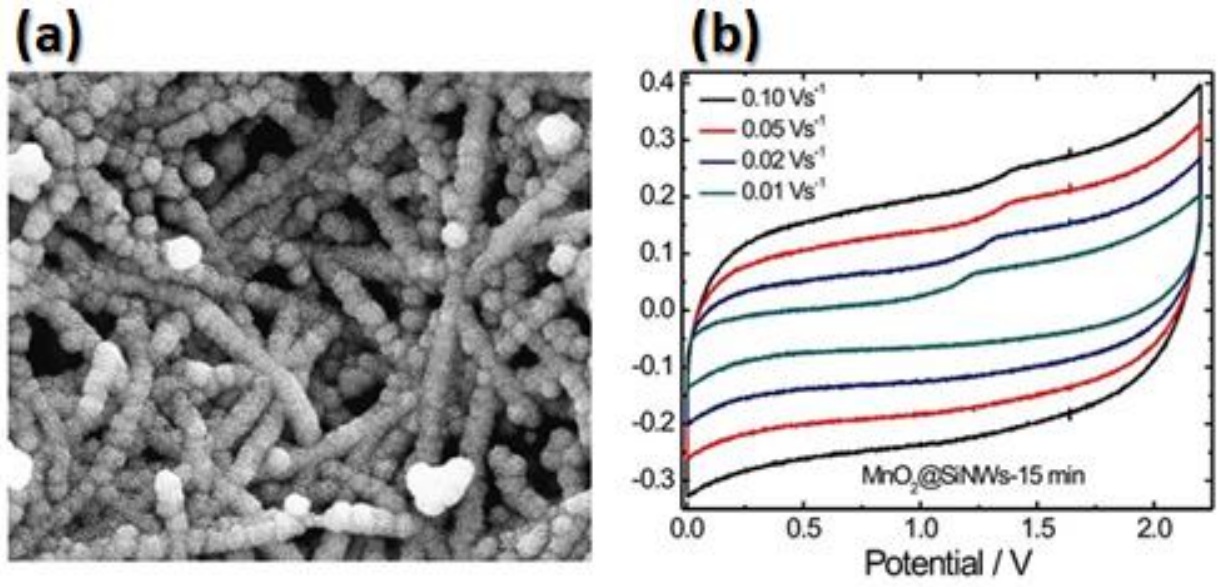

Figure 28: (a) SEM image and (b) CVs at various scan rates of MnO_2-coated silicon nanowires [12].

3. Limitations of the use of silicon nanowires as electrode

As reported above, silicon nanowires exhibit a high surface area which makes them a promising supercapacitor electrode material. However, the rapid oxidation of the silicon surface and the reactivity of silicon nanowires in aqueous electrolytes limit their use as electrode materials for supercapacitors [1, 7, 11, 12], and their application is only possible in organic and ionic liquid-based electrolytes.

4. Objectives

To overcome these limitations, two strategies were proposed to inhibit the chemical instability of the wires: i) several studies have shown that SiNWs-based electrodes exhibit good stability and quasi-ideal capacitive behavior in an organic electrolyte composed of Tetraethylammonium tetrafluoroborate (NEt_4BF_4) and in propylene carbonate (PC) [10]. ii) Post-coating SiNWs with carbon [11], silicon carbide [7] or nano-flakes of MnO_2 [212] allows improving the electrochemical stability of SiNWs.

The main advantage of organic electrolytes is the electrochemical stability window (2-3 V) which stores a large amount of energy. However, the use of organic electrolytes remains limited due to their lower ionic conductivity (0.05 $S.cm^{-1}$), high cost compared to aqueous electrolytes, high flammability and toxicity. Thus, post-coating SiNWs with highly pseudo-capacitive of chromium nitride (CrN) should have advantages such as high conductivity combined with the large surface area.

5. Experimental

The growth of SiNWs and the deposition of CrN were carried out in collaboration with the two laboratories; Department of Microelectronics and Microsensors, Rennes (France) and of the Interdisciplinary Laboratory of Electronic Spectroscopy (LISE), Namur (Belgium).

5.1. Fabrication of silicon nanowires SiNWs on a silicon wafer

Single-side polished silicon (100) oriented n-type wafers (arsenic-doped, 0.001-0.005 $Ohm.cm^{-1}$ resistivity) were used as substrate. The substrate was degreased in acetone and isopropyl alcohol, rinsed with Milli-Q water, and cleaned in a piranha solution (3:1 concentrated H_2SO_4/ 30% H_2O_2) for 15 min at 80 °C followed by copious rinsing with Milli-Q water. The surface was further dried under a stream of nitrogen. Silicon nanowires (Si NWs) were prepared using the vapor-liquid-solid (VLS) mechanism [23].

The process is based on metal-catalyst-directed chemical vapor deposition of silicon. First, a thin film of gold (4 nm thick) was thermally evaporated on the Si substrate. Gold nanoparticles were obtained on the surface by metal dewetting. In a second step, the gold-coated surface is exposed to the silane gas at a pressure of 0.4 T (flow rate equals 40 sccm) at 500 °C for 60 min leading to the growth of Si NWs.

*5.2.*Deposition of CrN onto the SiNWs

Chromium nitride (CrN) layers were deposited onto the SiNWs array by bipolar magnetron sputtering [22]. The use of bipolar sputtering (Magpuls QP-1000/20 10 kW pulse unit) with two chromium targets (7.5 × 35 cm, 99.99% purity, from Neyco), instead of conventional DC sputtering is beneficial for well-crystallized nanostructures. The current was set at 5 A, with a duty cycle of 75% and a frequency of 1250 Hz. The deposition was achieved in Ar/N_2 gas mixture (150/120 sccm) at a pressure of 5 mTorr (0.66 Pa). Three deposition times were tested namely 175, 210 and 350 s to obtain CrN nanostructures with different thicknesses. The deposition times correspond to equivalent thicknesses of 290, 550 and 900 nm, as measured on a flat silicon substrate set in the chamber, using a stylus profilometer.

6. Results and discussion

6.1.Structural and surface characterization

The surface morphologies of the SiNWs and SiNWs-CrN electrodes are evaluated by SEM images as shown in **Figure 29**. **Figure 29a** displays the top view SEM image of SiNWs grown on a silicon wafer, revealing a high density of nanowires with an average diameter in the range of 30-80 nm.

(**Figure 29 b-d**) reveals that the SiNWs are covered uniformly with small cubic CrN crystallites. It can be also noticed a continuous increase of the CrN film thickness on the SiNWs substrate upon increasing deposition time. Such results are expected to have an impact on the specific capacitance of SiNWs-CrN electrodes. As the deposition time increases, the SiNWs tend to stand up: more ends of SiNWs are visible in top view. This effect can be attributed to stress generated during the deposition due to the misfit between CrN and Si nanowires [24]. In our case, the nanostructures are deposited on silicon substrates, which means that material quantity available is very low, and therefore, in contrast to powder, the Brunauer-Emmett-Teller (BET) analysis is not possible. The only possible way to estimate the surface area is from SEM images.

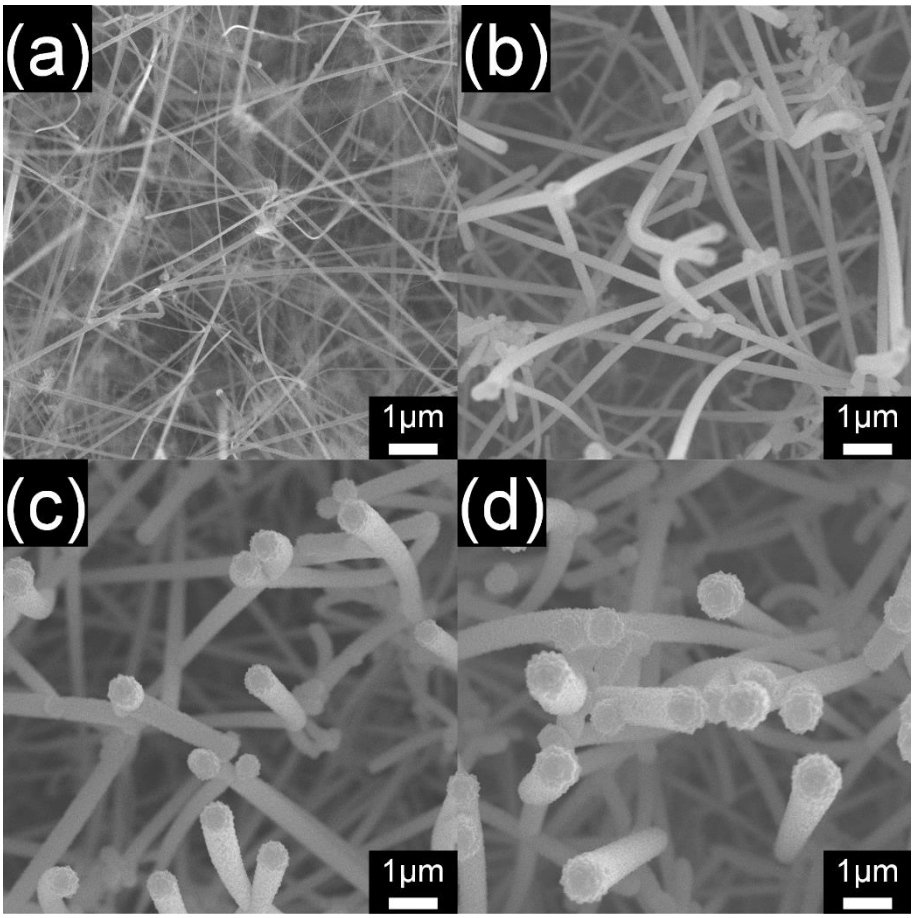

Figure 29: Top view SEM images of (a) raw SiNWs, (b) SiNWs-CrN 290 nm, (c) SiNWs-CrN 550 nm and (d) SiNWs-CrN 900 nm.

6.2.Physico-chemical characterization

The formation of CrN crystallites is confirmed by XRD measurement (**Figure 30**). The pristine SiNWs exhibit three diffraction peaks which can be assigned to silicon and gold nanoparticles (used for the SiNWs growth). XRD patterns of the SiNWs-CrN electrodes with different CrN thicknesses show the presence of two broad peaks at 37.4° and 43.1°, with a decrease of Si (111) peak intensity. This two distinct peaks can be assigned to the (111) and (200) diffraction planes of cubic CrN [25, 26].

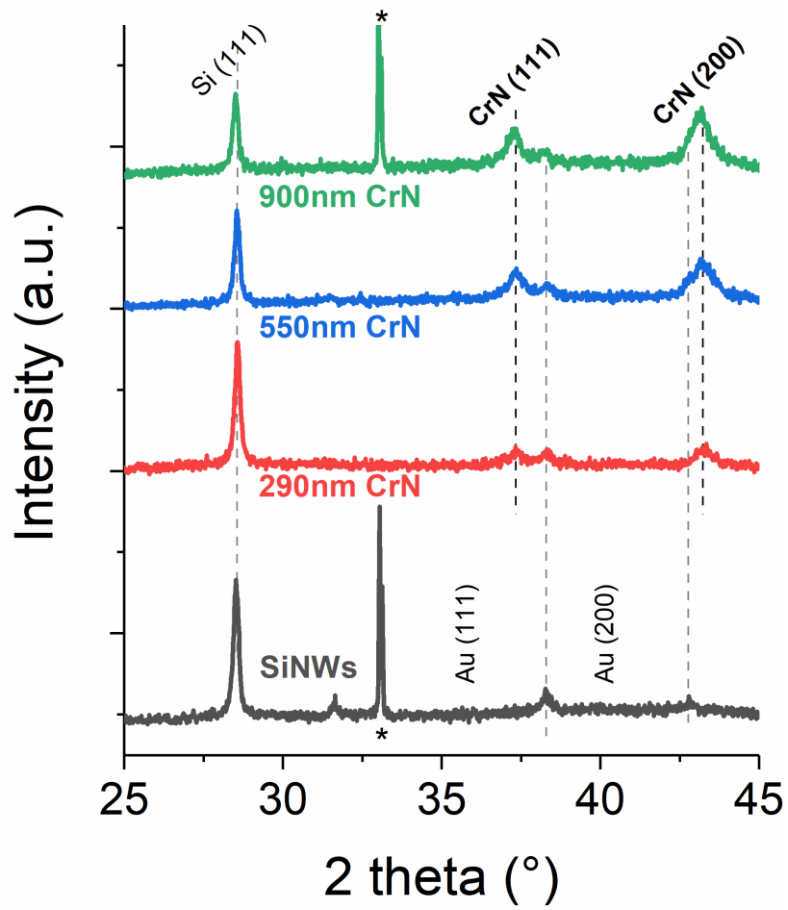

Figure 30: XRD pattern of SiNWs coated with CrN thin layers. The (*) corresponds to forbidden Si reflection, due to multiple diffractions in the Si substrate [32].

The surface chemistry compositions were investigated by XPS analyses (**Figure 31**). The surface of the as-grown SiNWs consists of Si/SiO_2, is confirmed by Si 2p and O 1s core-level spectra (**Figure 31a-b**). The high-resolution XPS spectrum of the Si 2p contains three contributions, centred at 99.3, 100.0 and 103.2eV attributed to Si $2p_{3/2}$, Si $2p_{1/2}$ and SiO_2, respectively [27]. The silicon oxide formation is also attested with a major peak at 532.6 eV (Figure 7b) [28]. These results are in good accordance with previously reported data [29]. Once the SiNWs are coated with CrN layers, the Si 2p signal vanishes while Cr 2p and N 1s signals appear, indicating a homogeneous coating of the analyzed surface (**Figure 31c-d**). The high-resolution XPS spectrum of Cr 2p signal consists of two major peaks due to Cr $2p_{3/2}$ and Cr $2p_{1/2}$ spin orbit coupling. The Cr $2p_{3/2}$ level can be fitted with three peaks centred at 574.3, 575.3 and 576.6 eV assigned to CrN, Cr (O, N) and Cr_2O_3, respectively [30].

The surface oxidation of chromium is confirmed by a contribution at 531.0 eV on O 1s level. Such surface oxidation is expected, as no sample etching is done before the analysis. The formation of CrN is attested

on the N 1s core level spectrum (**Figure 31c**) with a major contribution at 396.4 eV in addition to oxy-nitride formation detected at 398.3 eV [30, 31].

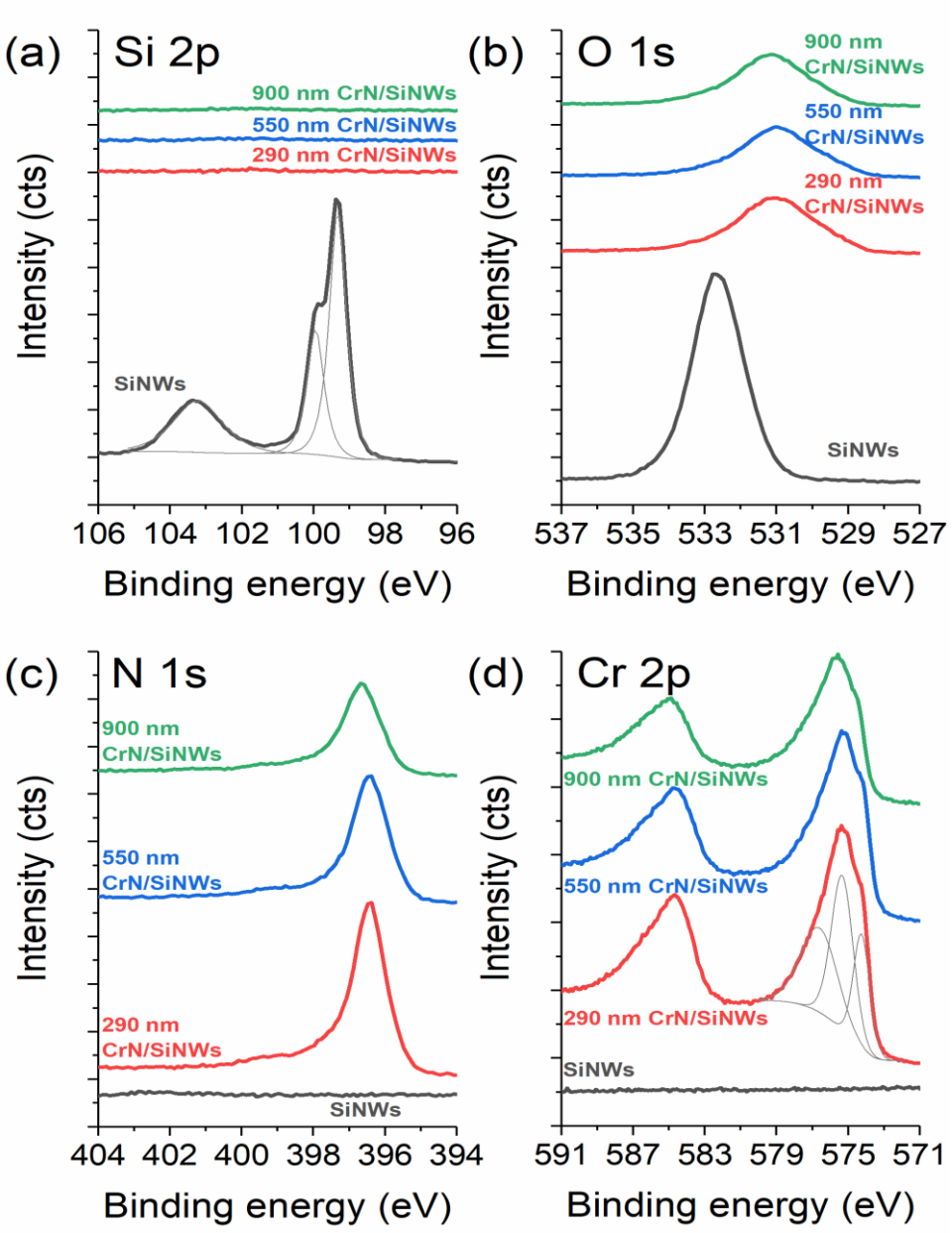

Figure 31: XPS analysis of SiNWs-CrN electrode materials: High resolution XPS spectra of (a) Si 2p, (b) O 1s, (c) N 1s and (d) Cr 2p core levels.

The SiNWs-CrN substrate was further characterized by transmission electron microscopy (TEM) (**Figure 32**). TEM images showed a herringbone structure due to the deposition of CrN on SiNWs. This peculiar nanostructure, which contains highly nanoporous channels, is expected to contribute to the electrode capacitance enhancement. The electron diffraction (ED) pattern of a silicon nanowire coated with CrN (500 nm) confirms the crystallinity of the CrN layer on the SiNW. The ED pattern exhibits multiples rings around the central spot, characteristic of the polycrystalline nature of the CrN film. The indexation of

these rings revealed the cubic structure of CrN film (Space group 225, $Fm\bar{3}m$). These results are in agreement with the XRD analyses.

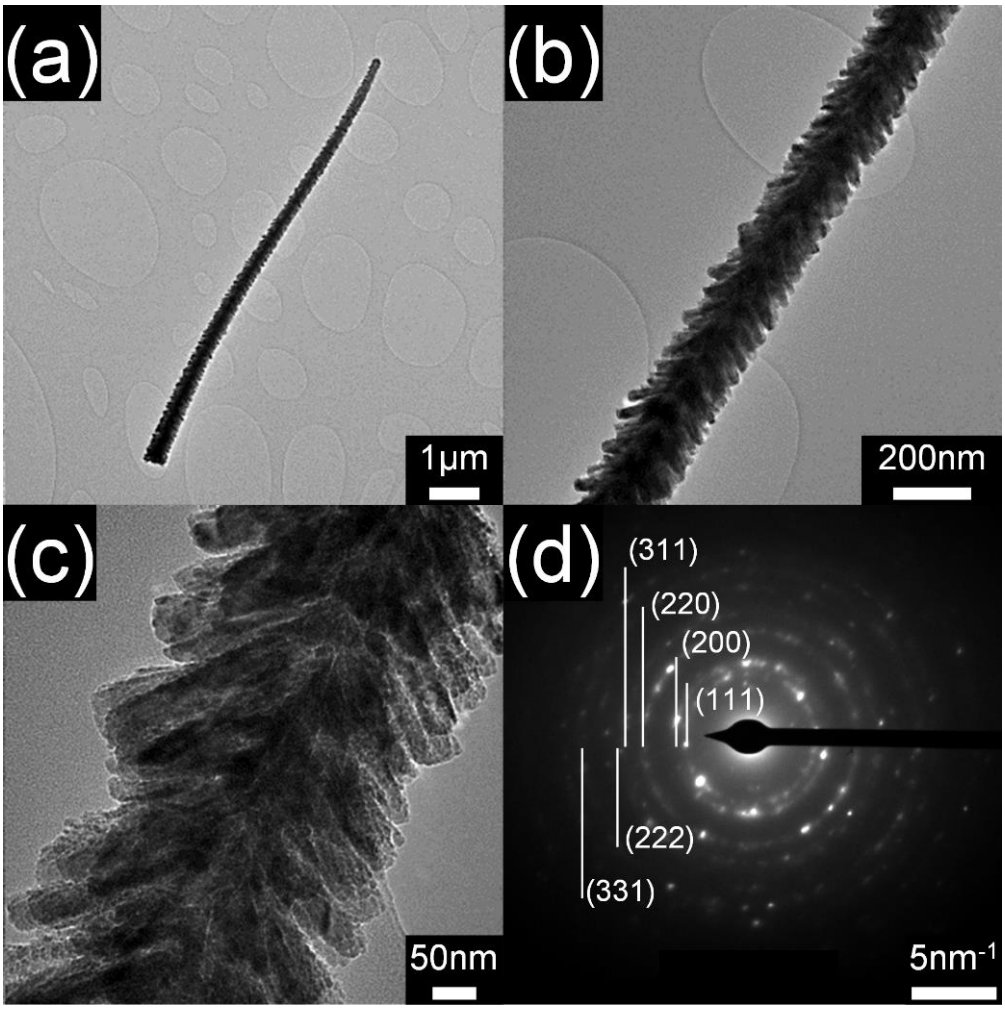

Figure 32: Transmission electron microscopy (TEM) images (a) to (c) and electron diffraction (d) of SiNWs-CrN (500nm).

6.3.Electrochemical characterization

Figure 33 displays the CV curves of the SiNWs and SiNWs-CrN (550 nm) electrodes recorded at the same scan rate of 100 $mV.s^{-1}$ in 0.5 M H_2SO_4 electrolyte. By comparison, SiNWs-CrN (550 nm) electrode has the largest area with enhanced capacitive current compared to pristine SiNWs, indicating higher specific capacitance. The areal capacitance of SiNWs at 100 $mV.s^{-1}$ was measured to be 0.16 $mF.cm^{-2}$ versus 54 $mF.cm^{-2}$ for SiNWs-CrN (550nm) electrode.

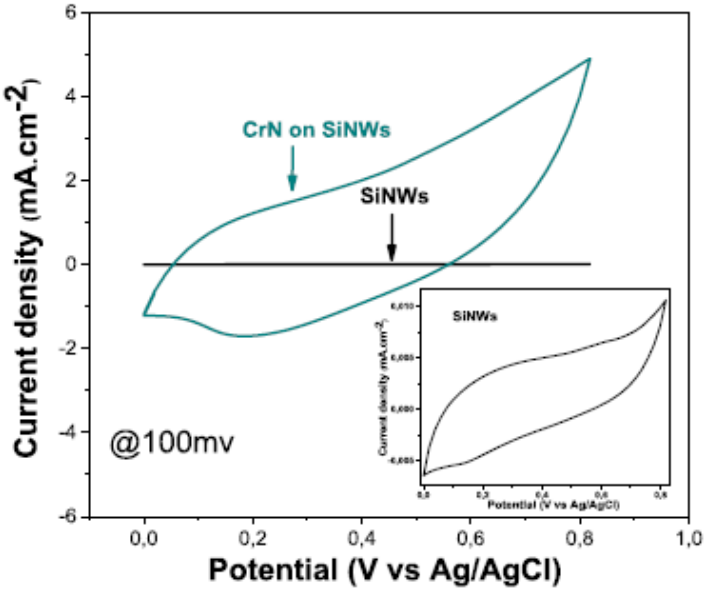

Figure 33: CV curves of SiNWs and SiNWs-CrN (550 nm) electrodes recorded in 0.5 M H_2SO_4 at a scan rate of 100 $mV.s^{-1}$. Inset CV of SiNWs.

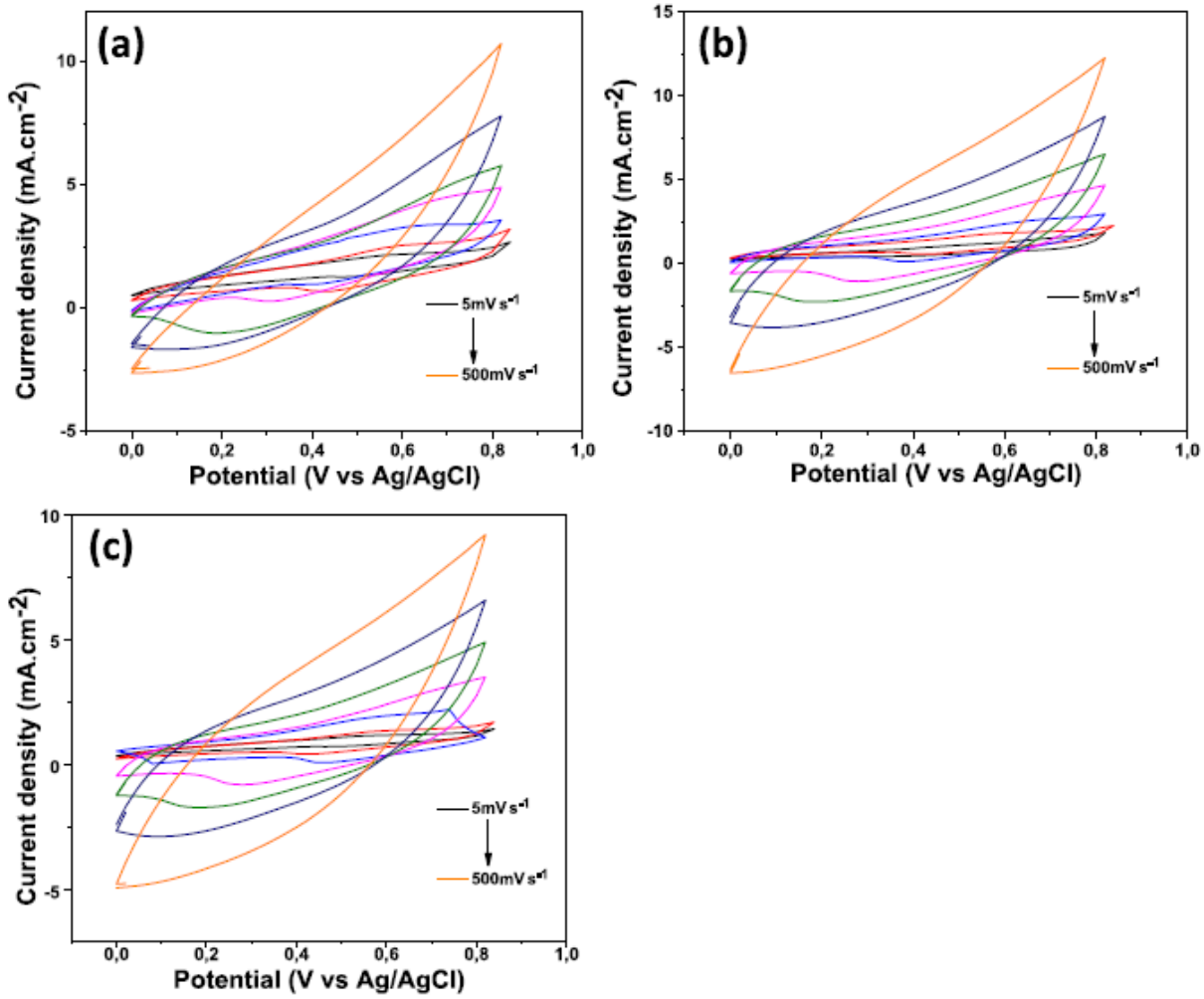

Figure 34: CV curves of (a) SiNWs-CrN 290nm. (b) SiNWs-CrN 550 nm and (c) SiNWs-CrN 900 nm at a scan rate of 100 $mV \cdot s^{-1}$.

Figure 34 depicts the CV curves of SiNWs-CrN electrodes obtained at various scan rates in a potential range of (0–0.8 V). The quasi-rectangular shapes of CV curves indicate that the SiNWs-CrN electrodes have obvious supercapacitive characteristics. However, at higher scan rates, CV curves become more distorted due to the increase of internal electrode resistivity.

GCD curves of SiNWs-CrN electrodes at a current density of 2 mA.cm^{-2} are displayed in **Figure 35**. SiNWs-CrN 900 nm electrode displays the smallest IR drop of (0.12 V) followed by SiNWs-CrN 550 nm (0.13 V) and 290 nm (0.19 V), respectively. It can be also seen that the IR drop decreases with increasing the CrN thickness, indicating the good conductivity of CrN layers. This can be explained by the increase of the CrN coating density, as observed in SEM analysis.

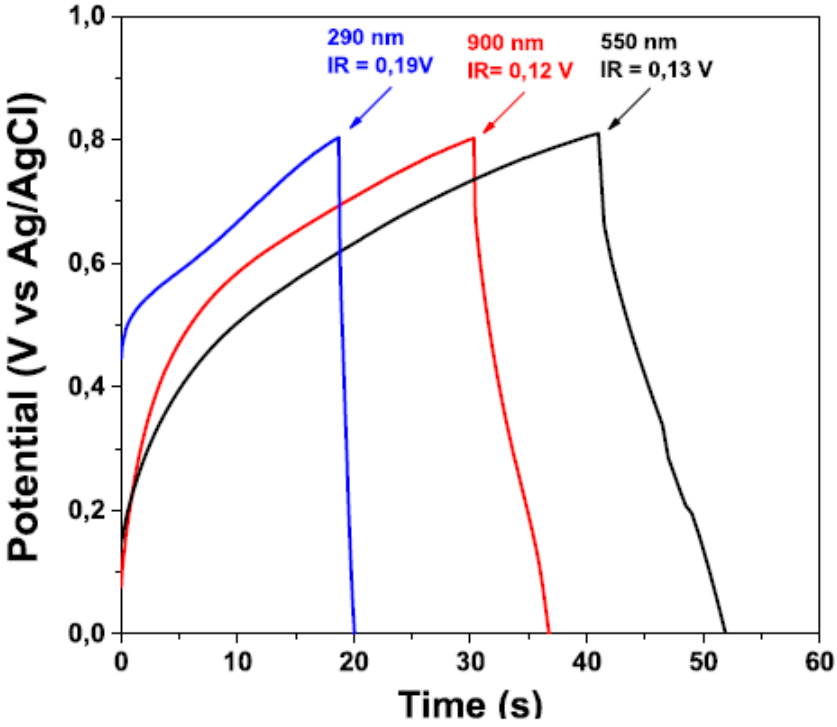

Figure 35: Charge-discharge curves of SiNWs-CrN electrodes with different CrN thicknesses recorded at 2 mA.cm^{-2}.

In contrast, to the SiNWs electrode which exhibits a capacitance of 1.55 mF.cm^{-2} under different scan rates, the areal capacitance values of the SiNWs-CrN electrodes, calculated from the CV curves (at a scan rate of 5 mV.s^{-1}) are as high as 80, 180 and 120 mF.cm^{-2} for 290, 550 and 900 nm CrN coated SiNWs, respectively. Furthermore, the areal capacitances were calculated from the GCD curves and found to be 5.2, 31.8 and 16.8 mF.cm^{-2} at a current density of 1.6 mA.cm^{-2} for 290, 550 and 900 nm CrN coated SiNWs, respectively. Since the areal capacitance of the SiNWs-CrN electrode reached 180 mF.cm^{-2} while

those of EDLC is limited to 1-100 µF.cm^{-2}. The charged storage mechanism of CrN coating is believed to be predominantly pseudo-capacitive.

The variation of the areal capacitance with scan rate and current density is displayed in **Figure 36**). The SiNWs-CrN 550 nm electrode has the highest capacitance value whereas the SiNWs-CrN 290 nm shows the lowest capacitance.

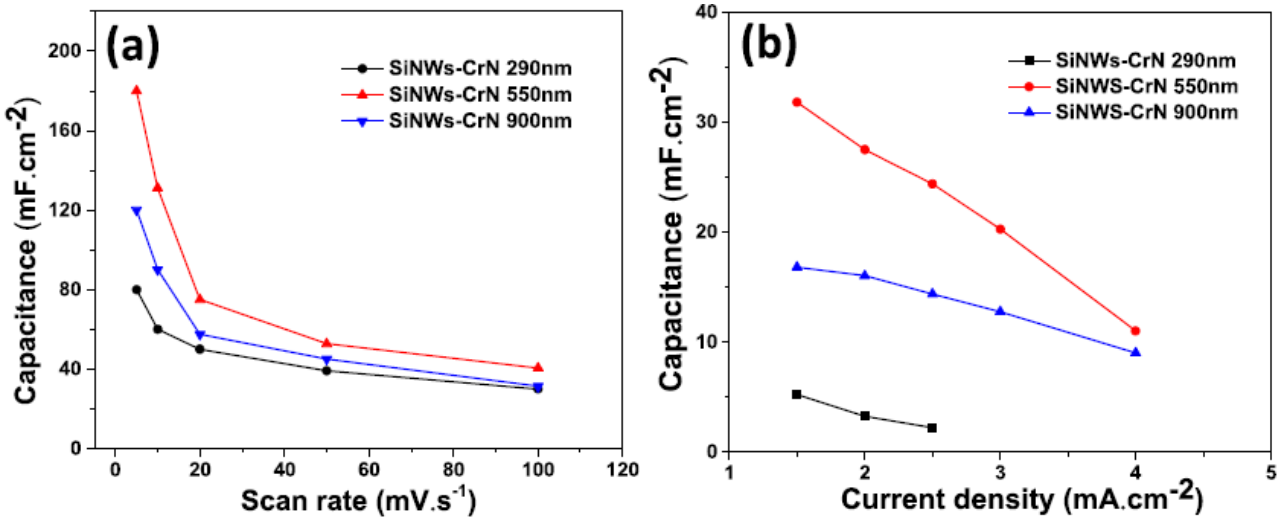

Figure 36: Variation of the areal capacitance of SiNWs-CrN at different (a) scan rates and (b) current densities.

To investigate the relationship between the thickness of CrN and the performances of SiNWs-CrN electrodes, we have varied CrN thickness from 290 to 900 nm. It is seen that the areal capacitance increase with the CrN thickness up to 550 nm, then is stabilized at 180 mF.cm^{-2} as thickness reaches 550 nm. At higher thickness, the capacitance decreases. We should recall that the TEM analysis showed that SiNWs-CrN electrodes having a herringbone structure with highly nanoporous channels (**Figure 32**) which is expected to contribute to capacitance enhancement of the electrode. Further increase of CrN thickness (from 550 to 900 nm) would lead to a capacitance decrease. The structural analysis by electron microscopy indicated that a continuous increase of the CrN film thickness on the SiNWs leads to part of the surface becomes inaccessible when the CrN thickness reaches 900 nm. This leads to insufficient ion transport and adsorption. Such behavior can be related to the amounts of CrN deposits and the surface area of different electrodes. Hence, both from a microstructural and an electrochemical characterization we can conclude that around 550 nm is an optimal thickness to obtain the highest areal capacitance.

The comparison of the areal capacitance of our electrodes with those of other nanostructures reported in the literature is summarized in **Table 8**. The areal capacitance of SiNWs-CrN 550 nm (130 and 31.8 $mF.cm^{-2}$ at 10 $mV.s^{-1}$ and 1.6 $mA.cm^{-2}$, respectively) is higher than of CrN thin film (in the range of 12.8 $mF.cm^{-2}$ at 1.0 mA cm^{-2})[21] . Much higher than of MnO_2-SiNWs electrodes where values of 21.296 and 13.38 $mF.cm^{-2}$ at 10 $mV.s^{-1}$ were reported in references [33] and [12], respectively. Also, much higher than of carbon-SiNWs electrodes (in the range of 25.6 $mF.cm^{-2}$ at 0.1 mA cm^{-2}) [11]. These results confirm the high performance of SiNWs-CrN composites for ECs application. The superior performance of SiNWs-CrN 550V nm can be attributed to the larger surface area (highly nanoporous channels), which can provide good contact between electrolyte and active material, resulting in an improvement in areal capacitance. It is worth to mention that thinner film (290nm) may not have sufficient CrN active material, whereas thicker film (900 nm) may block the diffusion of electrolyte ion into electrode internal structure and pores.

Table 8: performance of SiNWs-CrN 550nm electrode.

Film deposition	Capacitance ($mF.cm^{-2}$)	references
CrN-SiNWs	131 (10 $mV.s^{-1}$) 31.8 (1.6 $mA.cm^{-2}$)	This work
CrN thin film	12.8 (1.0 $mA.cm^{-2}$)	[21]
MnO_2-SiNWs	21.296 (10 $mV.s^{-1}$)	[33]
MnO_2-SiNWs	13.38 (10 $mV.s^{-1}$)	[12]
Carbon-SiNWs	25.6 (0.1 mA cm^{-2})	[11]

EIS measurement (**Figure 40**) depicts the Nyquist plots of SiNWs-CrN electrodes. The charge transfer resistance (R_{ct}) is calculated to be about 146, 89 and 83 Ω for SiNWs-CrN 290, 550 and 900 nm electrodes, respectively. This indicates that the CrN layers can reduce the charge transfer resistance and the electrodes can become more conductive as the thickness of the CrN layer increases.

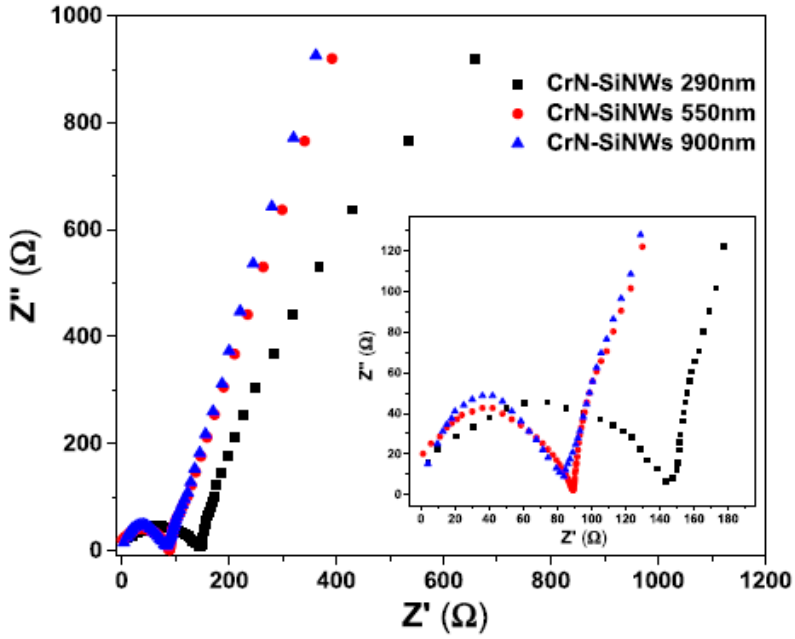

Figure 37: Nyquist impedance plots for CrN-SiNWs (290, 550 and 900 nm) electrodes.

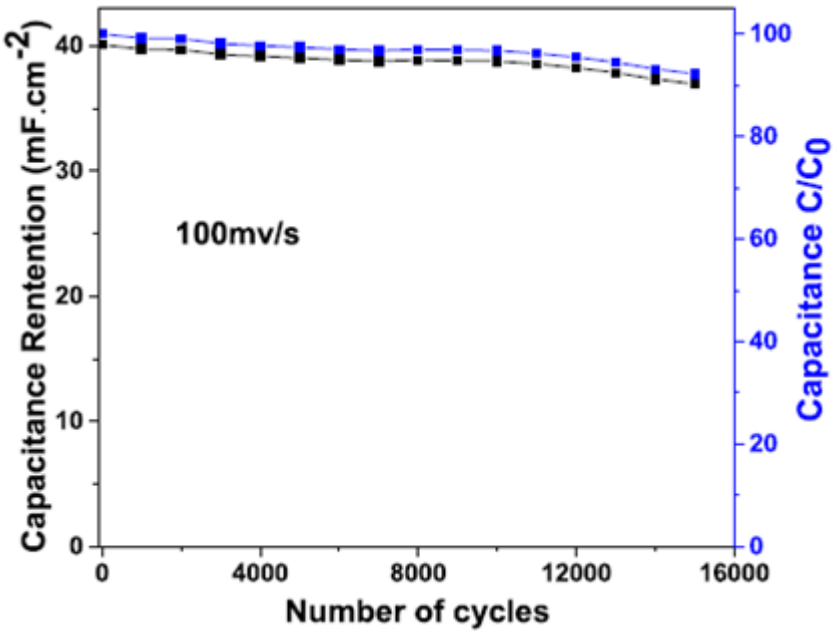

Figure 38: Evolution of the capacitance for CrN-SiNWs 550 nm electrode after 15000 consecutive cycles at a scan rate of 100 $mV.s^{-1}$.

The cycling stability of the SiNWs-CrN 500 nm electrode at a scan rate of 100 $mV.s^{-1}$ is presented in **Figure 41**. As can be seen, the electrode can sustain 92% of its initial capacitance value after 15000 cycles. Such cycling stability allows the use of these 3D SiNWs@CrN electrodes for micro-supercapacitors.

Conclusion

In this chapter, we reported the synthesis of 3 D nanostructured electrodes made of chromium nitride (CrN) layer deposited on silicon nanowires (SiNWs) arrays using bipolar magnetron sputtering method. SEM and TEM analysis showed that the SiNWs are covered uniformly with CrN forming a twisted bundle-like nanostructure with a high surface area. The results of electrochemical measurements showed that the SiNWs-CrN (550 nm) electrode has the highest areal capacitance of 180 $mF.cm^{-2}$ at a scan rate of 5 $mV.s^{-1}$ and 31.8 $mF.cm^{-2}$ at a high current density of 1.6 $mA.cm^{-2}$ with 92% of its initial specific capacitance value after 15000 cycles in 0.5 M H_2SO_4 electrolyte. These results suggest that coating SiNWs with transition metal nitride such as CrN is a promising way for the construction of high-energy storage systems.

References

[1] S. Ortaboy, J. P. Alper, F. Rossi, G. Bertoni, G. Salviati, C. Carraro, R. Maboudian, MnOx-decorated carbonized porous silicon nanowire electrodes for high-performance supercapacitors, Energy & Environmental Science 10(6) (2017) 1505-1516.

[2] X. Zhou, B. Xu, Z. Lin, D. Shu, L. Ma, Hydrothermal synthesis of flower-like MoS2 nanospheres for electrochemical supercapacitors, J. Nanosci. Nanotechnol 14(9) (2014) 7250-7254.

[3] P. Simon, Y. Gogotsi, Materials for electrochemical capacitors, Nature. Mater. 7 (2008)

845–854.

[4] M. Mandal, D. Ghosh, S.S. Kalra, C. K. Das, High-performance supercapacitor electrode material based on flower-like MoS_2/reduced graphene oxide nanocomposite. Int. J. Lat. Res. Sci. Technol, (2014) 3 65.

[5] G.R. Li, Z.L. Wang, F.L. Zheng, Y.N. Ou, Y.X Tong, ZnO@MoO3 core/shell nanocables: facile electrochemical synthesis and enhanced supercapacitor performances, J. Mater. Chem. 21 (2011) 4217–4221.

[6]] P.M. Kulal, D.P. Dubal, C.D. Lokhande, V.J. Fulari, Chemical synthesis of Fe_2O_3 thin films for supercapacitor application J. All. Compd 509 (2011) 2567–2571.

[7] J. P. Alper, M. Vincent, C. Carraro, R. Maboudian, Silicon carbide coated silicon nanowires as robust electrode material for aqueous micro-supercapacitor Appl. Phy. Lett 100.16 (2012) 163901.

[8] F. Thissandier, N. Pauc, T. Brousse, P. Gentile, S. Sadki, Micro-ultracapacitors with highly doped silicon nanowires electrodes Nanoscale Res. Lett 8.1 (2013) 38.

[9] N. Berton, M. Brachet, F. Thissandier, J. Le Bideau, P. Gentile, G. Bidan, S. Sadki, Wide-voltage-window silicon nanowire electrodes for micro-supercapacitors via electrochemical surface oxidation in ionic liquid electrolyte Electrochem. Commun 41 (2014) 31-34.

[10] F. Thissandier, P. Gentile, N. Pauc, T. Brousse, G. Bidan, S. Sadki, Tuning silicon nanowires doping level and morphology for highly efficient micro-supercapacitors Nano Energy 5 (2014) 20-27.

[11] R.R. Devarapalli, S. Szunerits, Y. Coffinier, M.V. Shelke, R. Boukherroub, Glucose-derived porous carbon-coated silicon nanowires as efficient electrodes for aqueous micro-supercapacitors ACS. Appl. Mater. Interfaces 8.7 (2016) 4298-4302.

[12] D. P. Dubal, D. Aradilla, G.Bidan, P. Gentile, T. J. Schubert, J. Wimberg, P. Gomez-Romero, 3D hierarchical assembly of ultrathin MnO2 nanoflakes on silicon nanowires for high-performance micro-supercapacitors in Li-doped ionic liquid Sci. Rep 5 (2015) 9771.

[13] A. Achour, M. Islam, I. Ahmad, L. Le Brizoual, A. Djouadi, T. Brousse, Influence of surface chemistry and point defects in TiN based electrodes on electrochemical capacitive storage activity Scrip. Mater. 153 (2018) 59-62.

[14] P. Yang, D. Chao, C. Zhu, X. Xia, Y. Zhang, X. Wang, H.J. Fan, Ultrafast-charging supercapacitors based on corn-like titanium nitride nanostructures Adv. Sci. 3-6 (2016) 1500299.

[15] E. Kao, C. Yang, R. Warren, A. Kozinda, L. Lin, ALD titanium nitride on vertically aligned carbon nanotube forests for electrochemical supercapacitors Sens. Actuators. A 240 (2016) 160-166.

[16] N. Ouldhamadouche, A. Achour, R. Lucio-Porto, M. Islam, S. Solaymani, A. Arman, A. Ahmadpourian, H. Achour, L. Le Brizoual, M. A. Djouadi, T. Brousse, Electrodes based on nano-tree-like vanadium nitride and carbon nanotubes for micro-supercapacitors J. Mater. Sci. Tech 34 (2018) 976-982.

[17] A. Achour, R. Lucio-Porto, S. Solaymani, M. Islam, I. Ahmad, T. Brousse, Reactive sputtering of vanadium nitride thin films as pseudo-capacitor electrodes for high areal capacitance and cyclic stability J. Mater. Sci.: Mater. Electron 29 (2018) 13125-13131

[18] X. Lu, M. Yu, T. Zhai, G. Wang, S. Xie, T. Liu, Y. Li, High energy density asymmetric quasi-solid-state supercapacitor based on porous vanadium nitride nanowire anode Nano Lett. 13.6 (2013) 2628-2633.

[19] A. Djire, J.B. Siegel, O. Ajenifujah, L. He, L.T. Thompson, Pseudocapacitive storage via micropores in high-surface area molybdenum nitrides Nano. Energy 51 (2018) 122-127.

[20] M. Arif, A. Sanger, A. Singh, Sputter deposited chromium nitride thin electrodes for supercapacitor applications Mater. Lett. 220 (2018) 213-217.

[21] B. Wei, H. Liang, Zhang, D., Z. Wu, Z. Qi, Z. Wang, CrN thin films prepared by reactive DC magnetron sputtering for symmetric supercapacitors J. Mater. Chem. A 5-6 (2017) 2844-2851.

[22] E. Haye, J. L. Colaux, P. Moskovkin, J. J. Pireaux, S. Lucas, Wide range investigation of duty cycle and frequency effects on bipolar magnetron sputtering of chromium nitride Surf. Coat. Tech 350(2018) 84-94.

[23] N. Verplanck, E. Galopin, J. C. Camart, V. Thomy, Y. Coffinier, R. Boukherroub, Reversible Electrowetting on Superhydrophobic Silicon Nanowires Nano Lett. 7 (2007) 813-817.

[24] M. Muraoka, N. Settsu, M. Saka, Residual-strain-induced nanocoils of metallic nanowires J. Nanosci. Nanotechnology 8 (2008) 439-442.

[25] P. Hones, R. Sanjines, F. Levy, Characterization of sputter-deposited chromium nitride thin films for hard coatings Surf Coat Technol 94(1997) 398-402.

[26] E.Haye, J. L. Colaux, P. Moskovkin, J. J. Pireaux, S. Lucas, Wide range investigation of duty cycle and frequency effects on bipolar magnetron sputtering of chromium nitride Surf Coat Technol 350 (2018) 84-94.

[27] M.A. Gharavi, S. Kerdsongpanya, S. Schmidt, F. Eriksson, N.V. Nong, J. Lu, B. Balke, D. Fournier, L. Belliard, A. le Febvrier, C. Pallier, P. Eklund, Microstructure and thermoelectric properties of CrN and CrN/Cr2N thin films J. Phys D: Appl. Phys 51 (2018) 355302.

[28] D.S. Jensen, S.S. Kanyal, N. Madaan, M.A. Vail, A.E. Dadson, M.H. Engelhard, M.R. Linford, Silicon (100)/SiO_2 by XPS Surf Sci. Spectra 20 (2013) 36–42.

[29] I. Kurylo, M. Dupré, S. Cantel, C. Enjalbal, H. Drobecq, S. Szunerits, O. Melnyk, R. Boukherroub, Y. Coffinier, Characterization of peptide attachment on silicon nanowires by X-ray photoelectron spectroscopy and mass spectrometry Analyst 142 (2017) 969–978.

[30] I. Milošev, H.H. Strehblow, B. Navinšek, Comparison of TiN, ZrN and CrN hard nitride coatings: Electrochemical and thermal oxidation Thin Solid Films 303 (1997) 246–254.

[31] H.C. Barshilia, N. Selvakumar, B. Deepthi, K.S. Rajam, A comparative study of reactive direct current magnetron sputtered CrAlN and CrN coatings, Surf. Coat. Technol. 201 (2006) 2193–2201.

[32] P. Zaumseil, High-resolution characterization of the forbidden Si 200 and Si 222 reflections J. Appl. Cryst 48 (2015) 528–532.

[33] F. Moulai, T. Hadjersi, M. Ifires, A. Khen, N. Rachedi, Enhancement of Electrochemical Capacitance of Silicon Nanowires Arrays (SiNWs) by Modification with Manganese Dioxide MnO 2 Silicon (2019) 1-12

Chapter 4.CrN-coated Carbon nanowalls as efficient and stable micro-supercapacitor

1. Introduction

Among the various energy storage systems, electrochemical capacitors (ECs) also called supercapacitors have attracted increasing attention as potential candidates, due to their high power density and long life cycle [1-4]. Carbon materials such as graphene [1], activated carbon [5], and carbon nanofibers [6] are widely used as promising materials for supercapacitors, owing to their high surface area, excellent conductivity, and electrochemical stability [7,8] Recently, carbon nanowalls (CNW) have been recognized as an emerging material for electrochemical applications due to their unique structure of two-dimensional self-aligned graphene sheets with high surface area (100-1500 $m^2.g^{-1}$) [9-11]. However, their integration as active material for supercapacitor applications remains limited by their low specific capacitances [9]. Thus, the deposition of nanostructures such as transition metal oxides, conductive polymers and transition metal nitride on CNW represents an appealing approach to increase their specific capacitance. For example, Dinh et al.[10] have fabricated CNW/ hydrous RuO_2 composite with an enhanced specific capacitance of 1000 $mF.cm^{-2}$ at 2 scan rate of $2mV.s^{-1}$. Furthermore, CNW-MnO_2 composite has been reported by Hassan et al. for EC application with a good specific capacitance of 851 F. g^{-1} at current density of $1mA.cm^{-2}$[11]. However, the moderate cyclic stability of transition metal oxides, as well as the high cost of ruthenium oxide are the main obstacles for their application as electrodes for electrochemical capacitors.

As an alternative, transition metal nitrides (TMNs) including TiN [12], VN [13], Ni_3N[14], have been invastigated as promising active materials for EC applications due to their high specific capacitance, excellent electrical conductivity and electrochemical stability [12, 15, 16]. Among TMNs, chromium nitride (CrN) [15,16] was highly studied for its excellent conductivity and electrochemical stability [16]. Thus, association of metal nitride and carbon-based material can drastically enhance the performance of supercapacitors [17–19], as demonstrated by Achour et al.[12] with the synthesis of TiN/CNT nanocomposite with excellent stability over 20,000 cycles. Therefore, the high conductivity of the CrN combined with the high surface area of CNW should be an ideal approach to improve the electrochemical performance.

In the present chapter, we report the synthesis of high-performance micro-supercapacitors based on CrN deposited on CNW electrodes. The CrN thin films were synthesized by magnetron sputtering on a vertically aligned CNW template in a one-step process. The electrochemical measurements revealed the enhanced performance of CNW-CrN micro-supercapacitors with higher areal capacitance values of 239.5 $mF.cm^{-2}$ and excellent stability over 30 000 cycles.

2. Carbon as supercapacitors electrode materials

Carbon-based materials are considered as potential electrode materials for application in micro-supercapacitors (µSC) due to their low cost and excellent chemical stability [1-4]. However, their specific capacitance remains limited by the active surface area of the electrode and the distribution of the pores [4]. The control of their specific surface and the pore size is crucial to ensure a good performance of the supercapacitor in terms of power and energy storage. Thus, several porous carbonaceous materials with well-controlled pore sizes have been synthesized [1-4].

Among carbon materials, activated carbon is the most widely used material in commercial supercapacitors because of its large surface area, relatively good electrical properties and low cost [4, 5]. It is generally produced by physical (thermal) and/or chemical activation of various types of carbonaceous materials (wood, charcoal, etc...) [4]. Depending on the activation methods and the precursors used, activated carbon can have a developed surface of up to 3000 $m^2.g^{-1}$ [4].

Next to activated carbon, carbon nanotubes (CNTs) are considered as promising electrode material thanks to their unique porous tubular structure and their superior electrical conductivity [4]. More recently, graphene, a new class of two-dimensional carbon nanostructures with a large specific surface area and high electronic conductivity [1-3] have been developed for application in supercapacitors. New nanostructured carbonaceous materials, carbon nanowalls, also called interconnected and vertically oriented graphene nanosheets have attracted major interest in recent years. Their open structure associated with a large specific surface (100 - 1500 $m^2.g^{-1}$) [9], good electrical conductivity and chemical stability, making them promising materials for supercapacitors [9-11]. Different methods based on the chemical vapor deposition process assisted by plasma (PECVD), radiofrequency RF/DC have been reported for the synthesis of CNW [1, 9-11]. Indeed the growth of CNW is due to the decomposition of the carbon

precursor, mixed with an active gas that is responsible for the nanostructuring of the material [1]. The morphology and quality of the CNW, namely the number per unit area, the length, the height and the thickness of the nanowalls, depend on the plasma conditions and the characteristics of the substrates [1]. Thus, coupling CNW with high pseudo-capacitive materials may offer benefits, such as enhanced faradaic capacitance and electrical conductivity of the composite. Dinh et al. [10] have reported the fabrication of CNW decorated with porous ruthenium oxide (RuO_2) with an excellent capacity of 1000 $mF.cm^{-2}$. However, the high cost, limited availability and environmental impact limit the use of RuO_2 for large-scale production. Other metallic oxides with low cost, abundance and low environmental impact such as manganese oxide (MnO_2) were used for the synthesis of the nano-composite CNW / MnO_2 electrode with a high specific capacitance of 851 Fg^{-1} [11]. Therefore, it would be interesting to use CNW coated with a CrN to enhance the surface area and improve the electrical conductivity of the CrN deposit.

3. Experimental

3.1. Synthesis of vertically aligned CNW films

The CNW films were deposited by expanding radio frequency (RF) discharge on silicon (100) oriented n-type wafers heated at 700 °C. The RF power was set at 300 W, while the Ar, H_2 and C_2H_2 gas flow rates were set to 1400, 25 and 2 sccm, respectively. The working pressure was about 100 Pa. The Ar plasma beam, acetylene (C_2H_2) and hydrogen (H_2) were used as carrying, precursor and active gas, respectively. The deposition time was fixed at 60 min. More experimental details are reported elsewhere [9].

3.2. Deposition of CrN on the CNW

Chromium nitride (CrN) thin films were deposited directly on the as-prepared CNW by bipolar magnetron sputtering [20, 21] (Magpuls QP-1000/20 10 kW pulse unit) with two chromium targets (7.5 × 35 cm, 99.99% purity, from Neyco) **(Chapter 3)**.

4. Results and discussion

4.1. Structural and surface characterization

Figure 39 display the top view scanning electron microscopy (SEM) images of CNW and CNW-CrN samples of different CrN thickness (290, 550 and 900 nm). **Figure 39a** confirms the vertical growth of carbon sheets with high surface area and honeycomb structure on the Si substrate. **Figure 39b-d** reveals that the CrN layer is uniformly coated over the CNW sheets. The large accessible surface area is an important parameter for easy penetration of ions through the active material. It is visible that the surface area decreases with increasing CrN deposit thickness (**Figure 39 d**), due to the plugging of the CNW by the CrN deposit. Such morphology change is expected to influence the electrochemical performance of the CNW-CrN samples.

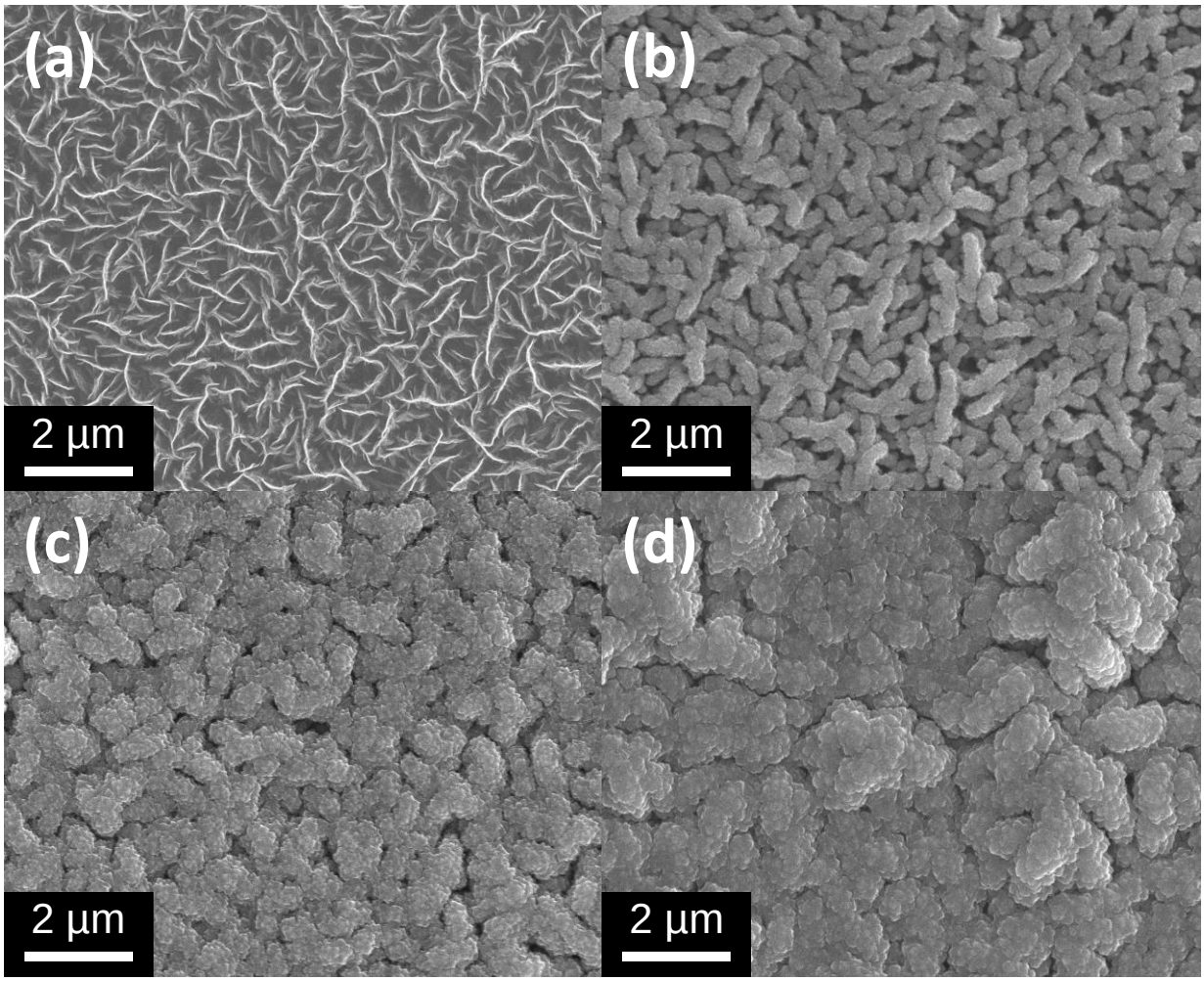

Figure 39: Top view SEM images of (a) CNW, (b) CNW-CrN 290 nm, (c) CNW-CrN 550 nm and (d) CNW-CrN 900 nm.

4.2. ***Physico-Chemical characterization***

Figure 40a depicts the XRD patterns of the prepared CNW and CNW-CrN with different CrN thicknesse. The pristine CNW does not exhibit any diffraction peak, indicating its amorphous nature. However, the XRD patterns of the CNW-CrN electrodes show the presence of diffraction peaks at around 37.4°, 43.1° and 63.1° which can be assigned to the (111), (200) and (220) diffraction planes of cubic CrN (Space group 225, $Fm\bar{3}m$) [21, 23]. The increase of the peak intensity is in accordance with a higher thickness of the CrN deposit.

Interestingly, no preferential growth direction was observed, while the deposition under similar conditions generally leads to (111) texturization [21]. The absence of preferential orientation is attributed to the very rough surface of the CNW, leading to the CrN growth in all directions, as confirmed by SEM observation.

The structure and morphology were further assesed by TEM analysis (**Figure 40 b**): the formation of small and cubic crystallites pointing at the surface is confirmed and the selected area diffraction pattern reveals a crystallized structure. The indexation of the pattern indicates experimental d-spacing of 2.416, 2.079, 1.420, 1.202, and 0.849 Å, respectively attributed of (111), (200), (220), (222) and (422) planes, in good agreement with the XRD data and formation of cubic CrN.

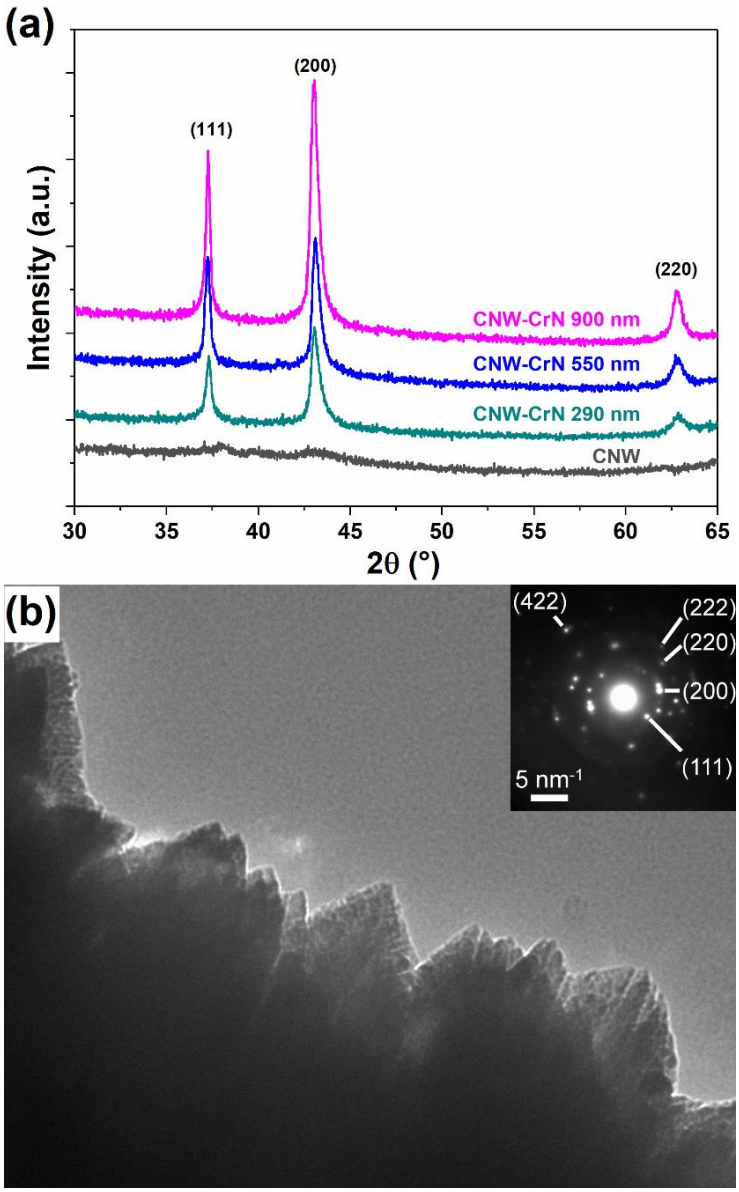

Figure 40*:* (a) XRD pattern of the CNW coated with CrN thin layers with different thicknesses. (b) TEM image of CNW-CrN 550 nm and selected area diffraction pattern in the insert.

The surface chemical composition of the CNW-CrN sample was investigated by X-ray photoelectron spectroscopy (XPS) analysis. The XPS survey spectrum (**Figure 41a**), shows the presence of C, Cr, and N, which confirms the formation of CrN on the CNW surface. The high-resolution XPS spectrum of Cr 2p peak consists of two major components attributed to Cr $2p_{1/2}$ and Cr $2p_{3/2}$ (**Figure 41b**). The high-resolution Cr $2p_{3/2}$ peak can be fitted with three peaks assigned to CrN, Cr (O, N) and Cr_2O_3 at binding energies of 574.3, 575.3 and 576.6 eV, respectively [24]. As the samples have not been etched, surface oxidation is expected and confirmed by the intense O 1s level centered at 531.0 eV (**Figure 41c**) [24,25]. **Figure 41d** displays the high-resolution N1s spectrum with a major contribution at 396.4 eV, which confirms the formation of CrN. Besides, a second wide contribution is observed at 398.3 eV, attributed to

"organic" nitrogen, namely nitrogen bound to C or O atoms. Indeed, this contribution is wide, and probably contains in the energy range 397.5-399eV several sub-contributions (which are not fitted separately here), such as imine, amine or nitrile groups, as often observed in plasma functionalization of carbon materials [26].

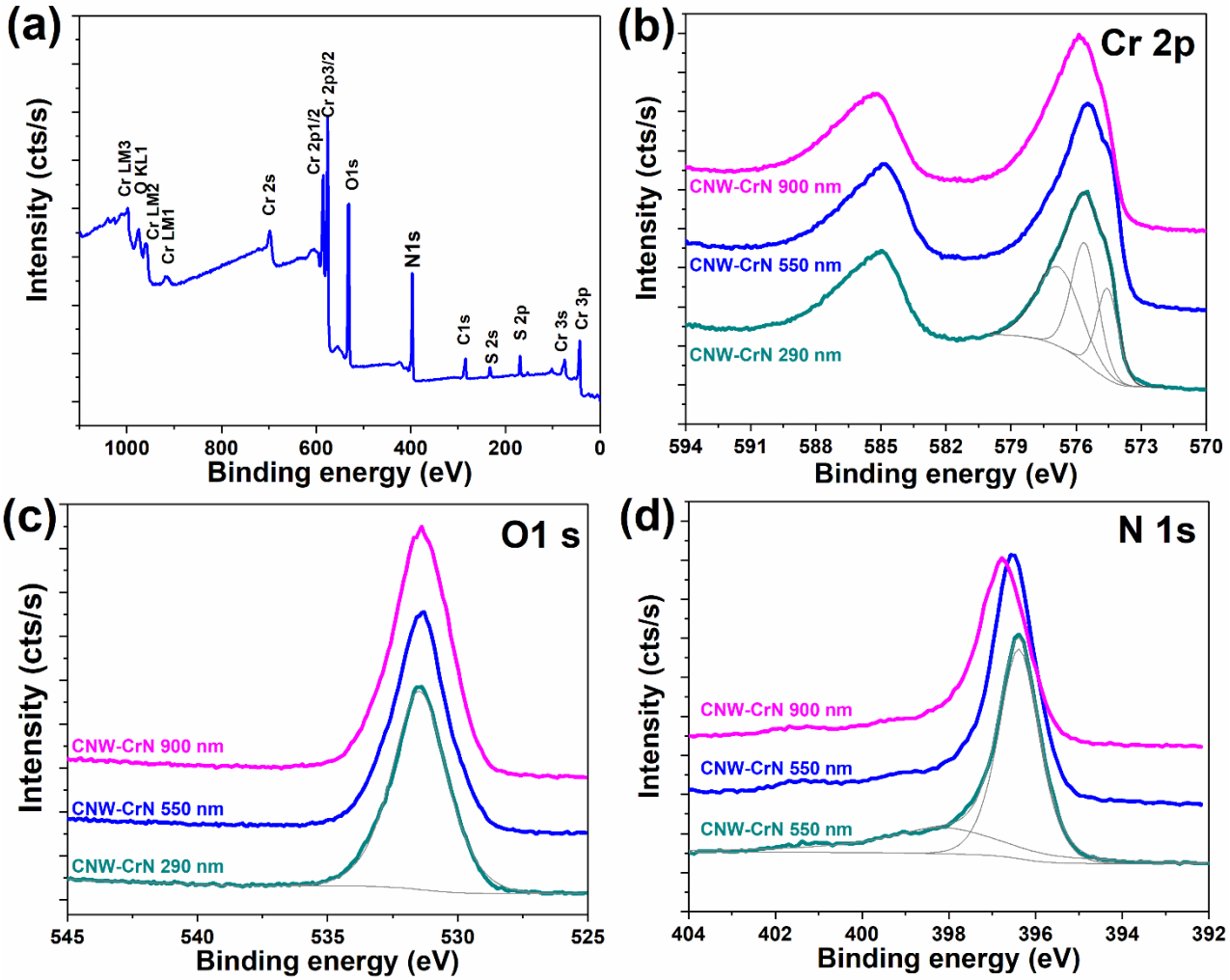

Figure 41: XPS analysis of the CNW-CrN electrode materials: (a) Survey spectrum and high-resolution XPS spectra of (b) Cr 2p (c) O 1s and (d) N 1s core levels.

4.3. Electrochemical measurement of CNW-CrN electrodes

The CVs of the CNW and CNW-CrN electrodes at a scan rate of 100 $mV.s^{-1}$ exhibit rectangular shape, indicating good super-capacitive behavior of the electrodes (**Figure 42a**). Compared to pristine CNW, the CNW-CrN 550 nm electrode exhibits the largest CV area with enhanced capacitive current, indicating higher capacitive performance. In addition, the areal capacitance was measured to be 0.11 $mF.cm^{-2}$ versus 75.9 $mF.cm^{-2}$ for the CNW-CrN 550nm electrode at 100 $mV.s^{-1}$.

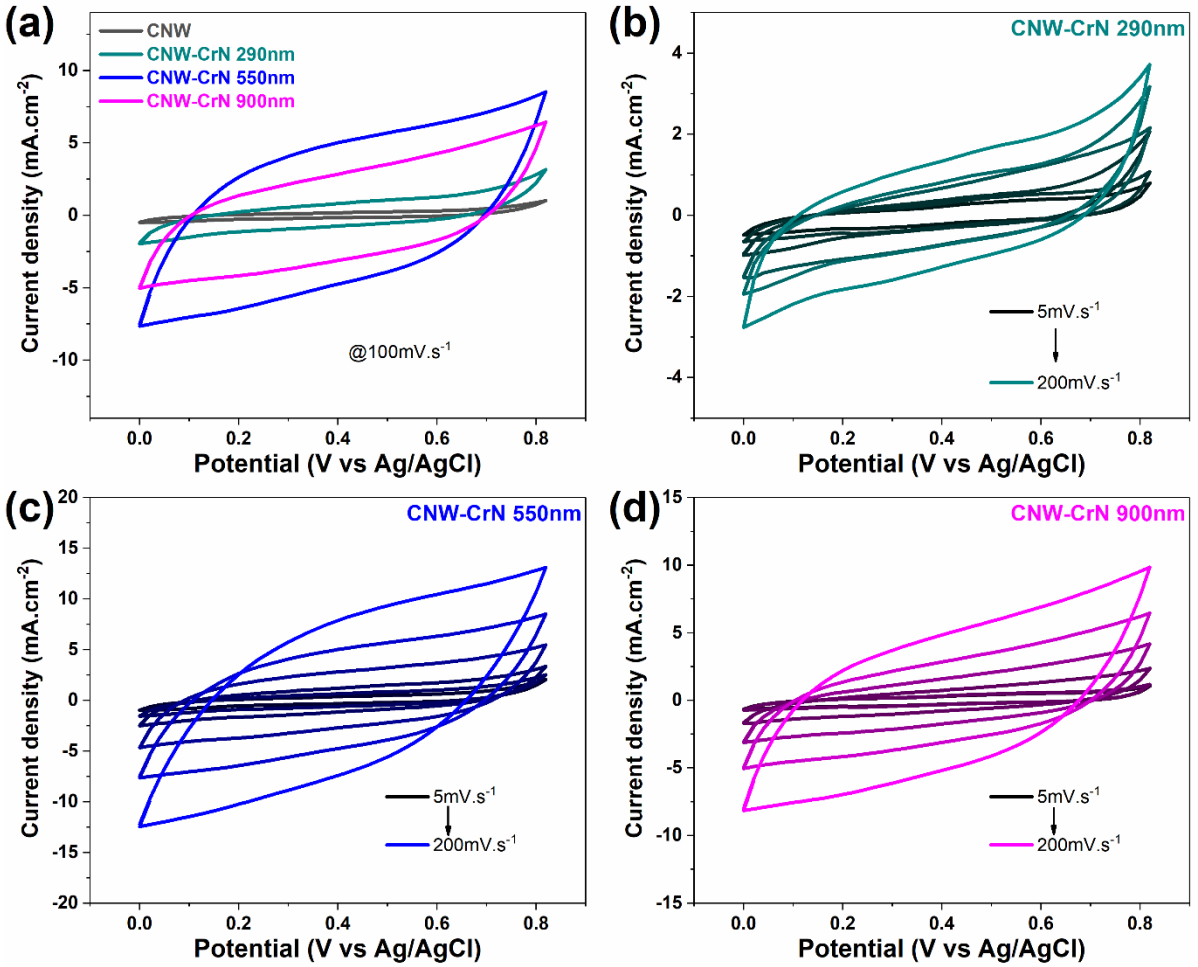

Figure 42: (a) CV curves of the CNW and CNW-CrN (290 nm, 550 nm and 900 nm) electrodes at a scan rate of 100 mV.s^{-1}. (b-d) CV curves of the CNW-CrN electrodes at various scan rates.

Figure 42a-c displays the CVs of the CNW-CrN electrodes with different CrN thickness of 290, 550 and 900 nm obtained at various scan rates in a potential range of (0 - 0.8 V). The quasi-rectangular shape of the CV curves indicates the capacitive characteristic of the CNW-CrN electrodes even at a high scan rate of 200 mV.s^{-1}. In addition, no redox behavior was observed, excluding the faradaic reaction and confirming the capacitive behavior of the CNW-CrN electrodes in the H_2SO_4 electrolyte. Furthermore, the areal capacitance values of the CNW-CrN electrodes, calculated from the CV curves (at a scan rate of 5 mV.s^{-1}) are as high as 60, 301 and 170 mF.cm^{-2} for the 290, 550 and 900 nm CrN coated CNW, respectively.

The GCD curves of the CNW-CrN electrodes recorded at a current density of 0.3 mA.cm^{-2} are displayed in **Figure 43**. The CNW-CrN 290 nm exhibits the highest IR drop of (0.09V) versus (0.015 V) for the CNW-CrN 550 and 900 nm, indicating the good conductivity of the CrN layers, which is beneficial for the transfer of ions and improve the rapid charging-discharging of the CrN active material.

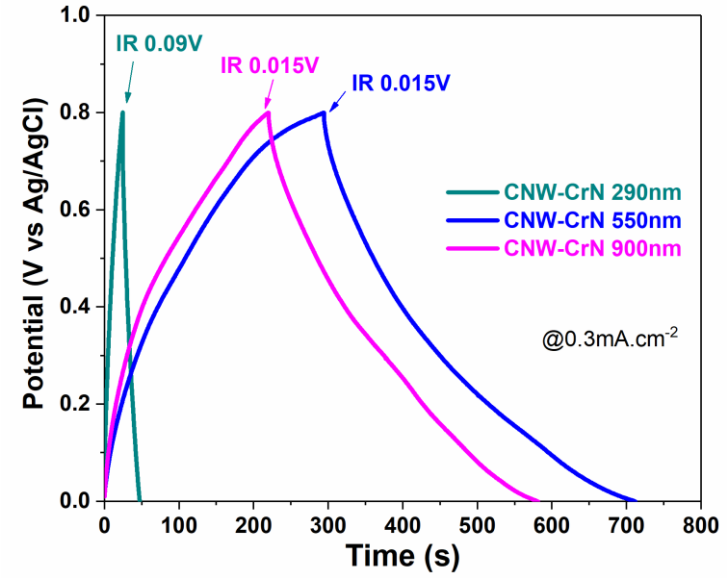

Figure 43: Galvanostatic charge-discharge curves at a current density of 0.3 mA.cm^{-2}.

The influence of the CrN thickness on the charge-discharge plots was further investigated. In contrast to the CNW electrode which exhibits a capacitance of 0.53 mF.cm^{-2} at a current density of 0.3 mA.cm^{-2}, the areal capacitances of the CNW-CrN electrodes were found to be 11, 156.5 and 135.5 mF.cm^{-2} at a current density of 0.3 mA.cm^{-2} for the 290, 550 and 900 nm CrN coated CNW, respectively. The capacitance values increase with the CrN thickness to reach a maximum for a CrN thickness of 550 nm. The increase of the CrN active material results in increased areal capacitance. Increasing the CrN thickness from 550 to 900 nm led to a decrease of the space between walls covered with CrN as observed by SEM images (**Figure 39d**), resulting in a decrease in areal capacitance. Similar loss of capacitance was observed for porous CrN coating deposited at a glancing angle [27] and CrN coated silicon nanowires [28]. The effect was attributed to (i) an optimal deposit thickness and (ii) the intrinsic conductivity of the CrN deposit; indeed, the capacitance increases with the thickness of the CrN deposit. However, if the CrN deposit is too thick, it starts to plug the porosity of the carbon nanowalls, as observed in SEM photographs (Figure 1d), reducing the accessible active area for the electrolyte, and in fine, the areal capacitance. Moreover, a too high CrN deposit is not favorable, as the electrical conductivity of CrN is only in the medium range (about 0.05 Ω.cm measured on a CrN coating deposited on Si substrate under similar condition)[20] decreasing the charge transfer mechanisms if the thickness is too high.

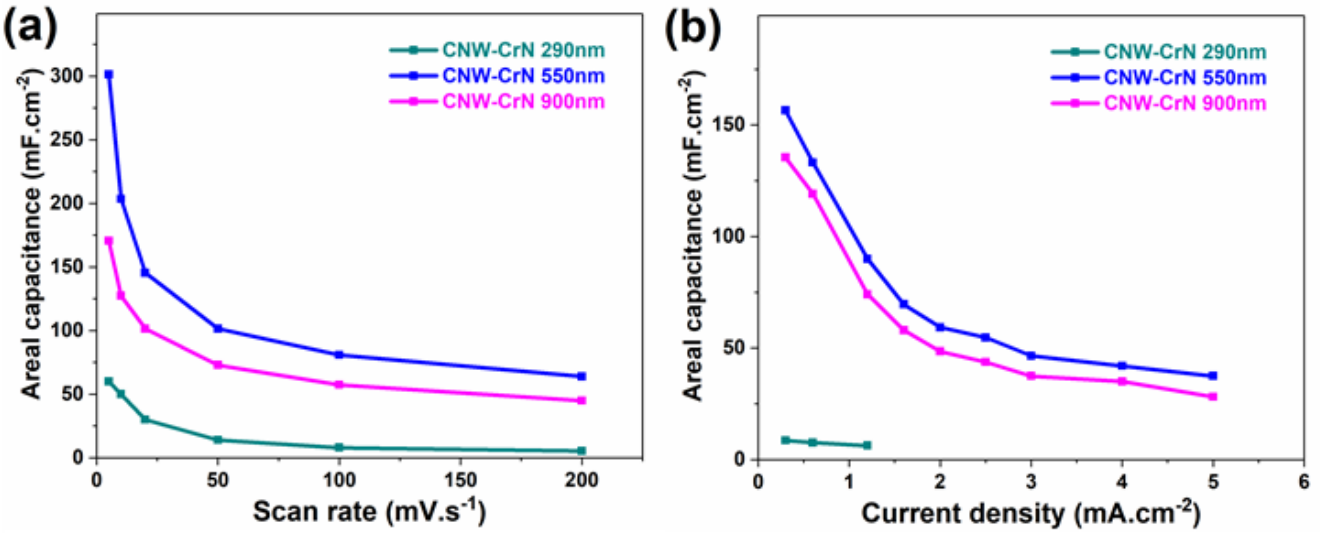

Figure 44: Variation of the areal capacitance of the CNW-CrN at different (a) scan rates and (b) current densities.

Figure 44 displays the variation of the areal capacitance with scan rate and current density. The areal capacitance values decrease upon increasing the scan rate and current density. This capacitance reduction can be attributed to the limited diffusion of the electrolyte into the active material [9, 27, 29]. Moreover, in the case of the CNW-CrN 550 nm electrode, a relatively high capacitance of 37.5 $mF.cm^{-2}$ is retained at a high current density of 5 $mA.cm^{-2}$. These results confirm the high-rate capability of the CNW-CrN electrode.

The cycling stability of the CNW-CrN 550 nm electrode was further evaluated by repeated CV cycles at a scan rate of 100 $mV.s^{-1}$ (**Figure 45a**). It can be observed that the areal capacitance first slightly increased after 500 cycles, which can be attributed to the electrochemical activation of the CNW-CrN electrode;[29] then the capacitance decreased by 2 % after 19000 cycles. After 30000 cycles, 92.4% capacitance is still retained, which is remarkably higher than the capacitance of transition metal nitrides, such as TiN[13, 17] and CrN [15, 16, 27, 28] previously reported.

The quasi-similar EIS plots obtained before and after cycling confirm the very high stability of the CNW-CrN electrode (**Figure 45b**). In addition, the CV plots before and after cycling (**Figure 45c**) show quasi similar rectangular shapes. Moreover, no redox peak was observed after cycling, indicating the high electrochemical stability of the CNW-CrN electrode.

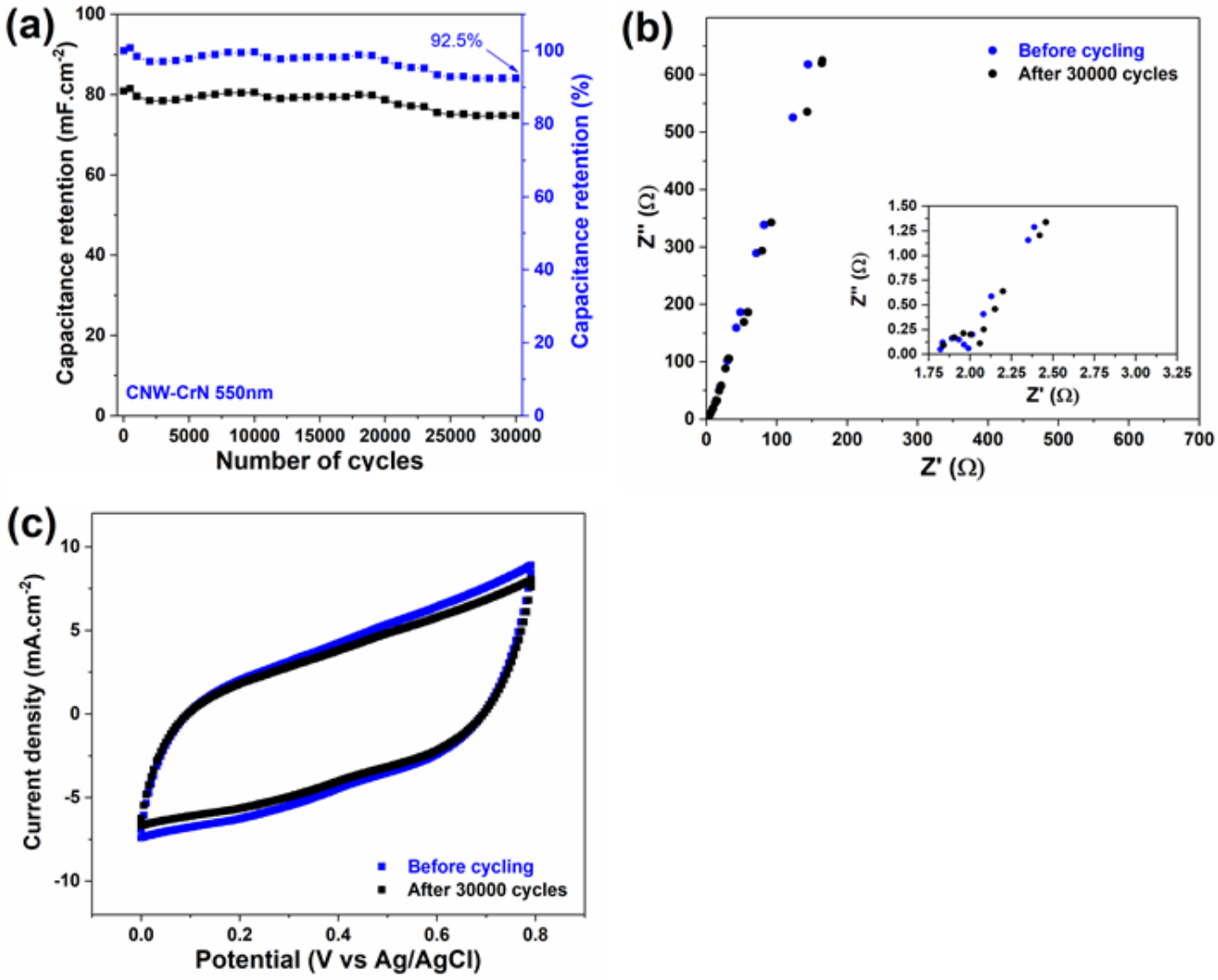

Figure 45: (a) Evolution of the capacitance for the CNW-CrN 550 nm electrode at a scan rate of 100 $mV.s^{-1}$. (b) Nyquist impedance plots for the CNW-CrN 550 nm before and after cycling. (c) CV curves for the CNW-CrN 550 nm before and after cycling.

4.4. The reason for the robust stability of CNW-CrN electrode

To better understand the good cycling stability of the CNW-CrN 550 nm electrode after 30000 cycles. SEM, XPS and XRD analyses were performed. **Figure 46** depicts the SEM images before and after cycling: no significant change in morphology and surface was observed. Furthermore, the chemical composition of the CNW-CrN 550 nm electrode (**Figure 47**) remains essentially the same after 30000 cycles. The XRD pattern (**Figure 48**) confirms that the structure of the post-cycled electrode remains cubic with (111), (200) and (220) orientations. Such results from the chemical, structural and electrochemical characterizations confirm the ultra-high stability of the CNW-CrN electrode.

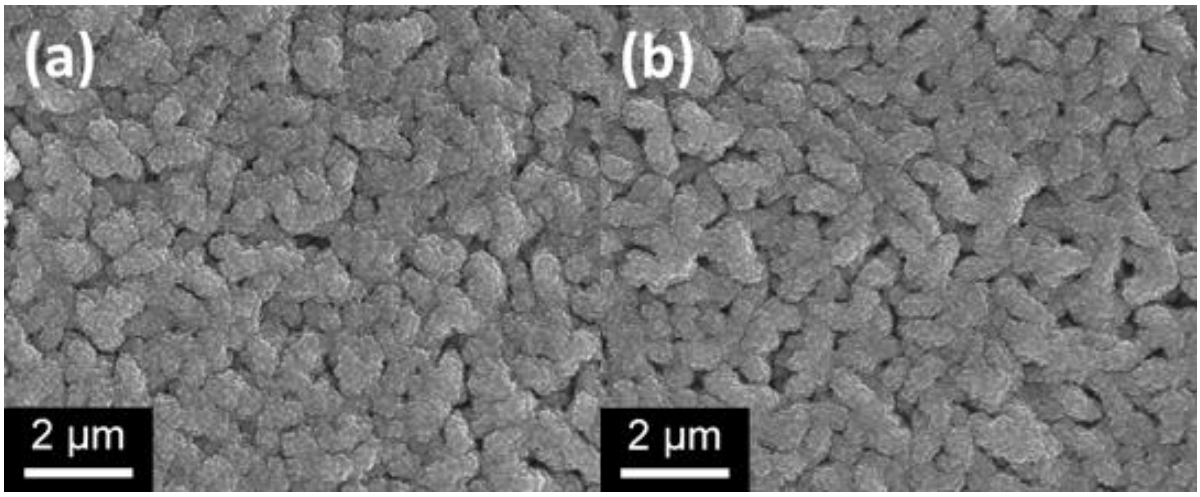

Figure 46: Top-view SEM images of CNW-CrN 550nm electrode (a) before cycling. (b) after 30000 cycles.

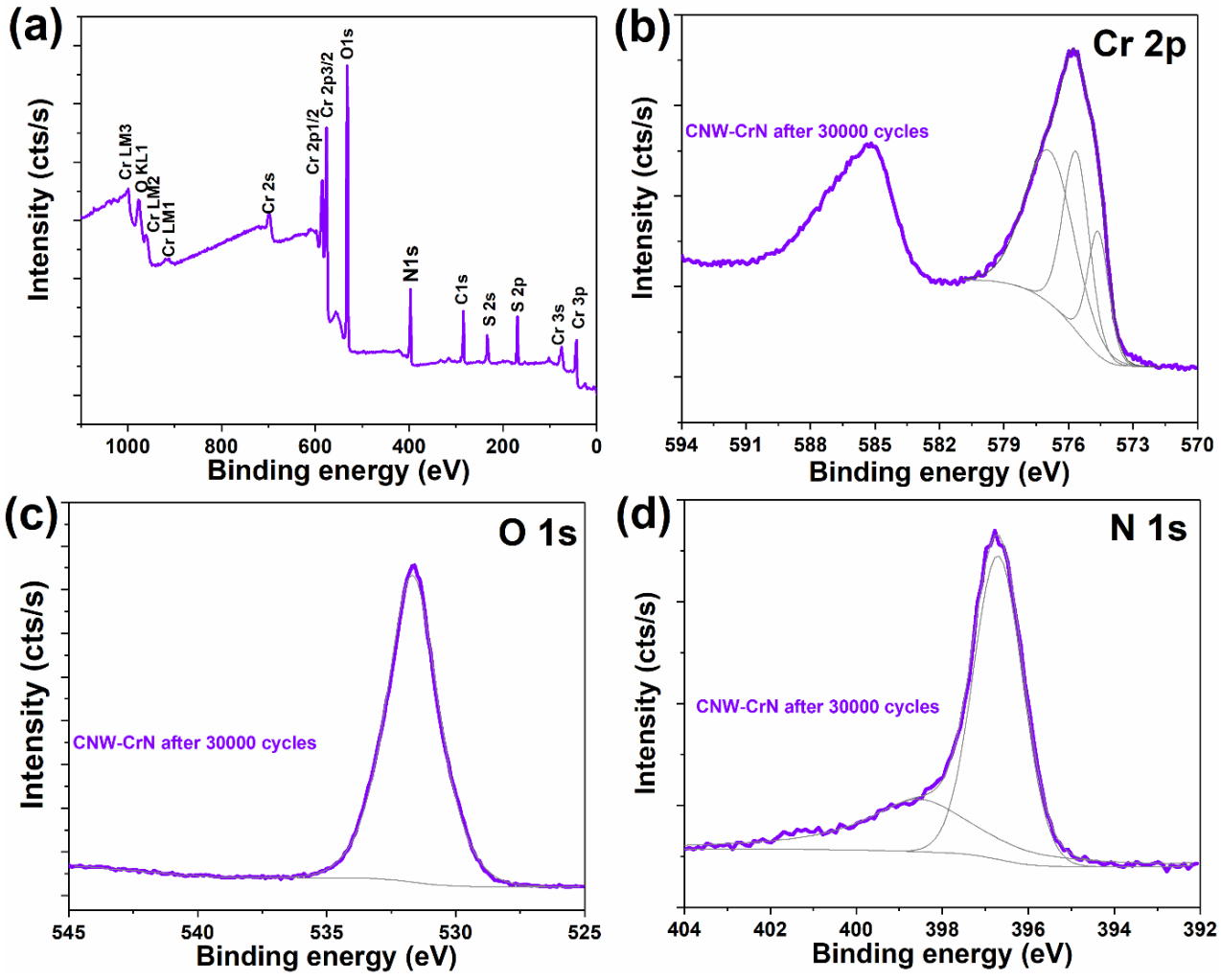

Figure 47: XPS analysis of CNW-CrN 550 nm electrode materials after 30000 cycles: Survey spectrum (a) and High-resolution XPS spectra of (b) Cr 2p (c) O 1s and (d) N 1s core levels.

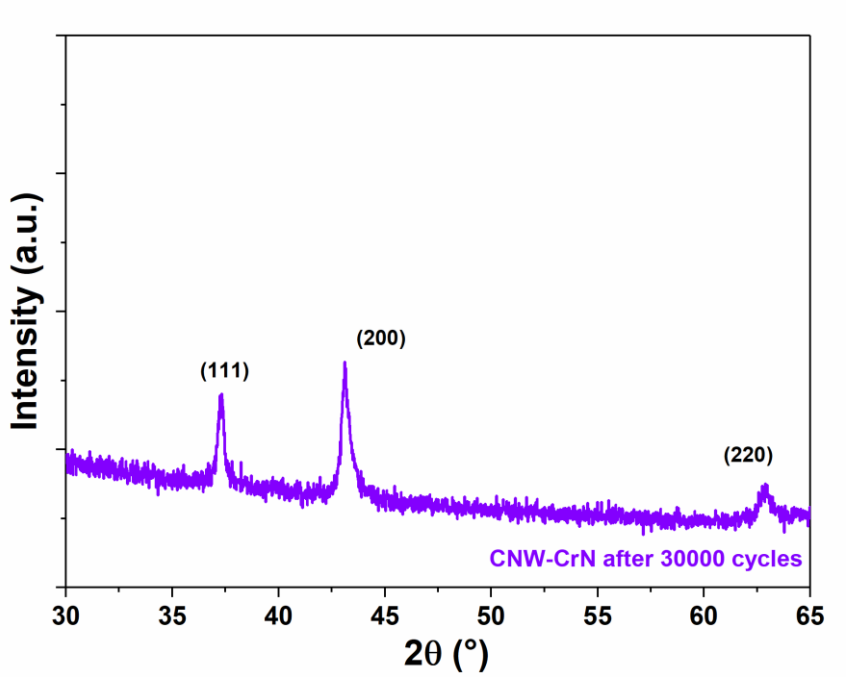

Figure 48: XRD pattern of CNW-CrN 550 nm electrode after 30000 cycles.

The comparison of the electrochemical performance (areal capacitance and cycling stability) of the CNW-CrN electrodes with those of transition metals nitrides reported in the literature is displayed in **Table 9**. To the best of our knowledge, the areal capacitance of CNW-CrN 550 nm electrode (80.8 and 90 $mF.cm^{-2}$ at 100 $mV.s^{-1}$ and 1.2 $mA.cm^{-2}$, respectively) is higher than that of CrN thin film [16] (in the range of 37.7 and 12.8 $mF.cm^{-2}$ at 100 $mV.s^{-1}$ and 1.0 $mA.cm^{-2}$, respectively), much higher than those of CrN-GLAD thin-film electrodes [27] (in the range of 35.4 at 1.2 $mA.cm^{-2}$), SiNWs-CrN electrodes [28] (in the range of 31.8 $mF.cm^{-2}$ at 1.6 $mA.cm^{-2}$) and CNT-TiN electrode [17] (in the range of 25.5 $mF.cm^{-2}$ at 100 $mV.s^{-1}$). These results confirm the high electrochemical performance of CNW-CrN composites for electrochemical capacitors application, which could be attributed to the large surface area of CNW combined with the excellent conductivity of CrN thin film.

Table 9: Performance of CNW-CrN electrode.

Electrodes	Areal capacitance	Cycling stability	Reference
CNW-CrN	80.8 mF.cm^{-2} at 100 mV.s^{-1} 90 mF.cm^{-2} at 1.2 mA.cm^{-2}	92.4% after 30000 cycles	This work
CrN-GLAD	35.4 at 1.2 mA.cm^{-2}	94.5% after 10000 cycles	Haye et al.[27]
SiNWs-CrN	31.8 mF.cm^{-2} at 1.6 mA.cm^{-2}	92% after 15000 cycles	Guerra et al.[28]
CrN thin film	37.7 mF.cm^{-2} at 100 mV.s^{-1} 12.8 mF.cm^{-2} at 1.0 mA.cm^{-2}	92.1% after 20000 cycles	Wei et al.[16]
CNT-TiN	25.5 mF.cm^{-2} at 100 mV.s^{-1}	90.9% after 20000 cycles	Achour et al.[17]

4.5. Electrochemical measurement of CNW-CrN//CNW-CrN µSC

The electrochemical performance of a symmetric *CNW-CrN//CNW-CrN* µSC was assessed using a two-electrode configuration with CNW-CrN as positive/negative electrodes in a PVA-H_2SO_4 gel electrolyte. **Figure 49a** depicts the CV plots at different scan rates of 5-1000 mV.s^{-1}. All the CV curves exhibit a typical rectangular and symmetrical shape with enhanced current density upon increasing the scan rate, indicating good capacitive behavior. **Figure 49b** shows the GCD curves of the symmetric µSC at different current densities 1-10 mA.cm^{-2}. The GCD curves display a symmetric rectangular shape regardless of current density, indicating an excellent capacitive behavior.

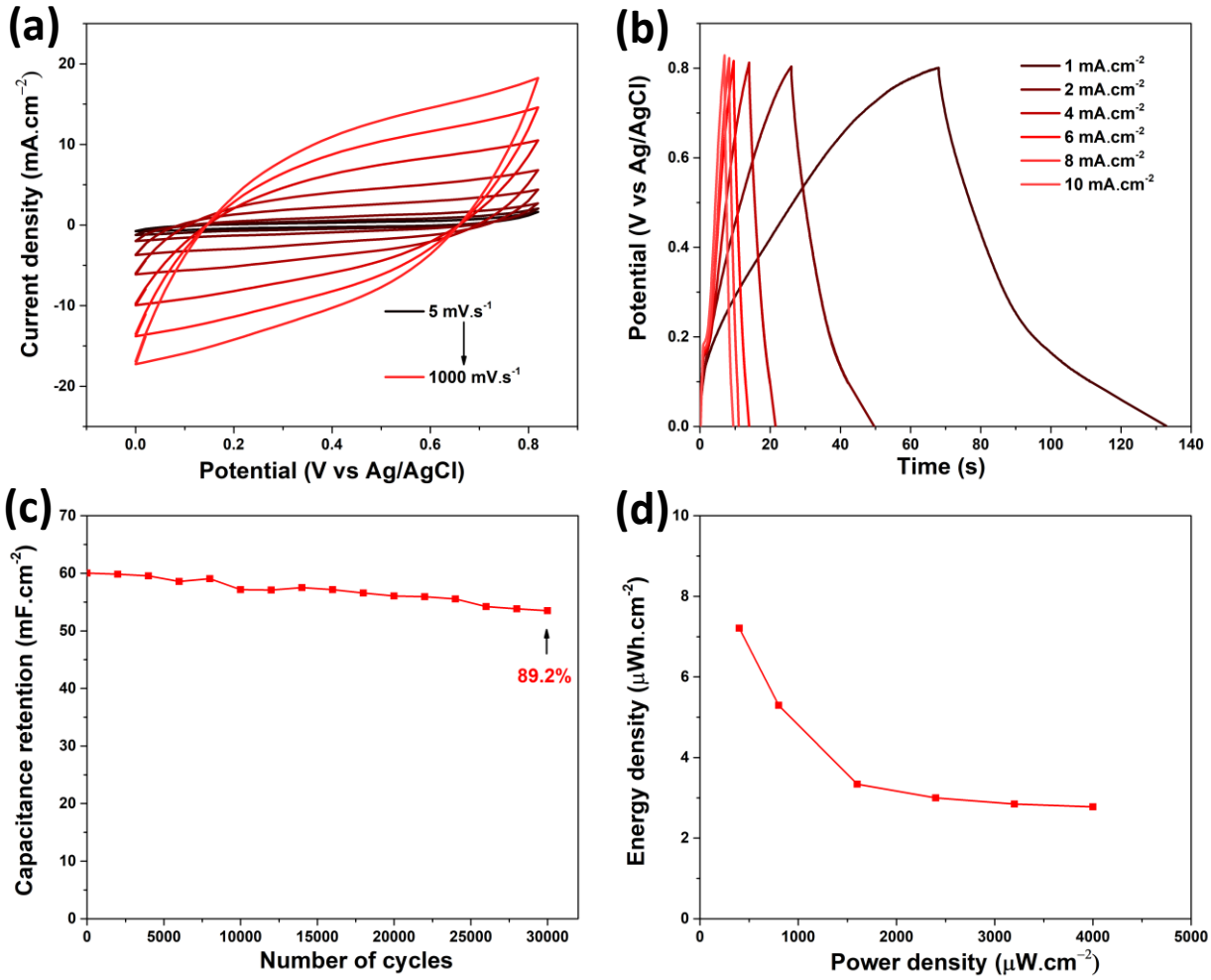

Figure 49: (a) CV curves of the CNW-CrN based µSC at various scan rates. (b) Galvanostatic charge-discharge curves at various current densities. (c) Evolution of the capacitance for the µSC at a scan rate of 100 $mV.s^{-1}$. (d) Ragone plot.

The areal capacitance values were calculated from GCD and found to be 81.1, 59.6, 37.6, 33.7, 32 and 31.2 $mF.cm^{-2}$ at current density of 1, 2, 4, 6, 8 and 10 $mA.cm^{-2}$ respectively. The areal capacitance of the symmetric CNW-CrN based µSC is higher than those of CrN based µSC [16, 27].

The cycling stability of the µSC device was further evaluated by continuous CV cycles at 100 $mV.s^{-1}$ (**Figure 49c**). The capacitance loss is only 10.8 % after 30000 cycles, which is significantly higher than CrN based µSC reported recently [16, 27].

Figure 49d depicts the Ragone plot (P vs E) relating the maximum power density and energy density of the symmetric CNW-CrN based µSC exhibited a power density of 400 $\mu W.cm^{-2}$ and 7.2 $\mu Wh.cm^{-2}$ at a current density of 1 $mA.cm^{-2}$. These results confirm the high performance of the CNW-CrN electrode for electrochemical capacitor applications.

4. Conclusion

In summary, we have reported the synthesis of thin film electrodes based on CrN coated carbon nanowalls (CNW) as long-life cycle micro-supercapacitors (μSC). SEM results revealed that the CNW-CrN electrodes exhibit a porous structure, which ensures easy electrolyte access to the large area of active electrode materials. Under optimized conditions, the CNW-CrN electrodes displayed a specific capacitance as high as 301 $mF.cm^{-2}$ at a scan rate of 5 $mV.cm^{-2}$ and 157.6 $mF.cm^{-2}$ at a current density of 0.3 $mA.cm^{-2}$ with a good cycling stability over 30,000 cycles in 0.5 M H_2SO_4 electrolyte. Furthermore, a symmetric μSC has was fabricated and achieved a capacitance of 31.2 $mF.cm^{-2}$ at a high current density of 10 $mA.cm^{-2}$ in 1M PVA-H_2SO_4 solid electrolyte. In addition, the symmetric device delivered a maximum energy density of 7.2 $\mu Wh.cm^{-2}$ at a power density of 400 $\mu W.cm^{-2}$. This work highlights the benefits of using CrN thin films deposited on carbon nanostructure as a promising material to achieve superior electrochemical properties.

References

[1] S. Vizireanu, B. Mitu, C. R. Luculescu, L. C. Nistor, G. Dinescu, PECVD synthesis of 2D nanostructured carbon material, Surface and Coatings Technology 211 (2012) 2-8.

[2] Liu, F.; Su, H.; Jin, L.; Zhang, H.; Chu, X.; Yang, W, Facile Synthesis of Ultrafine Cobalt Oxide Nanoparticles for High-Performance Supercapacitors, *Journal of Colloid and Interface Science 505* (2017) 796–804.

[3] Li, S.; Wen, J.; Mo, X.; Long, H.; Wang, H.; Wang, J.; Fang, G. Three-Dimensional MnO2 Nanowire/ZnO Nanorod Arrays Hybrid Nanostructure for High-Performance and Flexible Supercapacitor Electrode, *Journal of Power Sources 256* (2014)206–211.

[4] Chou, S.-L.; Wang, J.-Z.; Chew, S.-Y.; Liu, H.-K.; Dou, S.-X. Electrodeposition of MnO2 Nanowires on Carbon Nanotube Paper as Free-Standing, Flexible Electrode for Supercapacitors. *Electrochemistry Communications 10* (11) (2008) 1724–1727.

[5] Gamby, J.; Taberna, P. L.; Simon, P.; Fauvarque, J. F.; Chesneau, M. Studies and Characterisations of Various Activated Carbons Used for Carbon/Carbon Supercapacitors. *Journal of Power Sources 101* (1) (2001) 109–116.

[6] Kim, C.; Yang, K. S. Electrochemical Properties of Carbon Nanofiber Web as an Electrode for Supercapacitor Prepared by Electrospinning, *Appl. Phys. Lett. 83* (6) (2003) 1216–1218.

[7] Liu, C.; Yu, Z.; Neff, D.; Zhamu, A.; Jang, B. Z. Graphene-Based Supercapacitor with an Ultrahigh Energy Density. *Nano Lett. 10* (12) (2010) 4863–4868.

[8] Wang, Y.; Shi, Z.; Huang, Y.; Ma, Y.; Wang, C.; Chen, M.; Chen, Y. Supercapacitor Devices Based on Graphene Materials. *J. Phys. Chem. C 113* (30) (2009) 13103–13107.

[9] Guerra, A.; Achour, A.; Vizireanu, S.; Dinescu, G.; Messaci, S.; Hadjersi, T.; Boukherroub, R.; Coffinier, Y.; Pireaux, J.-J. ZnO/Carbon Nanowalls Shell/Core Nanostructures as Electrodes for Supercapacitors. *Applied Surface Science 481* (2019) 926–932.

[10] Dinh, T. M.; Achour, A.; Vizireanu, S.; Dinescu, G.; Nistor, L.; Armstrong, K.; Guay, D.; Pech, D. Hydrous RuO2/Carbon Nanowalls Hierarchical Structures for All-Solid-State Ultrahigh-Energy-Density Micro-Supercapacitors. *Nano Energy 10* (2014) 288–294.

[11] Hassan, S.; Suzuki, M.; Mori, S.; El-Moneim, A. A. MnO2/Carbon Nanowalls Composite Electrode for Supercapacitor Application. *Journal of Power Sources 249* (2014) 21–27.

[12] Achour, A.; Islam, M.; Ahmad, I.; Le Brizoual, L.; Djouadi, A.; Brousse, T. Influence of Surface Chemistry and Point Defects in TiN Based Electrodes on Electrochemical Capacitive Storage Activity. *Scripta Materialia 153* (2018) 59–62.

[13] Ouldhamadouche, N.; Achour, A.; Lucio-Porto, R.; Islam, M.; Solaymani, S.; Arman, A.; Ahmadpourian, A.; Achour, H.; Le Brizoual, L.; Djouadi, M. A.; et al. Electrodes Based on Nano-Tree-like Vanadium Nitride and Carbon Nanotubes for Micro-Supercapacitors. *Journal of Materials Science & Technology 34* (6) (2018) 976–982.

[14] Balogun, M.-S.; Zeng, Y.; Qiu, W.; Luo, Y.; Onasanya, A.; Olaniyi, T. K.; Tong, Y. Three-Dimensional Nickel Nitride (Ni3N) Nanosheets: Free Standing and Flexible Electrodes for Lithium Ion Batteries and Supercapacitors. *J. Mater. Chem. 4* (25) (2016) 9844–9849.

[15] Arif, M.; Sanger, A.; Singh, A. Sputter Deposited Chromium Nitride Thin Electrodes for Supercapacitor Applications. *Materials Letters* 220 (2018) 213–217.

[16] Wei, B.; Liang, H.; Zhang, D.; Wu, Z.; Qi, Z.; Wang, Z. CrN Thin Films Prepared by Reactive DC Magnetron Sputtering for Symmetric Supercapacitors. *J. Mater. Chem. 5* (6) (2017) 2844–

[17] Achour, A.; Ducros, J. B.; Porto, R. L.; Boujtita, M.; Gautron, E.; Le Brizoual, L.; Djouadi, M. A.; Brousse, T. Hierarchical Nanocomposite Electrodes Based on Titanium Nitride and Carbon Nanotubes for Micro-Supercapacitors. *Nano Energy 7* (2014) 104–113.

[18] Ghimbeu, C. M.; Raymundo-Piñero, E.; Fioux, P.; Béguin, F.; Vix-Guterl, C. Vanadium Nitride/Carbon Nanotube Nanocomposites as Electrodes for Supercapacitors. *J. Mater. Chem. 21* (35) (2011) 13268–13275.

[19] Wu, Y.; Ran, F. Vanadium Nitride Quantum Dot/Nitrogen-Doped Microporous Carbon Nanofibers Electrode for High-Performance Supercapacitors. *Journal of Power Sources 344* (2017) 1–10.

[20] Rassinfosse, L.; Colaux, J. L.; Pilloud, D.; Nominé, A.; Tumanov, N.; Lucas, S.; Pireaux, J.-J.; Haye, E. Using Ammonia for Reactive Magnetron Sputtering, a Possible Alternative to HiPIMS? *Applied Surface Science 502* (2020) 144176.

[21] Haye, E.; Colaux, J. L.; Moskovkin, P.; Pireaux, J.-J.; Lucas, S. Wide Range Investigation of Duty Cycle and Frequency Effects on Bipolar Magnetron Sputtering of Chromium Nitride. *Surf. Coat. Technol. 350 (*2018) 84–94.

[22] Haye, E.; Capon, F.; Barrat, S.; Boulet, P.; Andre, E.; Carteret, C.; Bruyere, S. Properties of Rare-Earth Orthoferrites Perovskite Driven by Steric Hindrance. *J. Alloys Compd. 657 (*2016) 631–638.

[23] Hones, P.; Sanjines, R.; Levy, F. Characterization of Sputter-Deposited Chromium Nitride Thin Films for Hard Coatings. *Surface and Coatings Technology 94–95 (1997)* 398–402.

[24] Milošev, I.; Strehblow, H.-H.; Navinšek, B. Comparison of TiN, ZrN and CrN Hard Nitride Coatings: Electrochemical and Thermal Oxidation. *Thin Solid Films 303* (1–2) (1997) 246–254.

[25] Barshilia, H. C.; Selvakumar, N.; Deepthi, B.; Rajam, K. S. A Comparative Study of Reactive Direct Current Magnetron Sputtered CrAlN and CrN Coatings. *Surf. Coat. Technol. 201* (6) (2006) 2193–2201.

[26] Felten, A.; Bittencourt, C.; Pireaux, J. J.; Van Lier, G.; Charlier, J. C. Radio-Frequency Plasma Functionalization of Carbon Nanotubes Surface O2, NH3, and CF4 Treatments. *J. Appl. Phys. 98* (7) (2005) 074308.

[27] Haye, E.; Achour, A.; Guerra, A.; Moulaï, F.; Hadjersi, T.; Boukherroub, R.; Panepinto, A.; Brousse, T.; Pireaux, J.-J.; Lucas, S. Achieving on Chip Micro-Supercapacitors Based on CrN Deposited by Bipolar Magnetron Sputtering at Glancing Angle. *Electrochimica Acta 324* (2019) 134890.

[28] Guerra, A.; Haye, E.; Achour, A.; Harnois, M.; Hadjersi, T.; Colomer, J.-F.; Pireaux, J.-J.; Lucas, S.; Boukherroub, R. High Performance of 3D Silicon Nanowires Array@CrN for Electrochemical Capacitors. *Nanotechnology 31* (3) (2020) 035407.

[29] Cho, S.; Han, J.; Kim, J.; Jo, Y.; Woo, H.; Lee, S.; Aqueel Ahmed, A. T.; Chavan, H. C.; Pawar, S. M.; Gunjakar, J. L.; et al. Calcium Nitrate (Ca(NO3)2)-Based Inorganic Salt Electrode for Supercapacitor with Long-Cycle Life Performance. *Current Applied Physics 17* (9) (2017)

Conclusions

The aim of this thesis was the development of composite electrodes based on chromium nitride (CrN) deposited on silicon, silicon nanwoires and carbon nanowalls for high-performance micro-supercapacitors (µSC).

The state of the art part describes the operating of supercapacitors and their storage mechanism. Then, a detailed bibliographic study was carried out on the composition of a supercapacitor (electrode, electrolyte, etc.) to determine the criteria for improving their electrochemical performance.

The electrode material is the key factor that determines the charge storage mechanism of the supercapacitor. Transition metal nitrides (TMNs) are considered as promising electrode materials for supercapacitors due to their high electrical conductivity. Among TMNs, chromium nitride (CrN) is considered as a potential candidate owing to its excellent electrical conductivity and chemical stability. Several studies have shown the major influence of the morphology and the specific surface on the electrochemical performance of electrodes. Thus, the control of the morphology and the specific surface can significantly enhance the areal capacitance of the electrodes. Furthermore, the nature of electrolyte is crucial which influence directly the performance of supercapacitors. The aqueous electrolytes seem to be suitable because of their low cost and excellent ionic conductivity which is important to reduce the cell resistance.

The bibliographic study allowed choosing the different elements for the development of high-performance electrodes i.e. *i)* highly doped silicon as a current collector. *ii)* Porous CrN thin film as the active material. *iii)* Aqueous electrolytes.

An original method combining physical vapor deposition (PVD) with glancing angle (GLAD) was used to fabricate porous CrN thin-film electrodes. This method allows controlling the morphology of our electrodes. A high porous structure was obtained for deposition angles of 45 ° and 60 ° which increase significantly their electrochemical performance. In the second part, we report the fabrication of micro-device with planar inter-digital configuration based on CrN electrodes. Indeed, the integration of CrN-based µSC on a silicon substrate allows reducing the series resistance and improving its power density.

Conclusions

The fabricated micro-device exhibits a lower resistance than the CrN electrodes with a high energy density of 2 $\mu Wh.cm^{-2}$ for a power density of 20 $\mu W.cm^{-2}$.

CrN thin films deposited at a glancing angle have shown a good electrochemical performance due to their high electrical conductivity. The third & fourth chapters deal with the study concerning the specific surface area of the CrN based-electrodes.

The results obtained showed that the use of silicon nanowires (SiNWs) as a template with a large specific surface area allowing capacitance enhancement of the CrN-based electrodes. The areal capacitance was increased by 1.3 fold with better cycling stability compared to thin-film CrN electrodes.

To further improve the electrochemical performances of CrN based electrodes, a nanostructured template consisting of aligned vertically carbon nanowalls are used. The obtained results show the growth of honeycombed carbon nanowalls with a large specific surface, which increases significantly the areal capacitance of the CNW-CrN based-electrodes. The areal capacitance was increased by 8 fold with robust electrochemical stability over 30000 cycles compared to CrN thin-film electrodes.

In conclusion, through this thesis, we have demonstrated the advantage of using chromium nitride (CrN) as supercapacitors electrode material. We have also shown that the use of nanostructured templates, in particular, carbon nanowalls and silicon nanowires with the high surface area can improve significantly the electrochemical performance of CrN based-electrodes.

Perspectives

In this thesis, micro-supercapacitors (µSC) were fabricated using low-cost chromium nitride (CrN) based material deposited by PVD. The effect of morphology and porosity was studied using a new GLAD technique was studied. Another way to improve the performance of CrN electrodes using high surface area templates consisting of silicon nanowires (SiNWs) and carbon nanowalls (CNW) was investigated. The fabricated electrodes showed good electrochemical performances in H_2SO_4 aqueous electrolyte. Their high performances were attributed to the good conductivity and chemical stability of CrN combined with the high surface area of nanostructured templates. These results could be very important for micro-supercapacitors design and application. The original work carried out open the way for future perspectives:

- The glancing angle deposition strategy can be generalized for other materials deposited by PVD to obtain electrodes with controlled porosity and improved electrochemical energy storage properties. The study of the electrochemical proprieties of other transition metal nitrides (TiN, VN, TiVN, RuN ...) or transition metal oxides (MnO_2, ZnO, NiO ...) developed using the glancing angle technique (GLAD) can be performed.
- Highly conductive nanostructures with a high surface area such as carbon nanowalls (CNW) and silicon nanowires (SiNWs) can be used as templates for the growth of transition metal compounds allows improving their electrochemical performances.
- The gel electrolyte used in this thesis is H_2SO_4/PVA. The operating electrochemical window is narrow. The working potential plays an important role on the energy storage in µSCs. So, developing a new electrolyte is quite important for the µSCs.
- The CrN based electrodes should be tested in an organic electrolyte or ionic liquid, which will increase the operating electrochemical window of the cell and therefore increasing their power and energy densities.

Finally, other active materials such as MnOx, VN, MoS_2, and Ni are being developed and evaluated to fabricate high-performance symmetric micro-supercapacitors.

Annex

Experimental and Measurement Method

Fabrication of inter-digital CrN based µSC

A symmetrical micro-supercapacitor (µSC) was fabricated using CrN thin films (CrN 45° or CrN 60°) as electrodes, as depicted in **Figure 1**. The technological process used for micro-device fabrication allows us to perform the collective fabrication of µSCs at a wafer scale. A 500 nm SiO_2 was first thermally grown at 1100°C on a 4-inch silicon wafer to provide good electrical insulation. Current collectors were then deposited using the evaporation of a 100 nm Ti / 400 nm Au layer, annealed at 250°C for 20min, and patterned with a conventional lift-off process. The current collectors were then protected by an insulating SU8 masking layer (800 nm thick) via a second photolithography step. To improve the resolution of the micro-device, a 2.5 µm N-LOF photoresist was deposited in the gap between the electrodes via a third photolithography step. A thin layer of 50 nm of Au was afterward deposited on the whole wafer, followed by the deposition of the active material. Both Au and active layers on the unwanted areas were finally lift-offs to obtain the final devices.

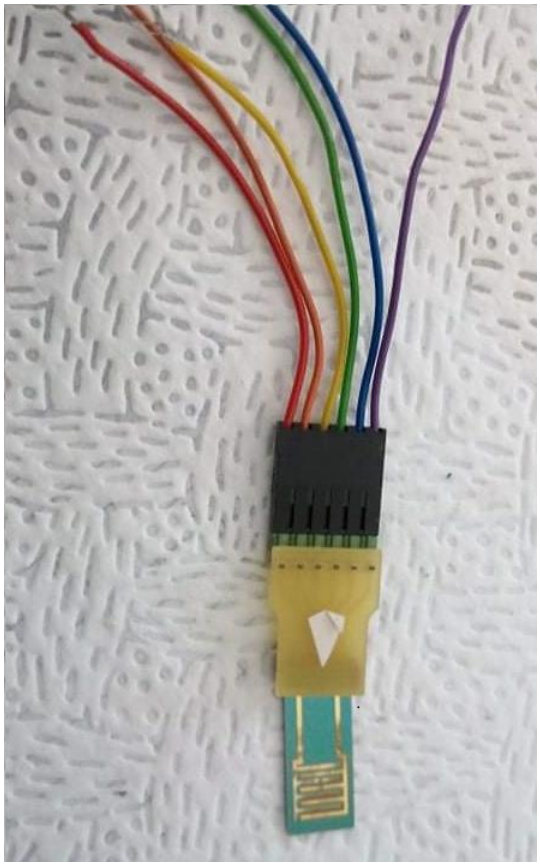

Figure 1: Photography of CrN based-micro-device with a connector.

Fabrication of symmetric CNW-CrN supercapacitor

Pair of CNW-CrN 550 nm films were used as positive/negative electrodes. PVA/H_2SO_4 was used as a solid electrolyte. 0.5 g of poly-vinyl-alcohol (PVA) was dissolved in 5 mL deionized water with vigorous magnetic stirring. 280 µL of H_2SO_4 was then added to the PVA solution and heated at 80 °C with magnetic stirring for another 10 min. The solid electrolyte was drop cast on the as-prepared electrode.

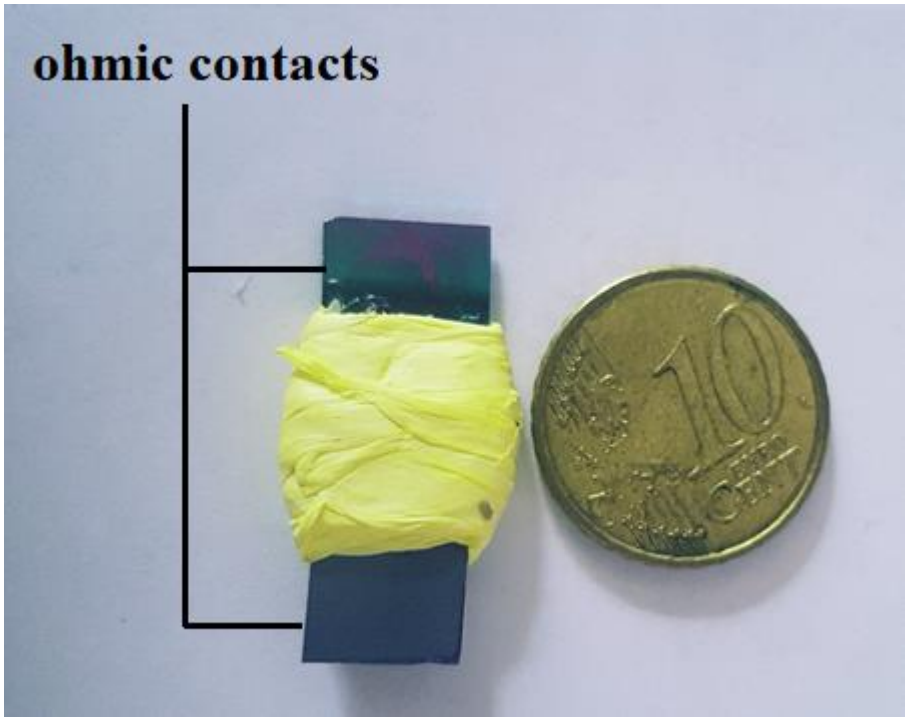

Figure 2: Photography of CNW-CrN based-micro-device.

Characterization methods

The main characterization techniques used are shown in this section. The characterization of the electrodes used was studied by scanning electronic microscope (SEM), transmission electron microscope (TEM), X-ray diffraction (XRD) and X-ray photoelectron spectroscopy. Besides, cyclic voltammetry (CV), galvanostatic charge/discharge and electrochemical impedance spectroscopy were used for the electrochemical evaluation of the as-prepared electrodes.

Structural and surface characterization

Scanning electron microscopy (SEM)

SEM is a method used for high-resolution surface imaging which provides information on the surface morphology and structure of the electrode.

In this thesis work, the morphology of the samples was characterized using scanning electron microscopy (SEM, JEOL JSM 7500F) at an accelerating voltage of 5 and 15 kV.

Transmission electron microscope (TEM)

Transmission electron microscopy (TEM) is a major analytical technique that provides structural information on nanostructured materials. The TEM uses a condensed, accelerated electron beam transmitted through a specimen to form an image at a significantly higher resolution than SEM microscopes.

In this thesis work, the samples were characterized using a T20 transmission electron microscope, working under 200 kV. Before measurement, the samples were deposited on a TEM grid for observation.

X-ray diffraction (XRD)

XRD is an effective technique to study the structure and the phases of materials by comparing the diffraction pattern collected from the samples with the diffraction patterns of known compounds. Resultant samples in the thesis were identified by X-ray diffraction (XRD) using an X-ray diffractometer D5000 MOXTEK with (Cu Kα) radiation (λ=0.154 nm) in the θ–2θ Bragg Brentano configuration.

X-ray photoelectron spectroscopy

XPS also called electron spectroscopy for chemical analysis (**ESCA)**, is an analytical technique widely used for the investigation of the chemical composition of solid surfaces with a thickness of 1 - 10 nm. For surface chemical analysis, XPS measurements were carried out on K-Alpha (Thermo Scientific, East Grinstead, England) using a monochromatic (Al Kα) X-ray beam, on a 300×300 μm^2 spot area in a spectrometer equipped with a flood gun for charge compensation. A Shirley background was subtracted from the spectra and the symmetric Gaussian functions were used during the peak-fitting procedure.

Evaluation of electrochemical properties

Three electrode configuration

Electrochemical studies of the single electrodes were carried out at room temperature using a PGSTAT128N potentiostat/galvanostat in a typical three-electrode electrochemical cell. The cell is composed of two parts screwed one in each other, one has a copper current collector and the other in Teflon filled with the electrolyte and has a hole at the bottom to enable the contact between the electrode

and the electrolyte. The as-prepared samples were used as working electrode, Ag/AgCl as a reference electrode and Pt foil as a counter electrode. In this cell, only the side coated with the active material was in contact with the electrolyte (S=0.5 cm2) and the other side was in contact with the current collector by using a silver paste to ensure good contact. The electrodes are characterized by cyclic voltammetry (CV), Galvanostatic Charge-Discharge (GCD) and electrochemical Impedance Spectroscopy (EIS).

Cyclic voltammetry (CV)

Cyclic voltammetry is one of the most used electrochemical techniques to evaluate the performances of supercapacitors. It consists of applying a linear potential sweep at a constant scan rate. The response current as a function of the potential is recorded during the scanning (**Figure 3**). The cyclic voltammetry is used to determine the electrochemical stability window, the behavior of the electrodes in the electrolyte (if they exhibit a capacitive or pseudo-capacitive behavior). It can be used also to assess the specific capacity and the cycling stability of the electrodes.

The CV curve of an ideal supercapacitor is rectangular (**Figure 3a**) without faradic reactions. However, the differences observed in (**Figure 3b**) can be explained by the presence of internal resistance (internal resistance of the active material, contact resistance, etc...).

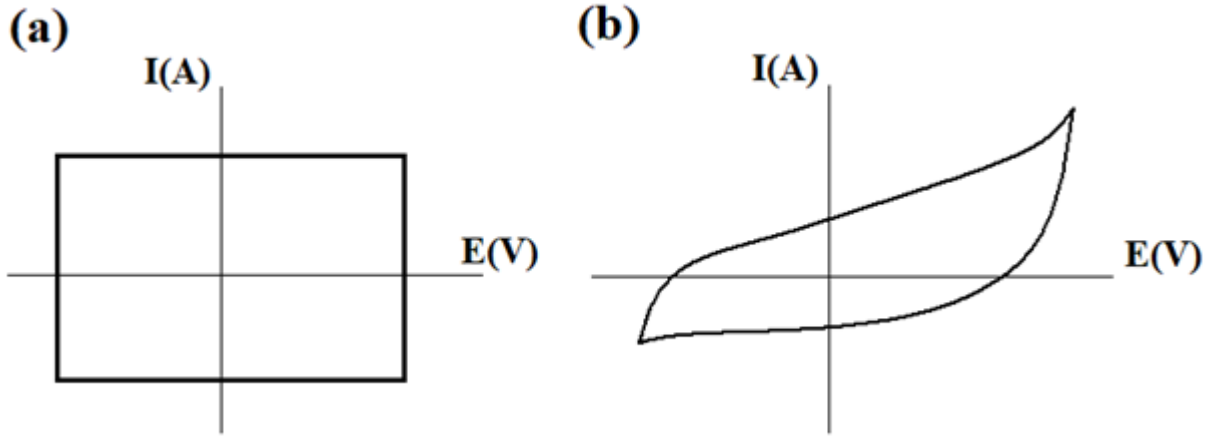

Figure 3: Cyclic voltammetry curves. (a) Ideal capacitive response. (b) Real capacitive response.

Galvanostatic charge / discharge (GCD)

GCD measurements consist of applying a constant current and measuring the potential as a function of time (**Figure 4**). The supercapacitor is charged by applying a positive current (+ i). However, when the potential reaches the value U_{max} (corresponding to the value of the electrochemical stability window), the

current is reversed (-i) implies the discharge of the supercapacitor. Galvanostatic cycling (multiple charge/discharge cycles) can be used also to determine the specific capacitance and cycling stability of the electrodes.

The resistance series (ESR) can be determined from the IR drop (ΔV) in the GCD curves. In order to have a maximum power density (Pm), the internal resistance should be minimized, since the power is inversely proportional to the ESR (**Equation I-6**).

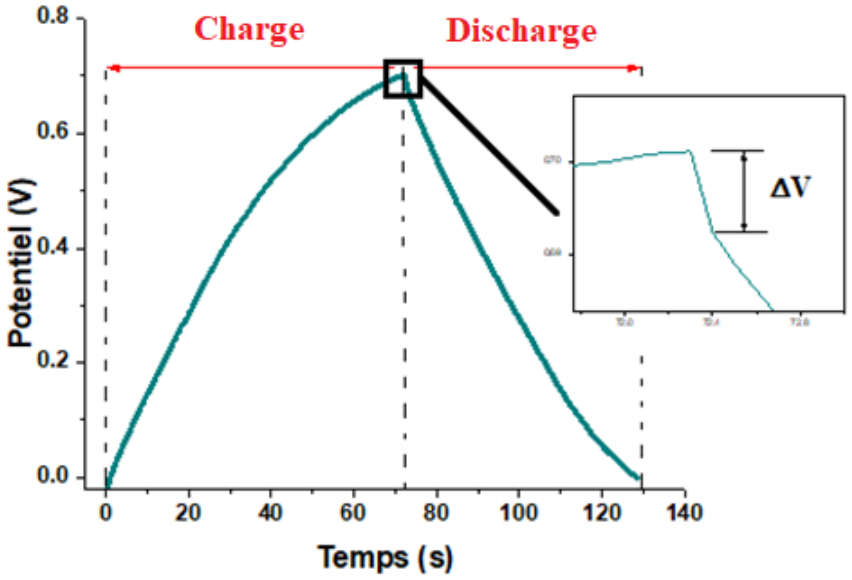

Figure 4: GCD curve at a current density of 40 µA.cm^{-2}.

Electrochemical impedance spectroscopy (EIS)

An ideal supercapacitor can be modelled as a pure capacitance in series with a pure resistance (**Figure 5a**). Therefore, the complex impedance of a supercapacitor is expressed like that of an RC circuit according to the expression:

$$Z = R + \frac{I}{jC\omega} \qquad \textbf{Equation 1}$$

R: The series resistance of supercapacitor (Ω)

C: The capacity (F)

ω: The pulsation = 2πf

At high frequencies, the impedance tends towards pure resistance. In contrast, at low frequencies, the impedance tends towards a pure capacity. The low-frequency part is characterized by a straight line corresponding to the diffusion of ions at the electrode-electrolyte interface (**Figure 5b**). At high

frequencies, the resistance of electrolyte (Re) can be obtained from the intercept of the Nyquist arc with the real axis. Also, the charge transfer resistance (Rct) is calculated from the diameter of the high-frequency arc.

In this thesis, EIS measurements are carried out at an open circuit (OCP) with a signal amplitude of 10 mV in a frequency range of 100 kHz–1 mHz.

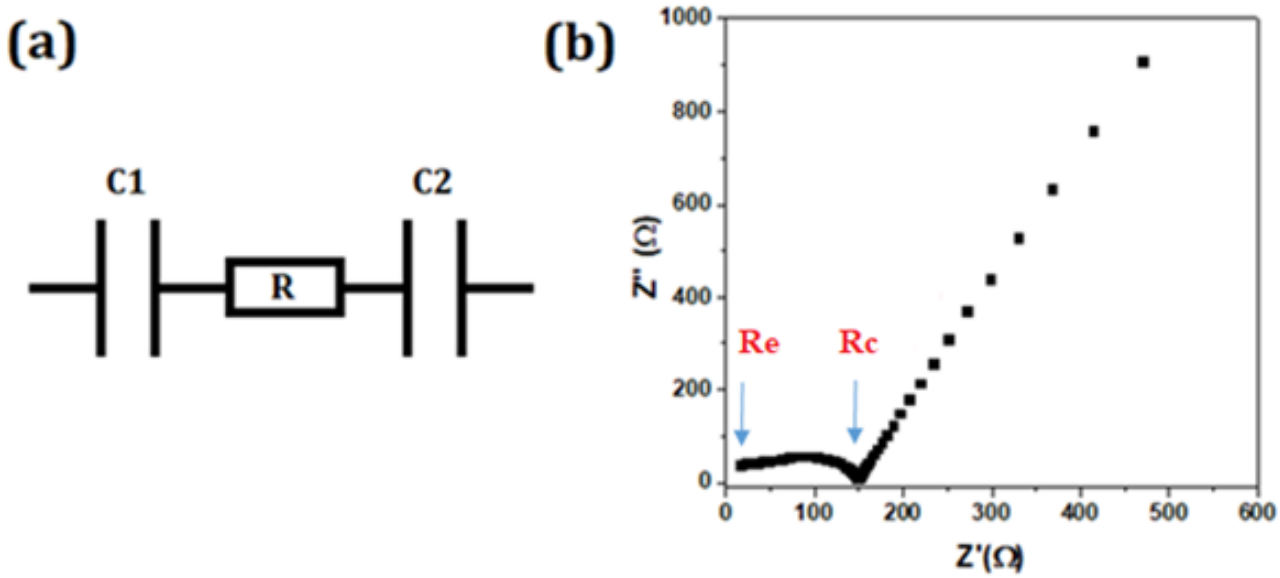

Figure 5: (a) Equivalent circuit of an ideal supercapacitor. (b) Nyquist diagram of CNW-ZnO electrode in 1 M KCl.

Capacitance assessment

The areal capacitance of the electrodes/micro-supercapacitor was determined from the CV and GCD curves. The surface of the electrodes in contact with the electrolyte is 0.5 cm^2 in the case of a three-electrode configuration, 0.02 cm^2 in the case of two-electrode inter-digital device configuration and 2 cm^2 for stacked configuration.

a) From CV curves

The areal capacitance C of the electrodes is calculated from the CV curves using **equation 2**:

$$C = \frac{\Delta i}{2v} \qquad \textbf{Equation 2}$$

C: The areal capacitance ($mF.cm^{-2}$)

Δi: The average of the intensity difference between the upper and the lower part of the CV curve (mA.cm^{-2})

v : The scan rate (mV.s^{-1}).

b) From GCD curves

The areal capacitance C of the electrodes is calculated from GCD curves using equation **3:**

$$C = \frac{I}{dV/dt} \qquad \textbf{Equation 3}$$

C: The areal capacitance (mF.cm^{-2})

I: The applied current density (mA.cm^{-2})

dV: The potential difference (V)

dt: The discharge time (s)

Electrochemical stability assessment

Cycling stability is an important parameter in a supercapacitor. It tells us about its lifespan. It can be assessed using a repeated CV or GCD cycles. In our studies, cycling stability was assessed from cyclic voltammetry (CV) curves.

Energy and power densities assessment

The energy density E is determined using the following equation:

$$E = \frac{C\,\Delta U^2}{2} \qquad \textbf{Equation 4}$$

The power density P is calculated according to the following equation:

$$P = \frac{E}{\Delta t} \qquad \textbf{Equation 5}$$

C: The areal capacitance (mF.cm^{-2})

ΔU: The potential difference (V)

Δt: discharge time (s)

Scherrer Equation

The Scherrer equation, in X-ray diffraction and crystallography, is a formula that relates the size of nano-crystallites in a solid to the broadening of a peak in a diffraction pattern. It is often referred to, incorrectly, as a formula for particle size measurement or analysis. It is used in the determination of size of crystals in the form of powder. The Scherrer equation can be expressed as:

$$T = \frac{K\lambda}{\beta \cos\theta} \qquad \textbf{Equation 6}$$

T: the mean size of the ordered (crystalline) domains

K: dimensionless shape factor with typical value of 0.9

λ: the X-ray wavelength.

β: the line broadening at half the maximum intensity (FWHM)

Θ: the Bragg angle